Organic and Inorganic Geochemical Signatures Associated with the 2011 Tohoku-oki Tsunami

January 2016

Tetsuya SHINOZAKI

Organic and Inorganic Geochemical Signatures Associated with the 2011 Tohoku-oki Tsunami

A Dissertation Submitted to
the Graduate School of Life and Environmental Sciences,
the University of Tsukuba
in Partial Fulfillment of the Requirements
for the Degree of Doctor of Philosophy in Science
(Doctoral Program in Earth Evolution Sciences)

Tetsuya SHINOZAKI

Contents

Abstract

To verify what kind of chemical component is transported onto the coastal land, and how long such a geochemical component is lasting, samples of the 2011 Tohoku-oki tsunami deposit and underlying and overlying soil were collected at Sendai, Odaka, Hasunuma, and Yamamoto, East Japan. I mainly focused on biomarkers and water-leachable ions as geochemical proxies which they represent organic matter and seawater component, respectively.

Characteristic biomarkers were detected at samples of Sendai, Miyagi Prefecture, and of Odaka, Fukushima Prefecture. Short-chain *n*-alkanes (C_{16}, C_{17}, C_{18}, and C_{19}) mainly elaborated from algae and fish were occurred at soil 2 cm deep from surface sandy tsunami deposit at Sendai. In addition to the short-chain *n*-alkanes, at Odaka, pristane and phytane that are elaborated from zooplankton, benthos, and fish were detected at soil immediately below sandy tsunami deposit. Moreover, diosterol that is derived from marine dinoflagellate was observed at tsunamigenic mud. No aquatic biomarker was presented further deep soil layer in both Sendai and Odaka and modern soil overlying tsunami deposit in Odaka, it is highly possible that these biomarkers were transported by the 2011 tsunami. Because they were detected at organic-rich soil layer not at tsunamigenic sand layer, transported aquatic biomarkers seems to adsorb to fine mineral particles and organic-rich matter but not to large, sand-sized particles. Moreover, according to the results of Sendai and Odaka, transported biomarkers seem to be preserved at least 2 years because sediment samples were collected more than 2 years after the 2011 tsunami. At Hasunuma, Chiba Prefecture, on the other hand, biomarkers were not detected in sand layer samples taken in June and August 2011, and October 2014, and no aquatic biomarkers were observed at both sandy tsunami deposit and pre-tsunami soil layer. Soil at Hasunuma contains sand probably from beach by wind because sampling locations were close to beach. The soil scattering sand might enrich permeability of allochthonous organic carbon. Therefore, transported biomarkers might pass through the soil layer by groundwater movement at Hasunuma.

At Hasunuma, tsunami-derived water-leachable ions showed highest concentrations at soil layer immediately below the sandy tsunami deposit from the samples taken in 2011 and then they were gradually decreased with depth. Soil can possess an amount of water rather than sand. Therefore, these

ions probably penetrate sand layer and concentrated at soil underlying sand layer. However, water-leachable ions recorded entirely low values not only at sand layer but also soil layer from samples taken in 2014. They probably diluted by post-tsunami rainfall, seepage, and seasonal changes in groundwater.

Suijin-numa, a small coastal lake, is located in Yamamoto, Miyagi Prefecture. Based on the comparison between pre- and post-tsunami lake bottom sediments, the 2011 tsunami eroded a significant thickness of the geological record over 1100 years including the paleotsunami deposit and volcanic tephra layer. It suggests that tsunami history in the coastal lake might not always be complete and the influence of tsunami erosion cannot be overlooked. Moreover, reworked thick muddy tsunami deposit can confuse estimation of the depositional age of event deposits. In order to reconstruct tsunami history accurately, we must be noted that the presence of erosion and reworking by tsunami inundation.

From the analysis of the 2011 tsunami deposit, I proposed that marine biomarkers and sea-water origin water-leachable ions were transported by tsunami inundation. Moreover, they seem to be easily preserved in organic silty mud rather than sand. Biomarkers have a possibility that it can be preserved for long time. It suggests that biomarkers have the potential as proxies for identifying marine-originated deposits on coastal land both tsunamigenic sand and reworked mud. Moreover, it may be utilized for prediction of precise tsunami inundation area. For further applications (e.g., research into paleotsunami), more case studies of modern and past tsunamis are required.

Keywords: 2011 Tohoku-oki tsunami, Tsunami deposit, East Japan, Geochemical analysis, Biomarker, Water-leachable ions, Erosion, Redeposition.

List of Figures

List of Tables

Chapter 1. Introduction

1.1 Background

A correct understanding of tsunami event is important to predict its magnitude, frequency, and timing. Because tsunami occur infrequently, current observational data for modern tsunamis and even though ancient document are not sufficient for a comprehensive understanding of tsunami event. Analysis of historical and prehistoric tsunamis (paleotsunami) using geological evidence is therefore required.

Tsunami deposit (Fig. 1-1) that is formed by tsunami flow is generally used for estimating paleotsunami event (e.g. Atwater, 1987; Dawson et al., 1988, 1995). To find tsunami deposit efficiently, geologists usually select lowland areas where sediments typically settle out of calm water (e.g., lakes, lagoons, ponds, marshes, and swamps) because these environments are assumed to be sites of continuous and uninterrupted sedimentation that are unlikely to be affected by erosion. As such an environment, many studies had been conducted in inter-ridge swales of strand plains (e.g., Nanayama et al., 2003; Jankaew et al., 2008; Sawai et al., 2012) or coastal lakes and lagoons (e.g., Minoura et al., 1994; Kelsey et al., 2005; Jackson et al., 2014).

Tsunami deposits form in various grain size, such as mud, sand, and boulder. Sandy tsunami deposit is especially used for paleotsunami research because it is easily identified from geological layer compared with mud, and it is easily formed at coastal area rather than boulder. Sandy tsunami deposit is mainly identified on the basis of geological, chemical, biological, archaeological, anthropological, geomorphological, and contextual feathers (Goff et al., 2012; Sawai, 2012). Especially, geological and biological features such as lateral changes in thickness and grain size of deposit (e.g. Minoura et al., 1996; Nanayama et al., 2007), presence of marine-origin microfossils (e.g. Hemphill-Haley, 1996; Sawai et al., 2008; Sawai, 2014) and others have been frequently utilized as identifying proxies. However, these characteristics do not always get preserved, in which case it is difficult to identify paleotsunami deposit. Moreover, sandy tsunami deposits do not seem to distribute up to the limit of tsunami inundation (Goto et al., 2011; Abe et al., 2012; Chagué-Goff et al., 2015). Therefore,

inundation distance estimated from the distribution of sandy tsunami deposits might result in underestimation (Fig. 1-2). In order to identify paleotsunami deposit or estimate precise tsunami inundation area, confirmation of new proxy is required.

Tsunami inundation causes salinization and soil pollution around coastal area that damages influence human activity (e.g., Szczuciński et al., 2005; Komai et al., 2012). The environmental damages means that evidences of tsunami inundation are preserved not only visible (boulder and sand) but also less-visible or invisible (mud and seawater) forms. If evidence of seawater inundation could be detected, it would be a good criterion for determining that sandy deposits have a marine source. Geochemical characteristic, such as major chemical components of seawater (e.g., sodium, chloride, and calcium) and biomarker that is molecular fossils originated from living organism, can remain for a while within inundation area after tsunami inundation (Fig. 1-3). If they are preserved as geologic evidence for long time, they can allow us to identify tsunami deposit, moreover, they can be utilized for accurate estimation of the inundation area. However, there is still little known about such geochemical characteristic; how much chemical components will be transported onto the coastal land, and how long such a chemical component will be lasting.

Analyzing a modern tsunami that have much and correct information leads to a better understanding of the behavior of geochemical characteristics associated with tsunami inundation. The 2011 Tohoku-oki tsunami is just such case study. The tsunami caused by the Tohoku earthquake (Mw 9.0) struck coastal areas in East Japan on March 11, 2011. After the tsunami, a number of research groups conducted urgent surveys based on sedimentological (e.g., Goto et al., 2011, 2012a, 2012b; Richmond et al., 2012; Szczuciński et al., 2012), micropaleontological (e.g., Pilarczyk et al., 2012; Tanaka et al., 2012), mineralogical (e.g., Jagodziński et al., 2012), and geomorphological (e.g., Tappin et al., 2012; Tanaka et al., 2014) approaches as well as geochemical (e.g., Chagué-Goff et al., 2012a, 2012b, 2014; Yoshii et al., 2013) approach. A lot of geochemical proxies have been utilized for tsunami research. In this thesis, I focused on stable carbon isotope ratio, biomarkers, and water-leachable ions as geochemical proxies. Water-leachable ions are one of standard geochemical proxy in tsunami research (e.g., Minoura and Nakaya, 1991), while biomarkers are new one in tsunami research.

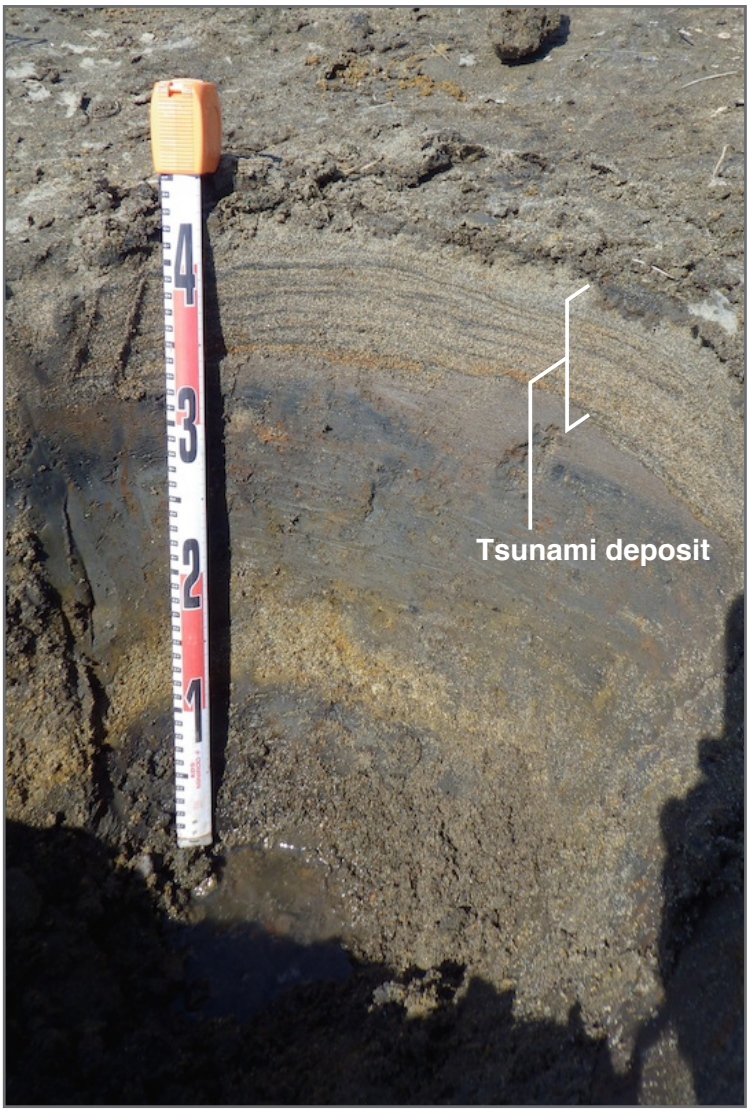

Fig. 1-1. Tsunami deposit formed by the 2011 Tohoku-oki tsunami. Photo taken at Minamisoma city, Fukushima Prefecture, Japan.

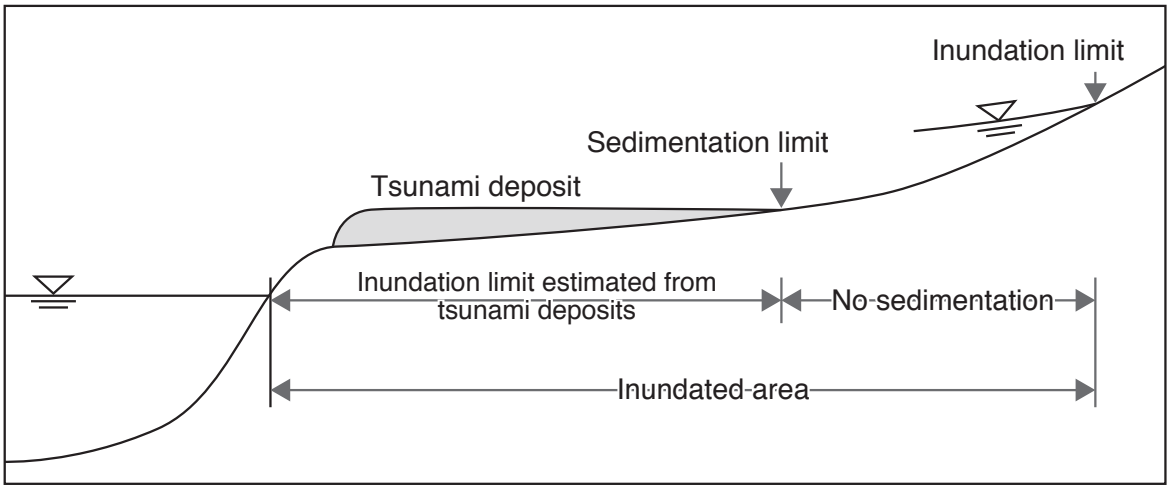

Fig. 1-2. Conceptual model of tsunami inundation.

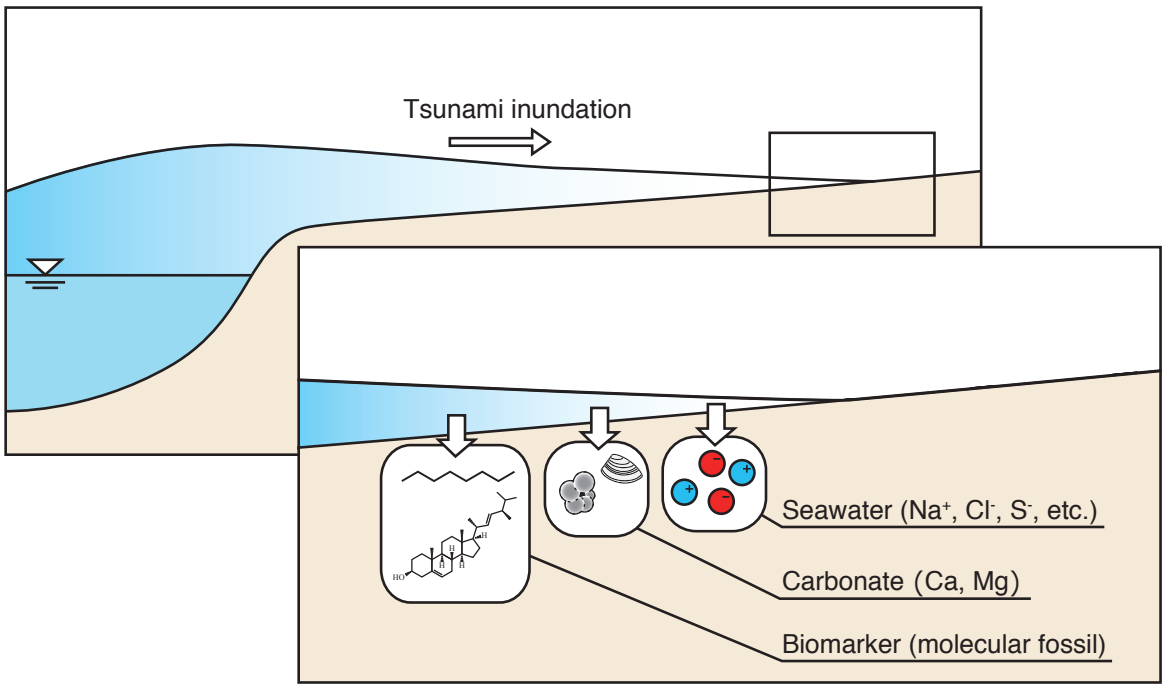

Fig. 1-3. Illustration showing geochemical characteristics transported by tsunami inundation.

1.2 Previous study

Minoura et al. (1987) in Japanese paper and Minoura and Nakaya (1991) in English paper were the first to report chemical evidence of a paleotsunami from lake sediment. They found high concentrations of Ca^{2+} and Mg^{2+} that were attributed to the reaction of seawater with the carbonic acid in lake water and to the skeletal carbonate associated with sandy layers. Then, geochemical analysis is applied for identifying historical and prehistoric tsunami deposit (e.g., Minoura et al., 1994; Chagué-Goff et al., 2002, 2012c; Goff et al., 2004, 2010; Nichol et al., 2010; Sawai et al., 2015b). Moreover, to get better understand geochemical behavior by tsunami inundation, numerous researchers applied geochemical analysis for modern tsunami, such as the 2004 Indian Ocean tsunami (e.g. Szczuciński et al., 2005; Srinivasalu et al., 2008; Raja et al., 2009), the 2009 South Pacific tsunami (Chagué-Goff et al., 2011), the 2010 Chile tsunami (Yoshii et al., 2013; Chagué-Goff et al., 2015), and the 2011 Tohoku-oki tsunami (Goto et al., 2011; Chagué-Goff et al., 2012a, 2012b, 2014; Yoshii et al., 2013).

Water-leachable ion is one of geochemical proxy. Immediately after the 2011 tsunami, high concentrations of water-leachable cations (e.g., Na^{+}, Mg^{2+}, Ca^{2+}, K^{+}) and anions (e.g., Cl^{-}, Br^{-}, SO_4^{2-}) were observed in the area inundated by the 2011 tsunami at Miyagi (Chagué-Goff et al., 2012b; Yoshii et al., 2013) and Fukushima Prefectures (Fujikawa et al., 2011). High concentrations of water-leachable ion were recorded at silty or muddy soil layer underlying thick (ca. >5 cm) sandy tsunami deposit and/or thin (<2 cm) sandy tsunami deposit. The concentrations were decreased with depth, suggesting downward penetration. Similar trend was observed from electrical conductivity (Fujikawa et al., 2011). Therefore, it is highly possible that saltwater flooded together with or after sand deposition penetrates the thick sand layer and reached the soil or concentrated muddy tsunami deposit. Because the finer textured and organic rich soil can hold more water than the sand, many seawater components likely became concentrated in the soil below the surface sand layer. Moreover, Yoshii et al. (2013) reported that the ratios of Na^{+}, Mg^{2+}, Br^{-}, and SO_4^{2-} to Cl^{-} are nearly the same in the tsunami deposits and in the tsunami inundated soil. It indicates that these characteristic of ions contaminated by tsunami inundation do not depend on whether or not tsunami deposits exist.

Chagué-Goff et al. (2012b, 2014) reported about the time variation of the concentration of water-leachable ions. Chagué-Goff et al. (2014) collected samples at the Sendai coastal plain 2, 5, and 11 months after the 2011 tsunami. Sulfate concentrations were even higher in February 2012 than they were in August 2011 in the soil at on site (site WP327 in the work of Chagué-Goff et al., 2014). However, concentrations generally decreased with time, particularly where the tsunami deposits and underlying soil were sandy (sites WP325 and WP326). The reports suggests that the concentration of water-leachable ions could generally decrease over time, most likely because it can easily be diluted by meteoric water such as precipitation and groundwater movement.

Goto et al. (2011) reported that >0.5 cm-thick sandy tsunami deposits were distributed over only 62% of the inundation distance at a shore-perpendicular transect on a coastal plain close to Sendai Airport. The deposit continued as a mud layer to the inundation limit, and they found these mud deposit contained high concentrations of water-leachable chloride. It suggests that geochemical analysis may be useful to estimate tsunami inundation area correctly.

Recently, biomarkers have just started to be utilized for tsunami research. Biomarkers are molecular fossil originating from living organisms. In general, biomarkers are used to reconstruct paleoenvironments and paleoclimates in geosciences (e.g. Brassell, 1993; Ohkouchi et al., 1997; Eglinton and Eglinton, 2008). Biomarkers have two advantages. One is their highly preservation potential. They have been confirmed to be stable on a geological time scale. For example, Abelson (1954) found that amino acids had been preserved in fossil shells for 360 million years. Another is the difference between terrigenous and marine biomarkers. For example, lower *n*-alkane homologs, notably C_{15}, C_{17}, and C_{19} *n*-alkanes, tend to be predominant in many algae, whereas higher *n*-alkane homologs, such as C_{27}, C_{29}, and C_{31}, tend to be predominant in leaf waxes of higher plants (Peters et al., 2007c). By using this characteristic, the variability of terrigenous organic carbon input by rivers into the ocean has been reconstructed by examining variations in long-chain *n*-alkanes in marine sediments (e.g. Yamamoto and Polyak, 2009). In that case, a terrestrial event was reconstructed from marine sediment by using biomarkers; in the study of tsunami research, it is proposed the opposite: that is, to attempt to reconstruct a marine event from terrestrial sediments by using biomarkers.

Alpar et al. (2012) firstly applied biomarkers to identify paleotsunami event using samples collected at southwest Turkey. They measured normal and branched alkanes, fatty acids, and sterols in three sand layers and two mud layers. They reported that marine-sourced biomarkers were present in at least one of the sand layers and concluded that this sand layer was most likely a tsunami deposit. However, marine-sourced biomarkers were not detected in the other two sand layers. Ünlü et al. (2012) conducted a biomarker analysis of semi-dry lagoon sediments in southwest Turkey. They reported that it was difficult to identify possible tsunami deposits from biochemical data. However, the results indicate some influxes of marine water in a freshwater environment. They reported characteristics of biomarker from event deposit, however, there is no report applying biomarker analysis for modern tsunami.

1.3 Objective and the organization of this thesis

To verify how and what kind of geochemical proxies are transported and preserved at coastal area by tsunami, geochemical analyses, especially water-leachable ions and biomarkers, were conducted for the samples of the 2011 Tohoku-oki tsunami deposit and underlying and overlying soil. Samples were collected at four sites (Sendai, Odaka, Hasunuma, and Yamamoto) where is affected by the tsunami. The reason why samples were collected at several site is to eliminate local effect. Moreover, samples were collected more than 2 years after the tsunami at Sendai and Odaka to confirm the preservation potential of geochemical characteristics. In Hasunuma, samples were collected in both 2011 (June or August) and October 2014 to discuss the time variation of geochemical characteristics. In Yamamoto, I firstly thought to verify what kind of geochemical characteristics were preserved for lake bottom. However, it seems that the lake at Yamamoto seems to be caught a severe lake bottom erosion and reworking from the comparison of lake bottom sediment between before and after the tsunami. Therefore, I mainly discussed about erosion and reworking from lake bottom sediment collected at Yamamoto.

This thesis is divided into 6 chapters: Chapter 1 gave introduction. Chapter 2 gave a description of the study area. Chapter 3 showed the methods of each analytical procedure. Chapter 4 showed the

results in each study area. Chapter 5 showed a discussion of behavior of geochemical characteristics and erosive action by the tsunami. Finally, chapter 6 summarized general conclusions. Parts of this doctoral thesis have published or submitted to the peer-reviewed journals (Shinozaki et al., 2015a, 2015b, submitted).

Chapter 2. Geological setting

2.1 Outline of study area

Study area was set up at four sites where is affected by the 2011 Tohoku-oki tsunami (Fig. 2-1). Samples were collected at three coastal lands (Sendai, Odaka, and Hasunuma) and one lake (Yamamoto) (Fig. 2-1). Study area, sample name, and sample collection date were summarized in Table 2-1.

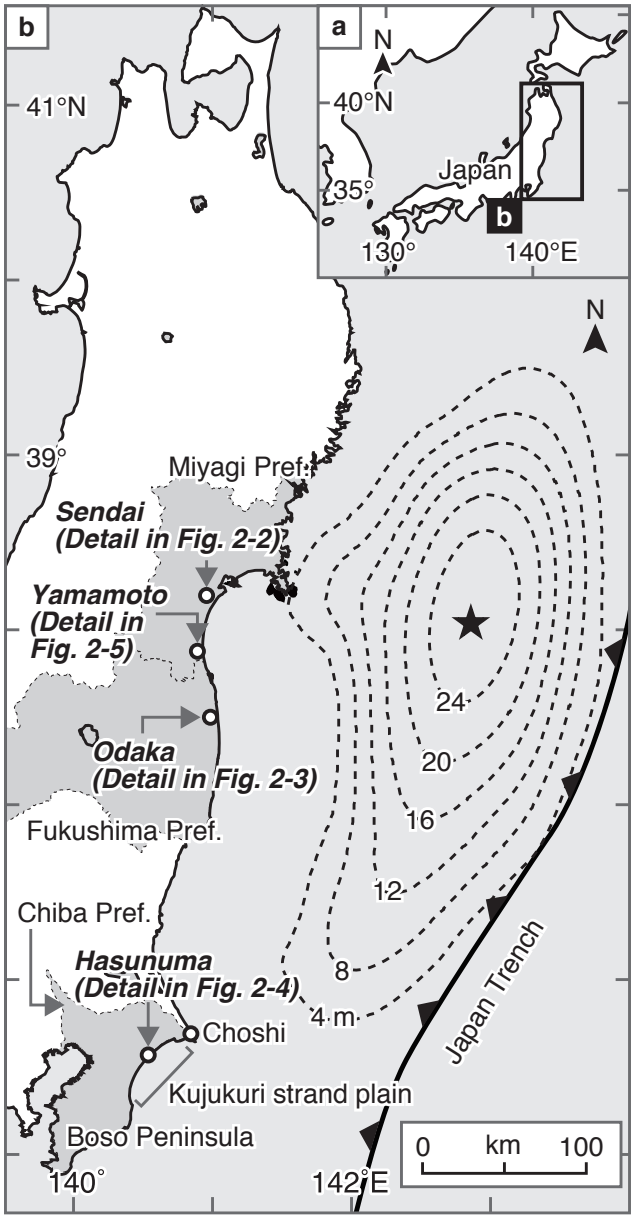

Fig. 2-1. Location maps. (a) Map of Japan. (b) Eastern Honshu; the epicenter of the main shock of the 2011 magnitude-9 Tohoku-oki earthquake (black star) and the coseismic slip distribution (dashed lines) are shown (Ozawa et al. 2011).

Table 2-1. Study area and collected sample name and date.

Study area	Sample name	Sample collected date
Sendai	SND-14	March 2013
Sendai	B-18	June 2011
Odaka	ODA-2	October 2013
Hasunuma	A5, A10, A13	August 2011, October 2014
Hasunuma	C1, C7, C10	June 2011, October 2014
Yamamoto	Slice 1–6	April 2014

2.2 Study area

2.2.1 Sendai

The Sendai Plain is alluvial lowland characterized by beach ridges formed parallel to the coast, natural levees, and back marshes (Fig. 2-2). The area has experienced several tsunami disasters before, with evidence of them preserved as sandy tsunami deposits (Abe et al., 1990; Minoura and Nakaya, 1991; Minoura et al., 2001; Sawai et al., 2008, 2012, 2015a).

The 2011 tsunami caused inundation to a distance of about 3.5–5.0 km inland around the study area (Geospatial Information Authority of Japan) (Fig. 2-2). The inundation height that is the tsunami vertical height above sea level was about 3.0–9.8 m around the study area (The 2011 Tohoku Earthquake Tsunami Joint Survey Group, 2011) (Fig. 2-2). Very coarse to medium sand was mainly transported from beach and dune sand (Szczuciński et al., 2012; Putra et al., 2013), and they covered rice paddies (Abe et al., 2012; Goto et al., 2012a). The more than 0.5 cm thick sand layer extended to 57–76% of the inundation distance where the tsunami inundated more than 2.5 km inland (Abe et al., 2012).

A 1.3-m-long sediment sample (SND-14) collected in March 2013 by the Geological Survey of Japan was used for analysis and discussion (Fig. 2-2 and Table 2-1). The sampling location was about 1.6 km inland from the shoreline and 0.2 m above sea level (Fig. 2-2). Before the tsunami, this site had been used as a rice paddy field, but after the tsunami it was still uncultivated in March 2013 when the sample was collected. In addition to the SND-14 samples, samples of sandy tsunami deposits and the overlying tsunamigenic mud deposit collected in June 2011 by Abe et al. (2012) was used for analysis and discussion (Transect B-18 in the work of Abe et al., 2012; Fig. 2-2 and Table 2-1). The sampling point of B-18 was about 1.7 km inland from the shoreline and about 2.1 km northeast of SND-14 (Fig. 2-2). These samples were also analyzed to examine when the geochemical characteristics had deposited.

2.2.2 Odaka

Odaka, Minamisoma city, Fukushima Prefecture, is located about 75 km south of Sendai (Fig. 2-1b). The lowland areas (<10 m a.s.l.) are surrounded by hills about 50 m high (Fig. 2-3). This area was also studied about historical and prehistric tsunami deposit (Sawai et al., 2012).

The 2011 tsunami caused inundation to a distance of about 2.6 km inland around the wide valley of study area (Geospatial Information Authority of Japan) (Fig. 2-3). The inundation heights around the study area were about 4.9–12.5 m (The 2011 Tohoku Earthquake Tsunami Joint Survey Group, 2011) (Fig. 2-3).

A 1.5-m-long sample (ODA-2) was obtained in October 2013 (Fig. 2-3 and Table 2-1). The sampling location was about 1.8 km inland and 1.1 m above sea level (Fig. 2-3). The location had been used for rice paddies before the tsunami, but after the tsunami it was still uncultivated in October 2013 when sample was collected.

2.2.3 Hasunuma

The Kujukuri strand plain is located on the eastern side of the Boso Peninsula, southern East Japan (Fig. 2-1b). The straight to slightly arcuate shoreline of the strand plain extends 60 km in a NE-SW direction. Hasunuma, Sanmu city, Chiba Prefecture, is located midway along this stretch of shoreline (Fig. 2-1b). Hasunuma area has a sandy beach (150–200 m wide), a foredune ridges (500–1000 m wide, up to 5 m in elevation), and an inter-ridge swale (Tamura et al., 2010).

Tide-gauge data recorded during the 2011 tsunami at Choshi, about 35 km northeast of Hasunuma, show that sea level began to rise 24 minutes after the main shock (Japan Meteorological Agency). It reached a first peak within 30 minutes. After that, sea-level repeatedly rose and fell. These data are consistent with both a video taken during the tsunami and an eyewitness account at Hasunuma. The second wave was higher than the first wave and inundated a greater area (Okazaki and Ohki, 2012). The 2011 tsunami caused inundation to a distance of about 1 km inland around Hasunuma (Geospatial Information Authority of Japan). The inundation height was about 2.3 m around sampling locations (The 2011 Tohoku Earthquake Tsunami Joint Survey Group, 2011).

Samples were collected at six locations (A5, A10, A13, C1, C7 and C10) from two transects (Transect A and C) in both 2011 (June or August) and October 2014 (Figs. 2-4 and Table 2-1). Sediment samples of 2011 analyzed in this study were provided from a part of sample collected in urgent survey conducted by the Geological Survey of Japan. The names of sampling locations agree with those presented by Matsumoto et al. (submitted). The study area is separated from the sea by a foredune and is dominanted by coniferous trees (*Pinus*) (Fig. 2-4a).

2.2.4 Yamamoto

Suijin-numa, a small coastal lake (about 200 × 100 m, 2.6 m maximum water depth), is located in Yamamoto town, southern edge of the Sendai Plain (Fig. 2-1b). The lake is situated about 600 m inland from the shoreline (Fig. 2-5a). The lake does not receive major river input but it does have narrow drainage (Fig. 2-5a and 2-5b). Lowland areas around the lake (about 2 m a.s.l.) are surrounded by hills, about 30 m high, of Pliocene sandstone (Fig. 2-5a).

Before the 2011 tsunami, Sawai et al. (2008) conducted paleotsunami research using lake bottom sediments at five locations. From the 1.5–2.0-m-long sediment samples, they found the 915 Towada-a (To-a) tephra layer, and two sand units that were formed by the historically documented 1611 Keicho and the 869 Jogan tsunamis. *Suijin-numa* was in a marine condition and became isolated from the sea by a beach-ridge plain between 3200 and 1100 cal yr BP (Sawai et al., 2008). Then peat was deposited. It contains more mud above the 1611 Keicho tsunami sand (Sawai et al., 2008). Thick peat and mud (ca. 60–180 cm thick) have been deposited continuously above the To-a layer.

About three years after the report of Sawai et al. (2008), the 2011 tsunami struck this area. Approximately 20–30 cm subsidence around this area was reported by the Geospatial Information Authority of Japan. The tsunami inundated about 1.9 km inland in this narrow valley (Geospatial Information Authority of Japan) (Fig. 2-5a). The inundation and run-up heights, the tsunami vertical height above sea level at the furthest point inland, were, respectively, up to 13.8 m and 9.8 m around this valley (The 2011 Tohoku Earthquake Tsunami Joint Survey Group, 2011) (Fig. 2-5b). Sandy and muddy tsunami deposits of ca. 30 cm thickness were formed over the valley floor (Abe et al., 2014;

Goto et al., 2014), which had been used mainly as a residential area along the coast and paddy fields. Immediately after the 2011 event, the lake water was pumped out. Then heavy machinery was moved onto the lake floor to remove rubble and to search for missing persons. However, according to a local administrator, the work was done in a limited area around the northeastern edge of the lake (Fig. 2-5b) because thick and very soft mud covered the central to west side of the lake, preventing machinery from reaching the area. Lake water naturally returned via the precipitation and ground water.

In April 2014, total six lake bottom sediments (Slice 1–6) were collected at four locations near the sampling locations used by Sawai et al. (2008) (Fig. 2-5b and Table 2-1). The sampling locations did not overlap the area where heavy machinery accessed.

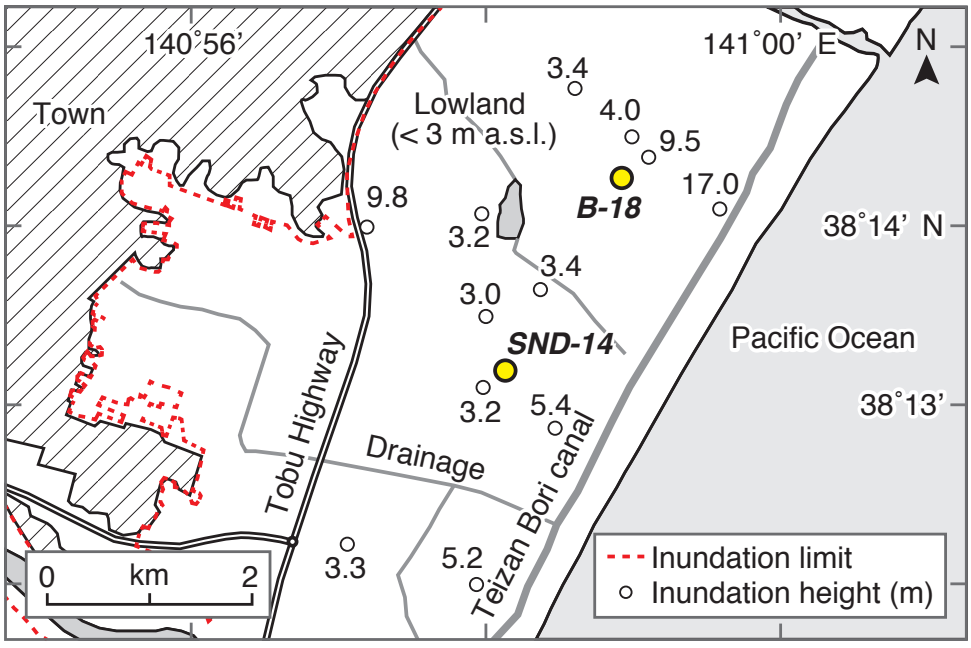

Fig. 2-2. Sendai study area. The study area has extensive flat lowlands (<3 m a.s.l.). The yellow circles show the sampling locations. The red dashed lines show the inundation limits of the 2011 tsunami, as obtained from the Geospatial Information Authority of Japan. Inundation height is the tsunami vertical height above sea level at an arbitrary point. The inundation height (m) is from The 2011 Tohoku Earthquake Tsunami Joint Survey Group (2011). Distance above sea level is expressed in meter units as m a.s.l.

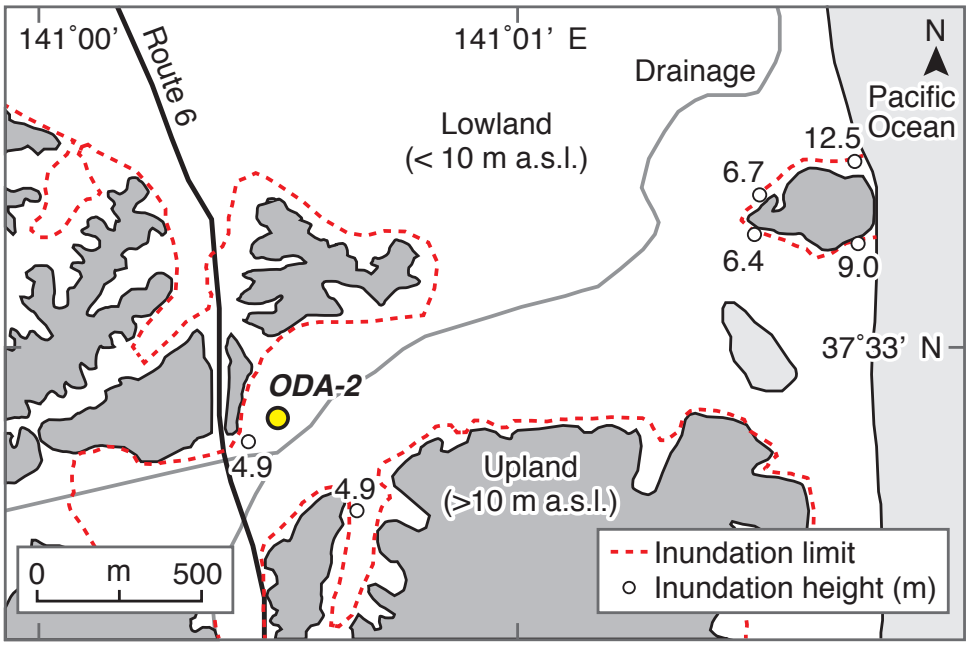

Fig. 2-3. Odaka study area. The yellow circle shows the sampling location. The red dashed lines show the inundation limits of the 2011 tsunami, as obtained from the Geospatial Information Authority of Japan. The inundation height (m) is from The 2011 Tohoku Earthquake Tsunami Joint Survey Group (2011). Distance above sea level is expressed in meter units as m a.s.l.

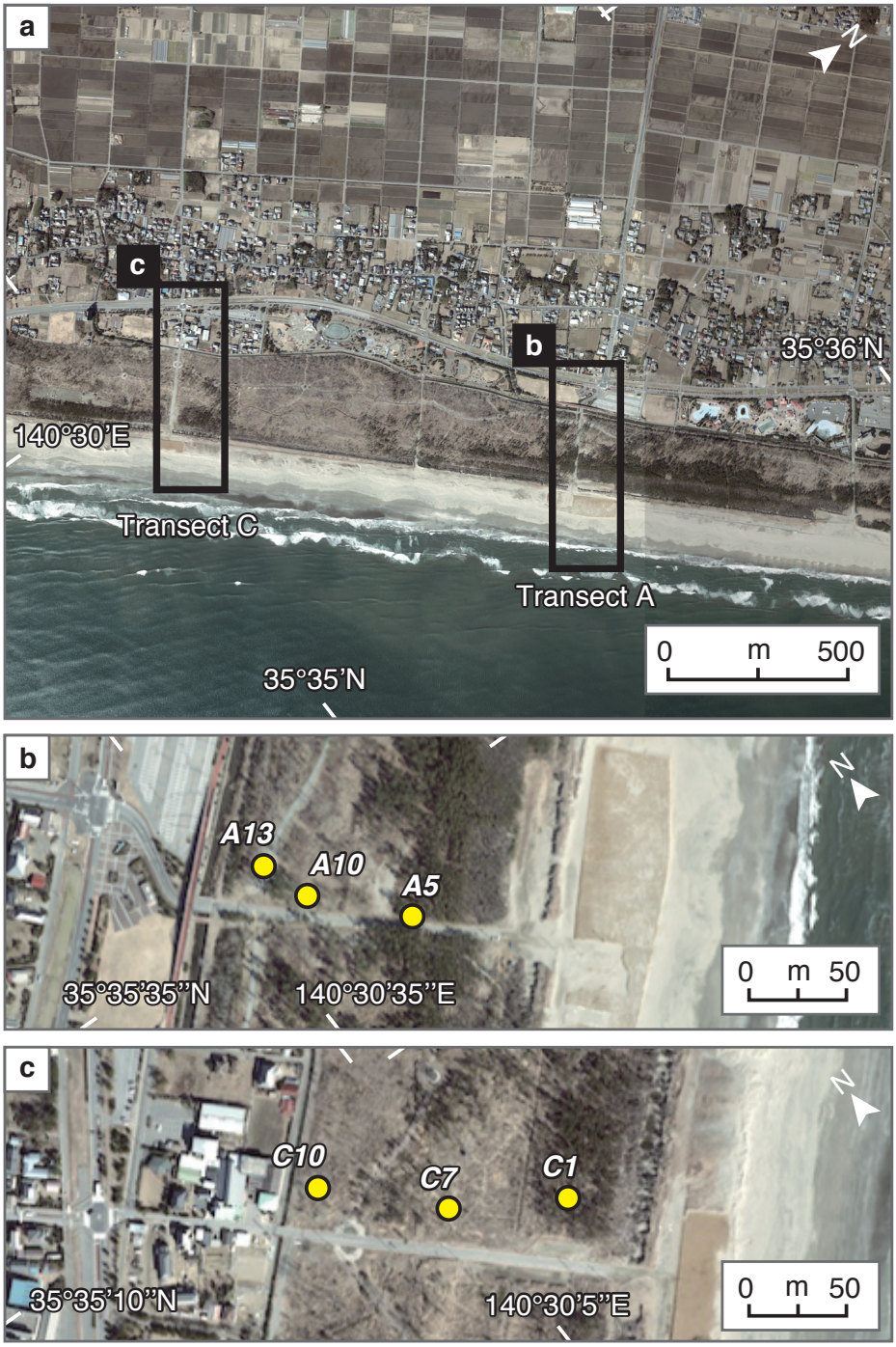

Fig. 2-4. Hasunuma study area. (a) Aerial photograph of the Hasunuma site (Geospatial Information Authority of Japan: CKT-2011-4-C27-1, 2). (b, c) Aerial photographs of the area around transects A and C showing the sampling locations (yellow circles). All photographs were taken on 11 February 2012.

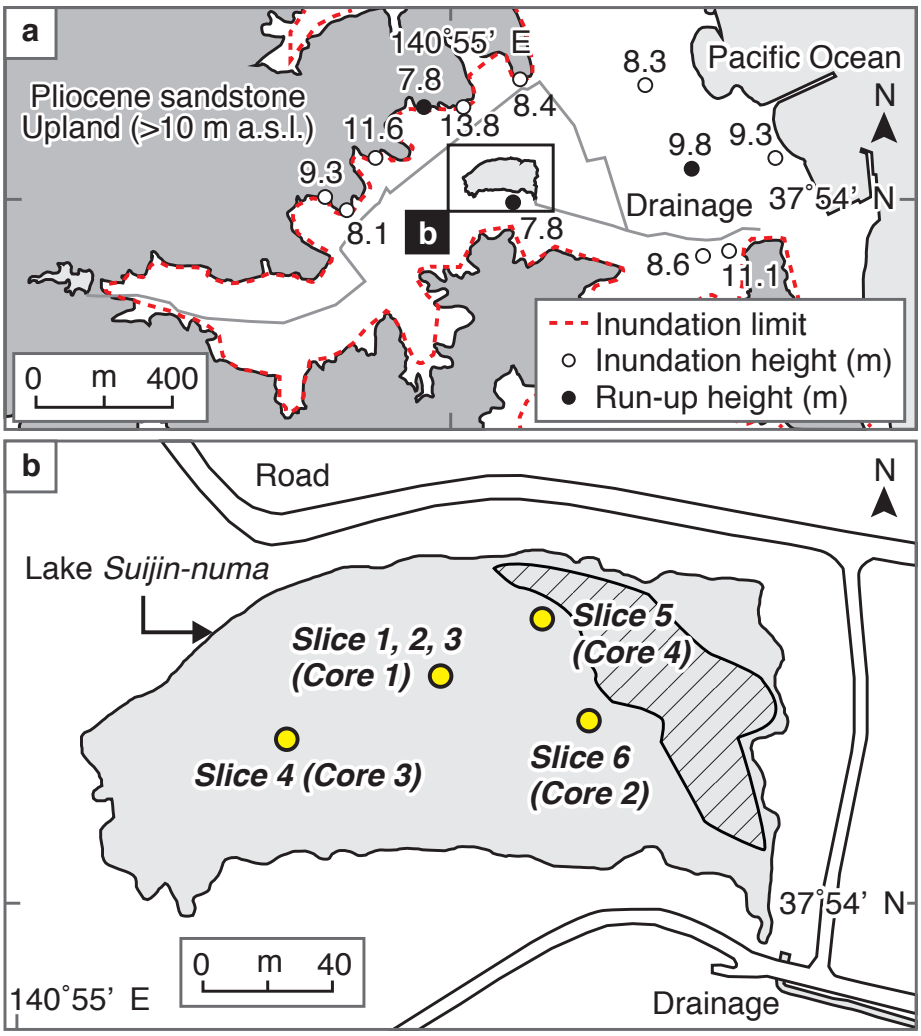

Fig. 2-5. Yamamoto study area. (a) The inundation limit is from the Geospatial Information Authority of Japan. Run-up height is the tsunami vertical height above sea level at the furthest point inland. The inundation and run-up heights (m) are from The 2011 Tohoku Earthquake Tsunami Joint Survey Group (2011). Distance above sea level is expressed in meter units as m a.s.l. (b) Six sediment samples were collected at four locations (yellow circles). Names of sample locations collected by Sawai et al. (2008) are written in parentheses. Heavy machinery that accessed the northeastern edge of the lake is shown as a shaded area.

Chapter 3. General methods

3.1 Sample collection and analytical procedures

Sediment samples were collected using handy geoslicer, consisting of a sample tray and a shutter plate (Fig. 3-1: Nakata and Shimazaki, 1997; Takada et al., 2002), or directly from walls of excavated pits. Collected samples were analyzed after pretreatment (See subsection 3.2.1). Analytical procedures were summarized in Fig. 3-2. Sample collecting methods and conducted analyses in each area were summarized in Table 3-1.

Fig. 3-1. Sample collection. (a) Collection of sediment sample using handy geoslicer. (b) Observation of sediment sample collected by handy geoslicer.

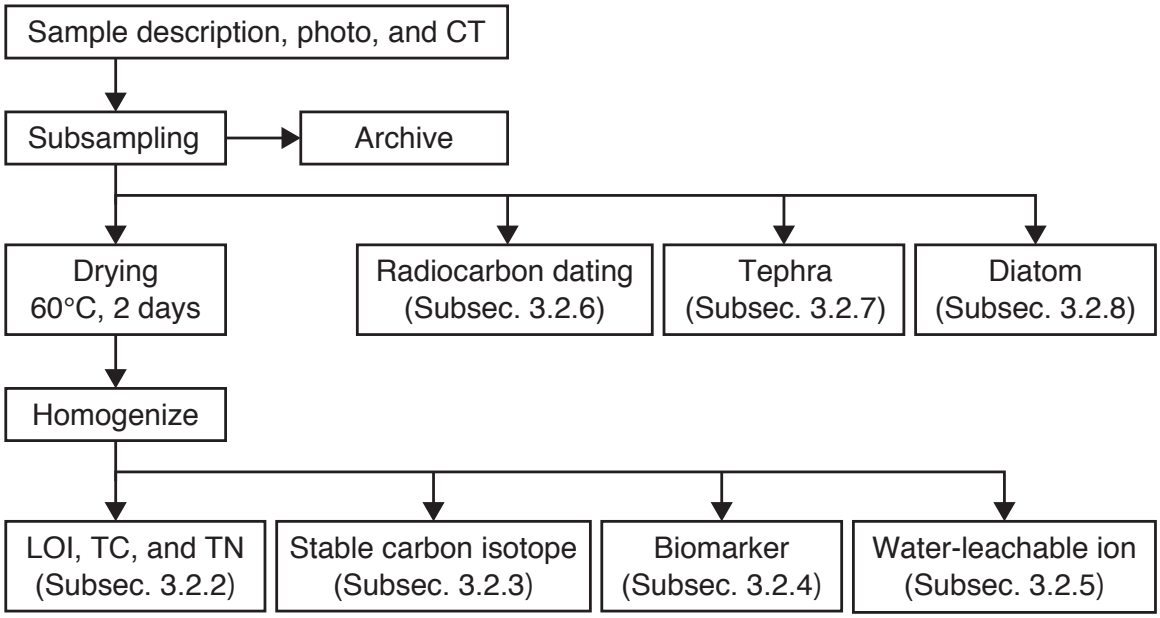

Fig. 3-2. Process flow scheme for sediment treatment.

Table 3-1. List of methods conducted in each study area.

Methods	Sendai	Odaka	Hasunuma	Yamamoto
Sample collection	2-m-long geoslicer	2-m-long geoslicer	1-m-long geoslicer and directly from wall pit	3-m-long geoslicer
Loss on ignition	✔	✔	✔	
Total carbon and Total nitrogen	✔	✔	✔	
$\delta^{13}C$	✔		✔	
Biomarker	✔	✔	✔	
Water-leachable ion			✔	
^{14}C dating				✔
Tephra				✔
Diatom				✔

3.2 Methods

3.2.1 Pretreatment

After sample description, taking photo, and X-ray computed tomography (CT), collected samples were kept at 4°C or –20°C until subsampling. The deposits were subsampled at vertical intervals of 1 or several cm. A part of each subsample was kept for archival purposes, and the remainder was used for analysis. For the analyses of loss on ignition (LOI), total carbon (TC), total nitrogen (TN), stable carbon isotope ratio ($\delta^{13}C$), biomarker, and water-leachable ions, subsamples were dried at 60°C for 2 days. Water content (%) was calculated from the sample weights before and after drying. The dried sample was then homogenized with an agate mortar and pestle. For the analyses of radiocarbon (^{14}C) dating, tephra, and diatom, subsamples were used without drying and homogenizing.

3.2.2 Loss on ignition, total carbon, and total nitrogen

LOI550 and LOI950 are respectively indicators of organic carbon and inorganic carbon (calcite) (Dean, 1974; Santisteban et al. 2004). About 1–2 g homogenized sample was weighed and ashed at 550°C for 4 h. LOI550 was calculated from the sample weights before and after ignition. Then it was further weighed and ashed at 950°C for 2 h. LOI950 was calculated from the sample weights before and after ignition at 950°C.

The homogenized sample was weighed in a tin cup, and TC and TN measurements were performed with an Elemental Analyzer (Flash EA 1112; ThermoFinnigan, Waltham, USA).

3.2.3 Stable carbon isotope ratio

$\delta^{13}C$ was determined for bulk ($\delta^{13}C_{bulk}$) and decalcified ($\delta^{13}C_{org}$) samples. An acid treatment is as follows: The homogenized sample weighed in a silver cup was decalcified with 300 μL of 3 N HCl for 3 days with sodium hydroxide and phosphorus(V) oxide. $\delta^{13}C$ was measured with an EA/IRMS (FlashEA 1112/DeltaPlus Advantage; Thermo Fisher Scientific). L-Alanine ($\delta^{13}C$ = –19.6±0.2‰; SI Science Co., LTD., Japan) was used as the standard for drift corrections.

3.2.4 Biomarker

Analytical procedure of biomarker analysis is as follows (Fig. 3-3): Lipids were extracted from the homogenized sediment samples to which 5α-cholestane and cholesterol had been added as internal standards. For extraction, an Accelerated Solvent Extractor (ASE200 system, Dionex, Sunnyvale, USA) was used at 100°C and 1000 psi for 15 min with about 40 mL dichloromethane/methanol (95:5). The extract was saponified with 1.0 M KOH/methanol for 2 h at 70°C. The neutral fraction was separated by extraction with hexane/dichloromethane (10:1). Column chromatography (Silica gel 60; Merck, Frankfurt, Germany; 0.040–0.063 mm) was then used to further separate the neutral fraction into four fractions: N1 (hydrocarbons), N2 (aromatic hydrocarbons), N3 (ketones), and N4 (alcohols and sterols). These fractions were separated with 2 mL hexane, 2 mL hexane/dichloromethane (2:1), 3 mL dichloromethane, and 4 mL dichloromethane/methanol (95:5), respectively. N4 fractions were converted to trimethylsilyl ether (TMS-ether) derivatives by using bis(trimethylsilyl)trifluoroacetamide (BSTFA) before analysis.

Gas chromatography with flame ionization detection (GC-FID, Agilent 6890N; Agilent Technologies Inc., USA) was used to analyze each hydrocarbon (N1), ketone (N3), and alcohol and sterol (N4). A Chrompack Capillary Column CP-Sil5CB column (60 m, 0.32 mm internal diameter, Agilent Technologies) was used. The oven temperature was increased from 50 to 120°C at 30 °C/min, and from 120 to 310°C (hold time: 35 min) at 6 °C/min. Each compound was identified by using GC-mass spectrometry (GC-MS, Agilent 5973 Network MSD; Agilent Technologies Inc., USA).

3.2.5 Water-leachable ion

Pretreatment of water-leachable ions was referred as the following methods outlined in Chagué-Goff et al. (2012b) (Fig. 3-4): 30 mL ultrapure water (18.2 MΩ cm) was added to 3 g homogenized sample. It was put on a shaker at 125 rpm for 24 hours. The supernatant was then filtered using a 0.45 μm disposable filter and split for cations and anions analyses. The subsamples for cation analysis (15 mL) were added nitric acid and made a final concentration of 1% volume per volume (v/v) of sample.

Water-leachable cations (Na^+, Mg^{2+}, Ca^{2+}, K^+, Mn^{2+}, and Sr^{2+}) were determined by inductively coupled plasma–atomic emission spectroscopy (ICP-AES, SPS3500DD; Seiko Instruments Inc., Japan), and water-leachable anions (Cl^-, SO_4^{2-}, Br^-, NO_3^-, F^-, and PO_4^{3-}) were determined by ion chromatography (IC-2001; TOSOH CO., Japan).

3.2.6 Radiocarbon dating

Organic sediment that had been passed through a 180-μm sieve or leaf were used for ^{14}C dating. Radiocarbon dating was conducted using accelerator mass spectrometry (AMS) by the Beta Analytic Inc., USA. The measured ^{14}C age was calibrated to calendar age using the IntCal13 calibration curve (Reimer et al., 2013) and software (Calib 7.1). Radiocarbon and calendar ages were expressed respectively as yr BP and cal yr BP.

3.2.7 Tephra

Volcanic glass contents, refractive-index of volcanic glass and orthopyroxene, and glass shard major element compositions were analyzed as tephra analysis by the Institute of Tephrochronology for Nature and History Co. Ltd., Japan. For volcanic glass contents, mud fraction was removed from subsample (6 g) using ultrasonic bath. Sample was dried at 80°C. Tephra particles were picked up under stereomicroscope. They were then filtered range from 1/4 to 1/8 mm or 1/8 to 1/16 mm. 250 particles range from 1/4 to 1/8 mm were counted and then volcanic glass contents, light and heavy minerals were calculated. Refractive-index of volcanic glass and orthopyroxene were measured with a Refractometer (RIM2000; Kyoto Fission-Trach Ltd., Japan). Glass shard major element composition was measured by Electron Probe MicroAnalyser (EPMA) using JXA8600 (JEOL Ltd., Tokyo, Japan).

3.2.8 Diatom

After the subsample was pretreated with 15% H_2O_2, it was mounted on slides with Pleurax medium (Mount Media; Wako Pure Chemical Inds. Ltd., Japan). The prepared slide was examined under a light

microscope at ×1000 magnification with oil immersion. At least 300 diatoms were counted in each sample.

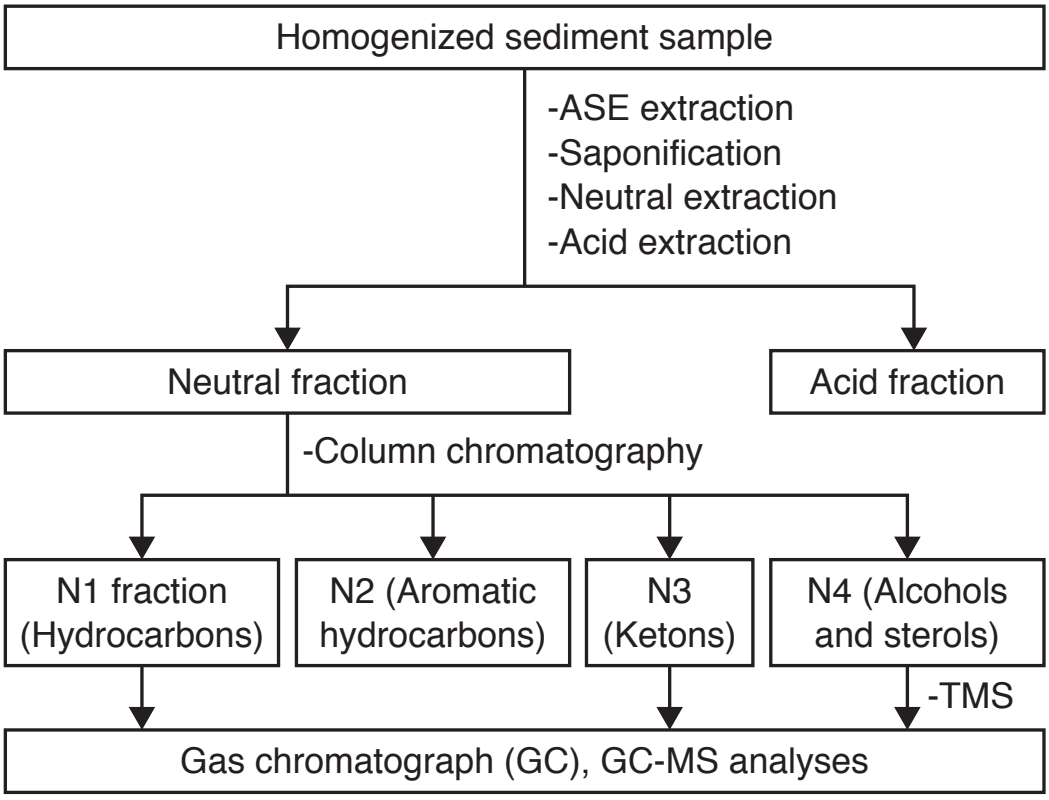

Fig. 3-3. Analytical procedure for biomarker analysis.

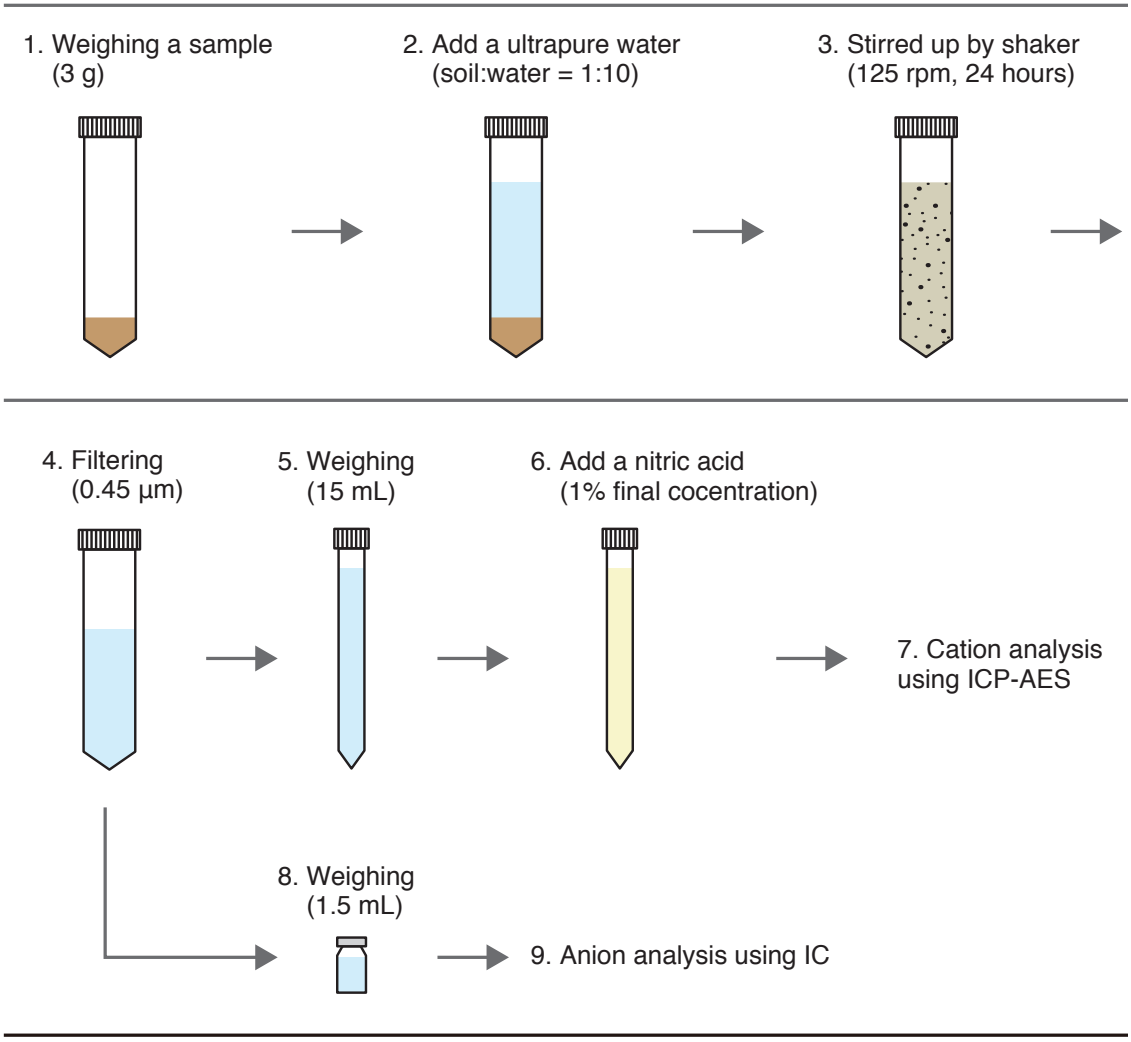

Fig. 3-4. Analytical procedure for water-leachable ions analysis.

Chapter 4. Results

4.1 Sendai

4.1.1 Stratigraphy

The SND-14 sample was collected using a 2-m-long geoslicer by the Geological Survey of Japan. The uppermost 12 cm was used for analysis. A 3-cm-thick fine sand deposit was observed at the top of the SND-14 sample (Fig. 4-1). Rice paddy soil (organic-rich mud) was beneath the sandy deposits. An approximately 2-cm-thick mud overlay was observed 1 month after the tsunami in this area, but it could have been removed by erosion or anthropogenic factors by the time sediment sample was collected 2 years later.

The B-18 sample was collected from walls of excavated pit in June 2011 by the work of Abe et al. (2012). The 2011 tsunami deposit was consisted of upper 1-cm-thick muddy and lower 3 to 5-cm-thick medium sand (Fig. 4-2). The sand contained mud clasts in lower part (Fig. 4-2).

4.1.2 Oraganic and inorganic contents and $\delta^{13}C$

Water content, LOI, TC, and TN were lower at the sand and higher at the soil in SND-14 sample (Fig. 4-1). TC and TN values were relatively low at a depth of 10–11 cm, as compared to those at the other soil depths (Fig. 4-1). The values of $\delta^{13}C$ were heavier in the sand layer (ca. –26‰) and lighter in the soil (–28 to –27‰) (Fig. 4-1). $\delta^{13}C_{bulk}$ and $\delta^{13}C_{org}$ were almost same values at the same layers.

4.1.3 Biomarkers

Biomarkers were measured in one layer in the sand (1–3 cm depth) and seven layers in the soil (3–4, 4–5, 5–6, 6–7, 7–8, 8–9, and 11–12 cm depth) from sample SND-14 (Fig. 4-1). *N*-alkanes occur as major components of the N1 fraction (hydrocarbons). They generally had a distribution with a maximum at C_{29} and other larger peaks at the odd-numbered *n*-alkanes (C_{23}, C_{25}, C_{27}, C_{31}, and C_{33}), whereas lesser peaks occurred at the even-numbered *n*-alkanes (C_{24}, C_{26}, C_{28}, C_{30}, and C_{32}) in every layer (Fig. 4-3a). Short-chain *n*-alkanes (C_{16}, C_{17}, C_{18}, and C_{19}) were observed only at a depth of 5–6

cm (Fig. 4-3b). Alkenones (see subsection 5.2.1), which occur as a component of the N3 fraction (ketones), were not detected in any layer, including at a depth of 5–6 cm. Sterols were observed as a component of the N4 fraction. Cholesterol and phytosterols, such as stigmasterol and *β*-sitosterol, were detected in every layer.

Figure 4-4 shows the hydrocarbon distribution of B-18 sample. Tsunamigenic mud (0–1 cm depth) contained short-chain *n*-alkanes and pristane as well as long-chain *n*-alkanes (Fig. 4-4a). While, there were long-chain *n*-alkanes (C_{21}–C_{33}) in the tsunamigenic sand but no characteristic hydrocarbons such as short-chain *n*-alkanes (Fig. 4-4b).

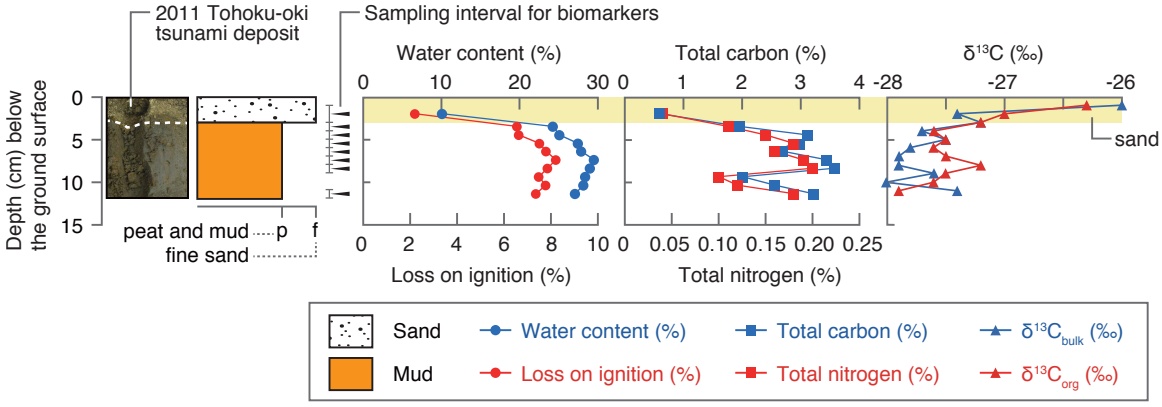

Fig. 4-1. Sediment sample photographs and lithology, depth profile of water content (%), loss on ignition (%), total carbon (%), total nitrogen (%), $\delta^{13}C_{bulk}$ (‰), and $\delta^{13}C_{org}$ (‰) in the SND-14 sample. Yellow band indicates tsunamigenic sand layer. Black arrowheads indicate sampling intervals for biomarkers.

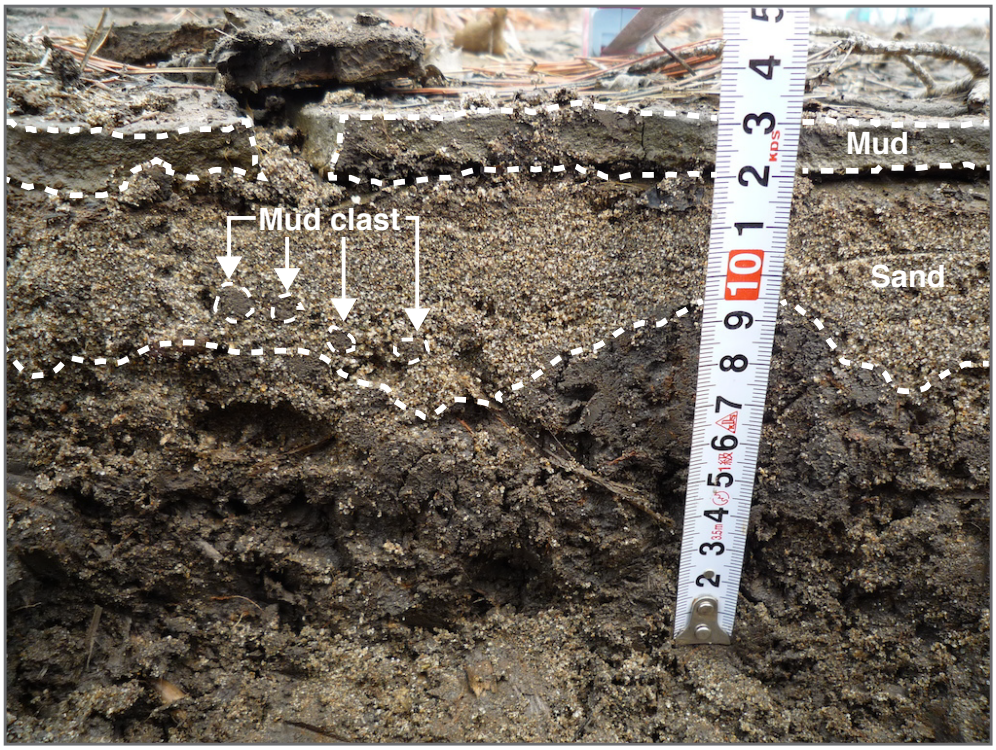

Fig. 4-2. Photograph of B-18 sample. Photo taken by Dr. Tomoya Abe.

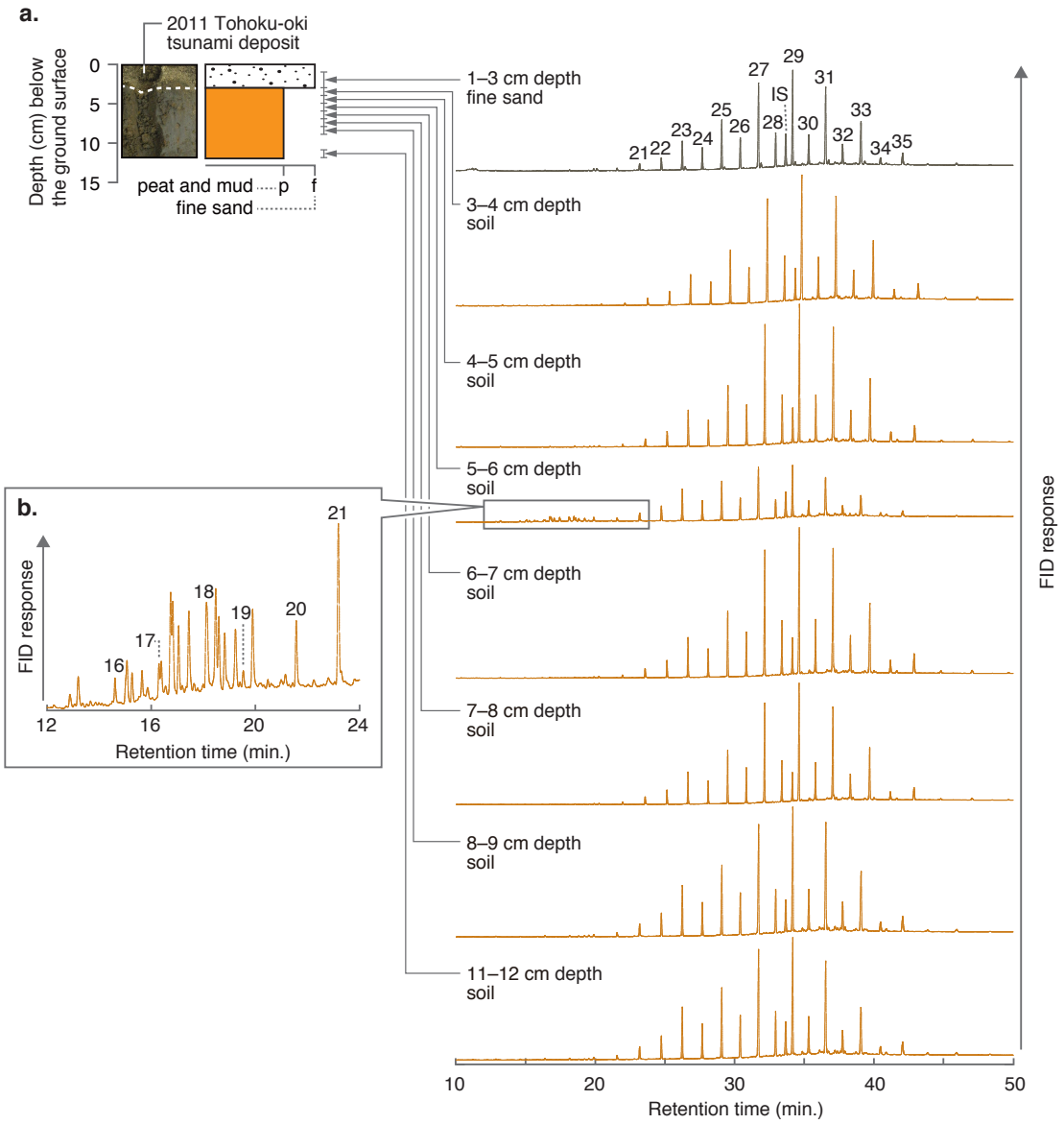

Fig. 4-3. Gas chromatographs of hydrocarbons (N1 fraction) obtained from sample SND-14. (a) Results for the layer at 1–12 cm depth. Gray and orange lines show the results for sand and soil, respectively. Numbers indicate carbon numbers of hydrocarbon, and IS represents the 5α-cholestane internal standards. (b) Expanded detail of the layer at 5–6 cm depth. Flame ionization detector (FID) response is a measure of the intensity of the signal, and retention time is the elapsed time at which the compound was detected.

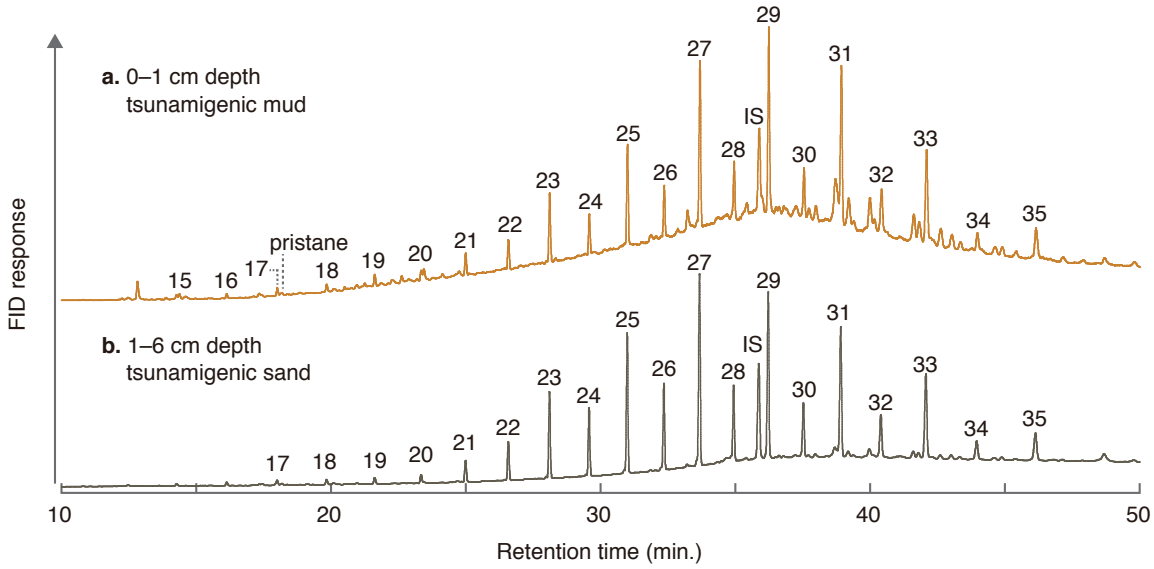

Fig. 4-4. Gas chromatographs of the hydrocarbon fraction obtained from samples at transect B-18: (a) mud and (b) sand. Numbers indicate carbon numbers of hydrocarbon, and IS represents the 5α-cholestane internal standards.

4.2 Odaka

4.2.1 Stratigraphy and organic content

The ODA-2 sample was collected using a 2-m-long geoslicer. The uppermost 35 cm was used for analysis. Sandy deposits were observed at depths of 8–15 and 18–20 cm (Fig. 4-5). A 4-cm-thick massive mud layer (4–8 cm depth) covered the upper sandy deposits. An organic-rich mud deposit was intercalated between the two sand deposits at 15–18 cm depth. The combination of sand and mud between 4 and 20 cm depth must have been deposited by the 2011 tsunami, because sand would not naturally have been present at this location. The uppermost 4 cm of soil appeared to have accumulated naturally after the tsunami.

Water content, LOI, TC, and TN were lower in the sand and they were higher in the mud, especially at depths of 1–8 and 15–18 cm (Fig. 4-5). Upper sand deposit (8–15 cm depth) was organic-poor than lower sand deposit (18–20 cm depth).

4.2.2 Biomarkers

Biomarkers were measured in three layers in the surface soil (1–2, 2–3, and 3–4 cm depth), 16 layers in the 2011 tsunami deposits (at 1-cm intervals from 4 to 20 cm depth), and three layers in the underlying soil (20–21, 21–22, and 22–23 cm depth) (Fig. 4-5). *N*-alkanes had a unimodal distribution with a maximum at C_{29}, with the exception of the layer at 20–21 cm depth (Fig. 4-6). There was a distinct distribution pattern in the 20 to 21 cm depth layer in which short-chain *n*-alkanes (C_{15}, C_{16}, C_{17}, C_{18}, and C_{19}), pristane (2,6,10,14-tetramethylpentadecane, $C_{19}H_{40}$, MW268), and phytane (2,6,10,14-tetramethylhexadecane, $C_{20}H_{42}$, MW282) were detected with a high baseline (Fig. 4-6). No alkenones were observed in any layers. Cholesterol, stigmasterol, and *β*-sitosterol were detected in every layer. In addition to these sterols, dinosterol (see subsection 5.2.1) was confirmed only in the 5 to 6 cm depth tsunamigenic mud layer (Figs. 4-7 and 4-8).

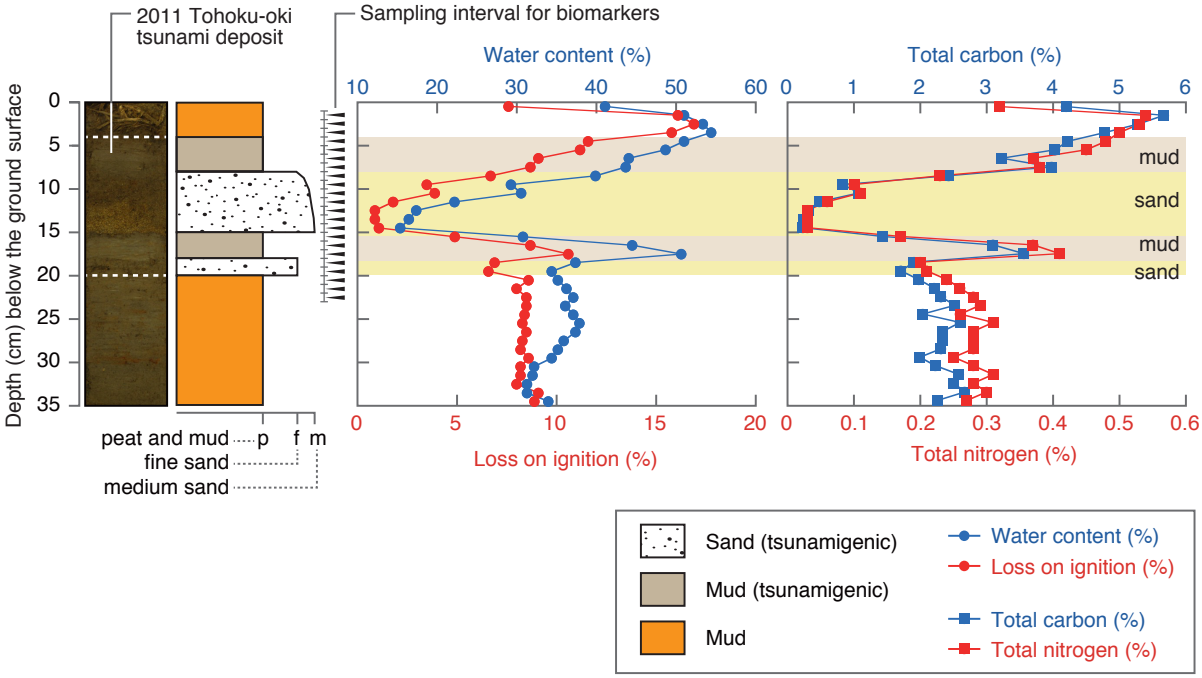

Fig. 4-5. Sediment sample photographs and lithology, depth profile of water content (%), loss on ignition (%), total carbon (%), and total nitrogen (%) in the ODA-2 sample. Yellow and gray bands indicate tsunamigenic sand and mud layers. Black arrowheads indicate sampling intervals for biomarkers.

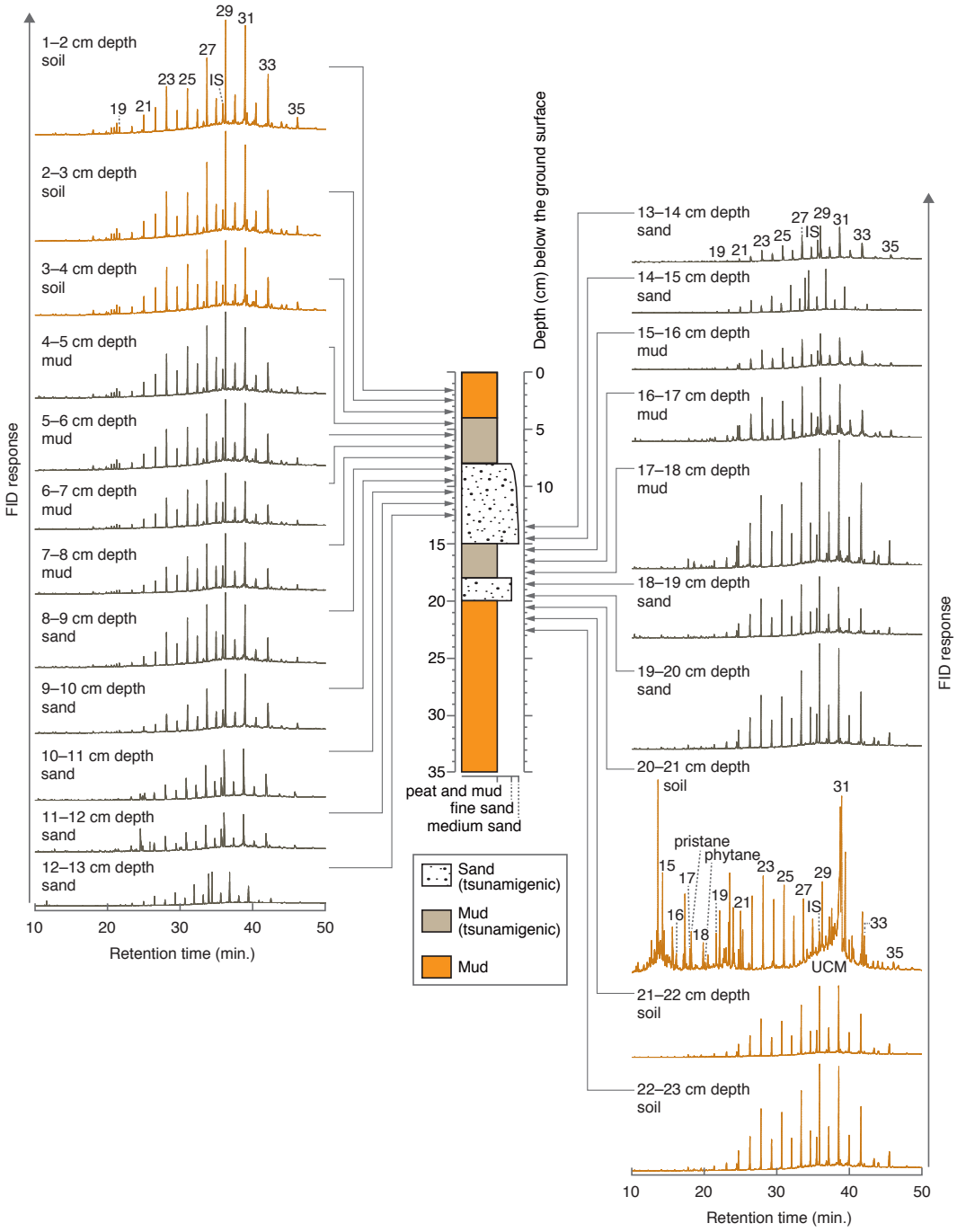

Fig. 4-6. Gas chromatographs of hydrocarbons obtained from sample ODA-2. Gray and orange lines show the results of tsunami deposits and soil, respectively. Numbers indicate carbon numbers of hydrocarbons, and IS represents the 5α-cholestane internal standards. UCM shows the existence of unresolved complex mixture.

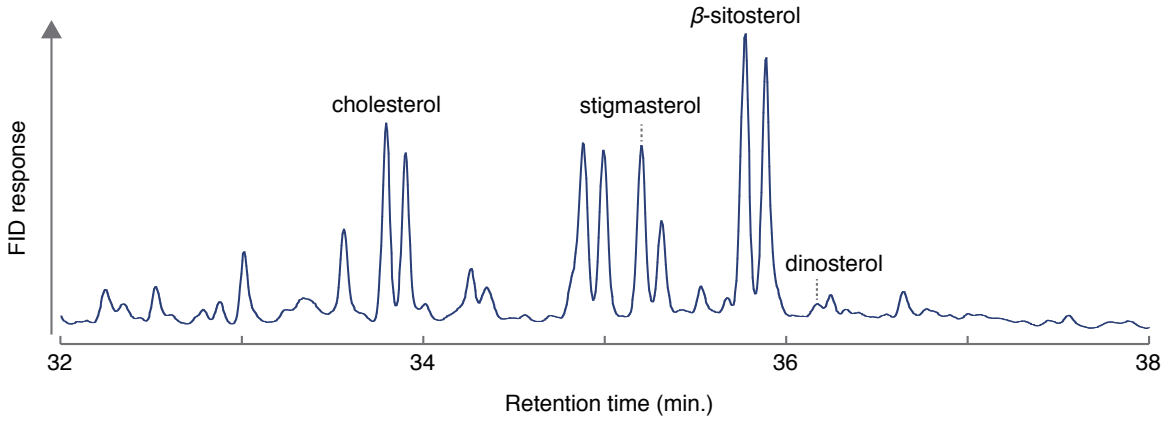

Fig. 4-7. Gas chromatograph results of the N4 fraction from sample ODA-2 at the 5–6 cm depth mud layer.

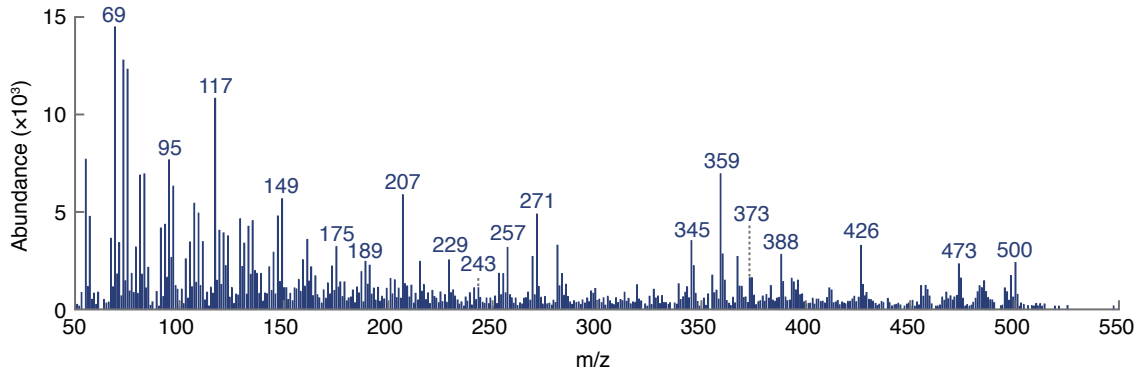

Fig. 4-8. Mass spectrum of dinosterol identified from sample ODA-2 at the 5–6 cm depth mud layer. Numbers are m/z values (mass-to-charge ratios).

4.3 Hasunuma

4.3.1 Stratigraphy

Transect A

In June and August 2011, 13 to 37 cm-long sediment samples were collected directly from wall pits by the Geological Survey of Japan. At location A13, it has collected only sand layer because it reached to the pavement. The tsunami deposit consisted of a very fine to medium sand layer (Fig. 4-9). The sand layer was 31 cm thick at location A5, and it overlaid an organic-rich soil with an erosive boundary. It was 20 cm and 13 cm thick at locations A10 and A13, respectively. Parallel lamination was observed in some parts of sand layer (Fig. 4-9). The sand contained much shell fragments. Mud clasts were observed in the sand at locations A5 and A13.

In 2014, 47 to 50 cm-long sediment samples were collected using 1-m-long geoslicer. The thickness of the sandy tsunami deposit at location A5 had changed from 31 cm to 24 cm (Figs. 4-9). The sand layer was capped by a modern 1–2 cm thick soil (Fig. 4-9). The contact between the sand and the overlying soil was gradual. The sandy tsunami deposit contained many fine roots and shell fragments concentrated layers. Difference of thickness of sand layer between 2011 and 2014 was caused by minor gap (a few meters) of sampling position.

Transect C

In 2011, 18 to 18.5 cm-long sediment samples were collected directly from wall pits by the Geological Survey of Japan. The tsunami deposit along transect C was composed of 12 to 13 cm thick very fine to fine sand (Fig. 4-10). At all three locations, the tsunami deposit overlay an organic-rich soil with an erosive boundary. Parallel lamination was observed in some part of sand layer at locations C7 and C10. Wavy lamination represented ripple cross-lamination was observed at location C7. The sand at location C10 contained plant fragments and shell fragments.

In 2014, 25 to 30 cm-long sediment samples were collected by using 1-m-long geoslicer. the tsunami deposits along transect C were capped by a modern 0.5–2 cm thick deposit (Fig. 4-10). The stratigraphic contact between the sand layer and overlying soil was gradual. The sandy tsunami deposit

contained many fine roots, but it could not be identified shell fragments at any of the three locations. Difference of thickness of sand layer between 2011 and 2014 was caused by minor gap (a few meters) of sampling position.

4.3.2 Organic and inorganic contents and $\delta^{13}C$

Transect A

At locations A5, A10, and A13, water content, LOI550, and TC and TN contents were approximately constant throughout the sand layer (Fig. 4-11). At location A5, they increased in the soil immediately beneath the sand layer and then decreased with depth. Soil was entirely poor in organic matter according to the low LOI550 (3.4–9.4%). LOI950 showed a prominent peak in 16–19 cm depth at location A5. $\delta^{13}C_{bulk}$ was heavier than $\delta^{13}C_{org}$ in the sand layer at every locations, but they were almost same in the underlying soil at location A5.

Transect C

Water content, LOI550, and TC and TN contents were approximately constant throughout the sand layer and relatively high in the soil beneath the sand layer and then decreased with depth (Fig. 4-12). Soil was entirely organic-poor according to the low LOI550 (2.1–14.8%). At location C7, $\delta^{13}C_{bulk}$ was heavier than $\delta^{13}C_{org}$ in the sand layer, but they were almost same in the underlying soil.

4.3.3 Biomarkers

Transect A

At location A5 collected in 2011, biomarkers were measured in three layers in the sand (16–19, 27–29, and 29–31 cm depth) and three layers in the soil (31–33, 33–35, and 35–37 cm depth). No hydrocarbons (N1 fraction) were detected in the sandy tsunami deposit, but long-chain *n*-alkanes (C_{21}–C_{35}) were generally detected in two soil samples (31–33 cm and 33–35 cm depth) (Fig. 4-13). The peaks of odd-numbered *n*-alkanes (C_{21}, C_{23}, C_{25}, C_{27}, C_{29}, C_{31}, C_{33}, and C_{35}) were larger than those of even-numbered *n*-alkanes (C_{22}, C_{24}, C_{26}, C_{28}, C_{30}, C_{32}, and C_{34}). Short-chain *n*-alkanes (C_{15}–C_{19}) were

absent in every layer (Fig. 4-13). Alkenones were not detected in either the tsunami deposit or the soil. Cholesterol and phytosterols such as stigmasterol and *β*-sitosterol were detected in every measuring layer.

At location A5 collected in 2014, biomarkers were measured in one modern soil layer (0–1 cm depth), four layers in the sand (1–3, 9–11, 17–19, and 23–25 cm depth), three layers in the underlying soil (25–27, 27–29, and 29–31 cm depth), and two layers in the bottom sand layers (31–33 and 37–39 cm depth). Long-chain *n*-alkanes (C_{23}–C_{33}) were generally detected, mainly in low concentrations, in soil samples (0–1 cm, 25–27 cm, 27–29 cm, and 29–31 cm depth) and in the sand layers immediately above and below the soil layers (1–3 cm, 23–25 cm, and 31–33 cm depth) (Fig. 4-14). No short-chain *n*-alkanes (C_{15}–C_{19}) or alkenones were detected. Cholesterol and phytosterols were detected in layer that was analyzed.

Transect C

At location C10 collected in 2011, biomarkers were measured in two layers in the sand (6–11 and 12–13 cm depth) and three layers in the soil (13–15, 15–17, and 17–18.5 cm depth). Long-chain *n*-alkanes (C_{29}–C_{33}) were detected only in the soil layer at 15–17 cm depth (Fig. 4-15). The odd-numbered *n*-alkane peaks were larger than the even-numbered peaks. In the sand layer at 6–11 cm depth, the C_{25} peak was highest, and peak height gradually decreased for hydrocarbons with both lower and higher carbon numbers (Fig. 4-15). No alkenones were detected. Cholesterol and phytosterols were detected in layer that was analyzed.

4.3.4 Water-leachable ions

Transect A

In 2011, at location A5, sodium, magnesium, calcium, potassium, and phosphate had little fluctuations in the sand layer, but their concentrations were abruptly increased in the soil immediately below the sand layer and gradually decreased with depth (Figs. 4-16 and 4-17). Bromide showed a similar trend, but it reached a maximum in a further deep soil layer (33–35 cm depth). Fluoride and

chloride contents were slightly higher in the sand layer than in the soil. Sulfate was higher in sand layer than underlying soil, however, it was represented the maximum value at the bottom of sample. Although nitrate was stable in sand layer, it was increased in the bottom of sand and decreased at soil layer. Maximum value of nitrate represents at the bottom of sample. At locations A10 and A13, most water-leachable ions had little fluctuations (Figs. 4-16 and 4-17). Sulfate gradually increased with depth at location A13.

In 2014, sodium was low at every location, but it was higher in the soil than in the sand layer (Fig. 4-16). Magnesium was mainly below the detection limit in the sandy tsunami deposit. Calcium and potassium were low in the sand layer and relatively high in the soil at locations A5 and A10. Calcium in the sand layer at locations A5 and A13 was higher than the sand layer collected in 2011. Water-leachable anions were mainly low in the sand layer at each location, but chloride, sulfate, and nitrate concentrations were relatively high both modern soil and soil just below the sand deposit, especially at locations A5 and A10 (Fig. 4-17). Water-leachable ions at modern soil were higher than or almost same with soil underlying sand layer (Figs. 4-16 and 4-17). It was probably caused by sea spray because sampling locations were up to 350 m away from the coastline.

Transect C

In 2011 along transect C, concentrations of water-leachable cations, sulfate, nitrate, fluoride and phosphate were low in the sand layer (Figs. 4-18 and 4-19). Their concentrations increased in the bottom of sand or soil just below the sand layer, and then they gradually decreased with depth (Figs. 4-18 and 4-19). Chloride was low in both the sand layer and the soil. Bromide was low in the sand layer and high in the soil.

In 2014, water-leachable cations were low in sand layer and they were higher in the soil than in the sand layer (Fig. 4-18). Magnesium was below the detection limit in most sand layer samples. Water-leachable anions were mainly low in the sand layer at every location, but concentrations of chloride, sulfate, nitrate, and phosphate were relatively high both overlying and underlying soil, especially at locations C1 and C7 (Fig. 4-19). Bromide was below the detection limit in most sand

layer. Water-leachable ions were higher at modern soil than sand layer (Figs. 4-18 and 4-19), resulting from sea spray.

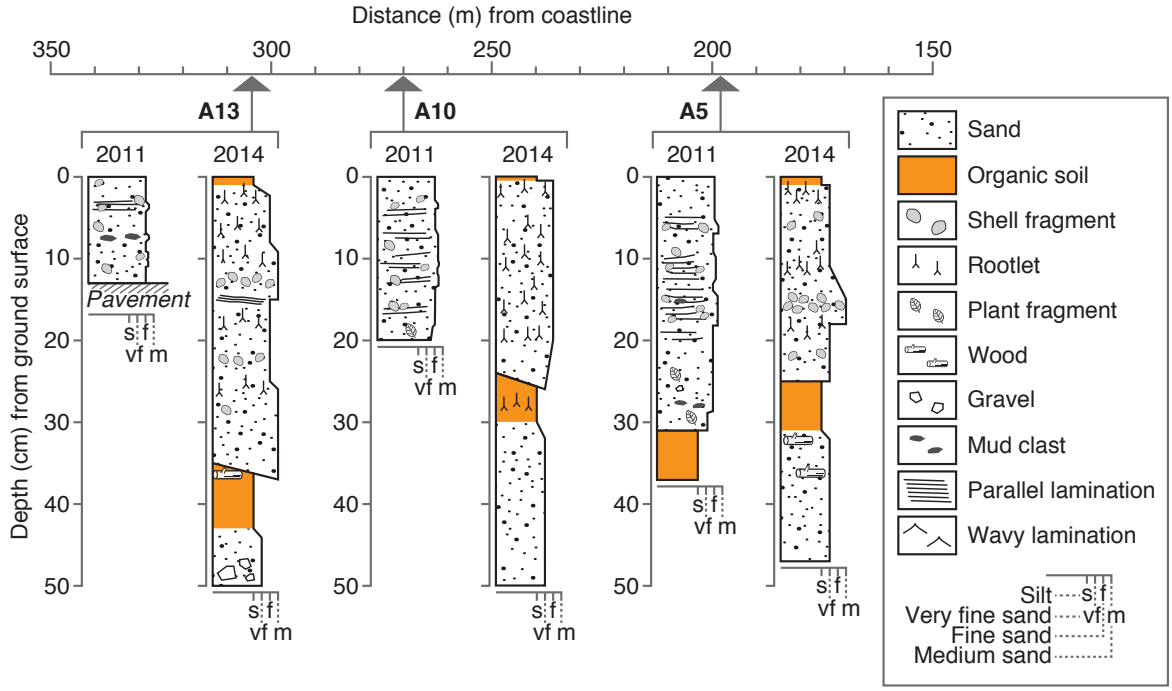

Fig. 4-9. Sediment sample lithology in the transect A at Hasunuma collected in 2011 and 2014. X-axis shows the distance (m) of sampling locations from coastline. At location A10, samples were collected just only from the sand layer in 2011. Sampling reached to pavement at location A13.

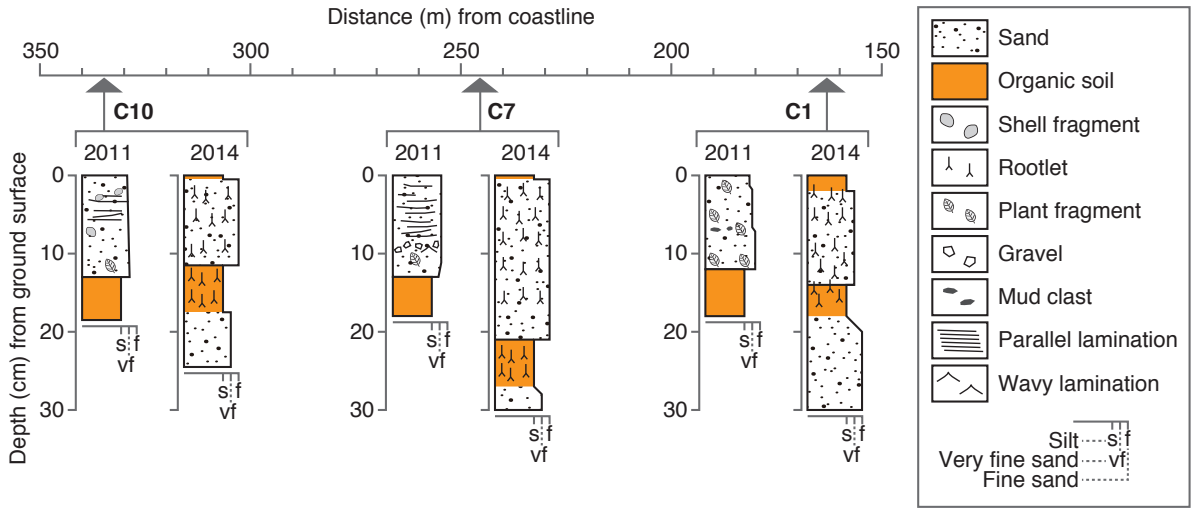

Fig. 4-10. Sediment sample lithology in the transect C at Hasunuma collected in 2011 and 2014. X-axis shows the distance (m) of sampling locations from coastline.

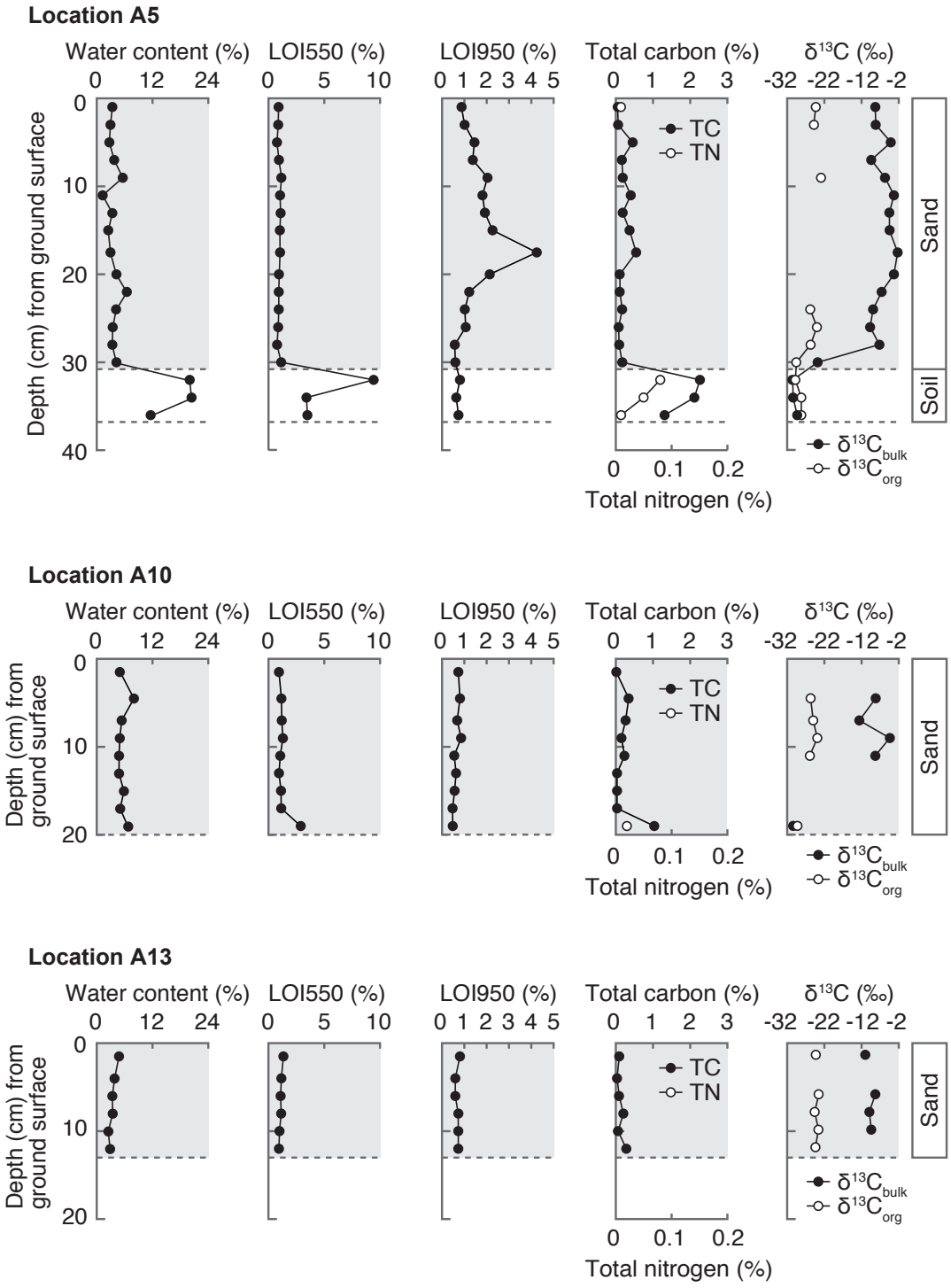

Fig. 4-11. Depth profiles of water content, LOI550, LOI950, total carbon, total nitrogen, $\delta^{13}C_{bulk}$, and $\delta^{13}C_{org}$ along transect A in 2011. Missing data shown in total nitrogen and stable carbon isotope both $\delta^{13}C_{bulk}$ and $\delta^{13}C_{org}$ indicates values below the detection limit.

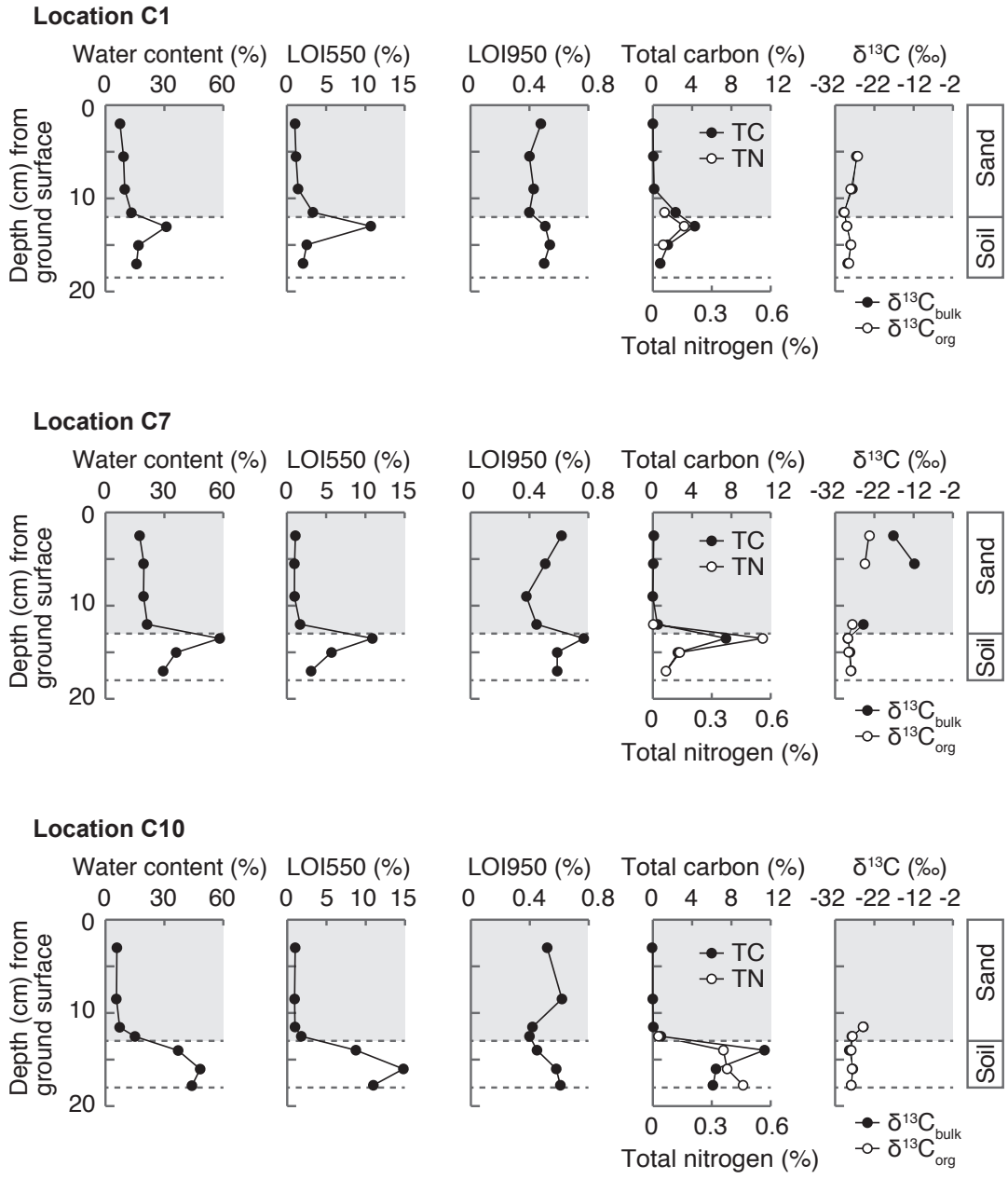

Fig. 4-12. Depth profiles of water content, LOI550, LOI950, total carbon, total nitrogen, $\delta^{13}C_{bulk}$, and $\delta^{13}C_{org}$ along transect C in 2011. Missing data shown in total nitrogen and stable carbon isotope both $\delta^{13}C_{bulk}$ and $\delta^{13}C_{org}$ indicates values below the detection limit.

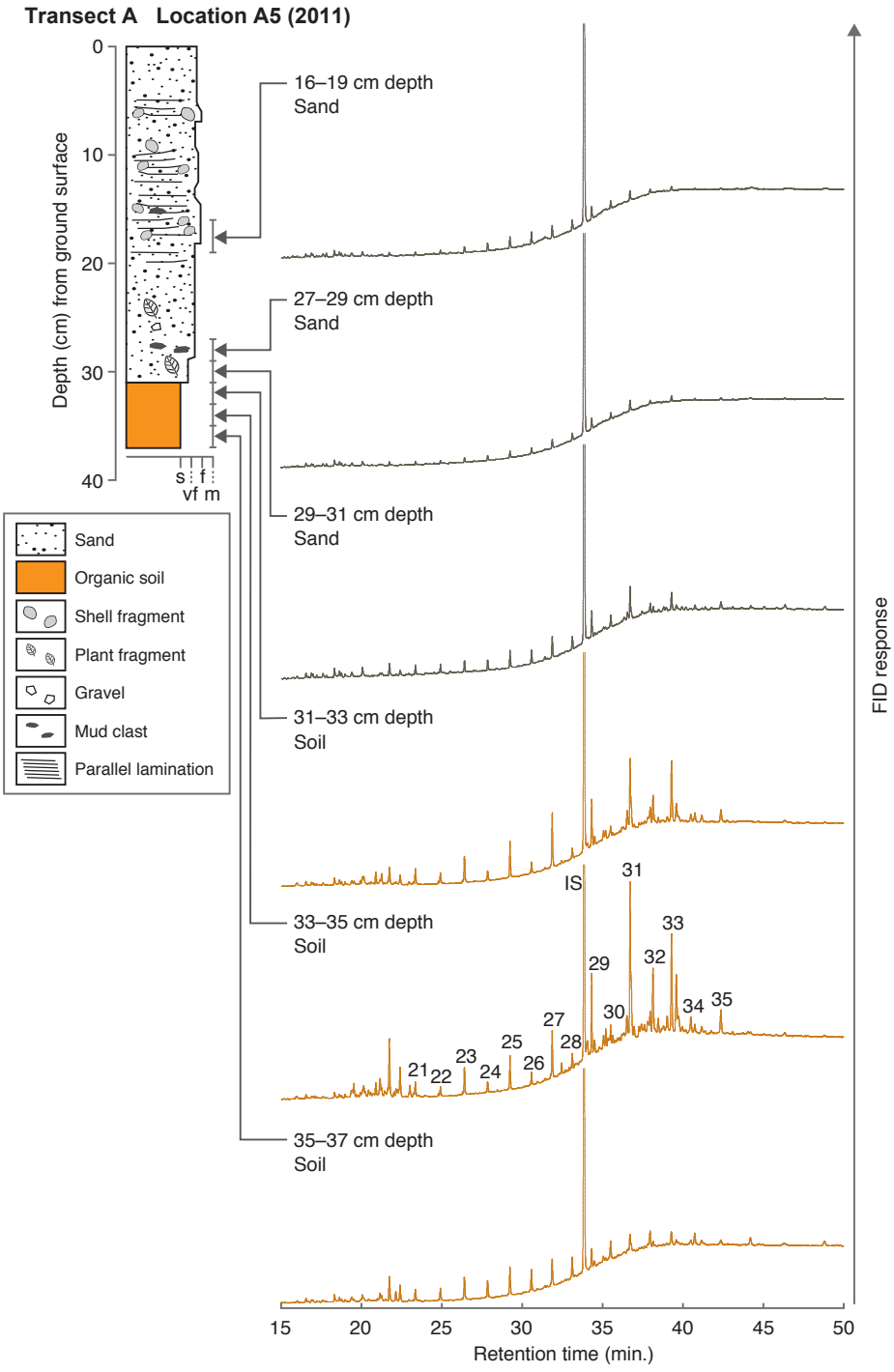

Fig. 4-13. Gas chromatographs of hydrocarbons (N1 fraction) at location A5 in 2011. Black and gray lines of chromatograph show the results of sand and soil, respectively. Numbers indicate carbon numbers of hydrocarbons, and IS is 5α-cholestane, used as an internal standard.

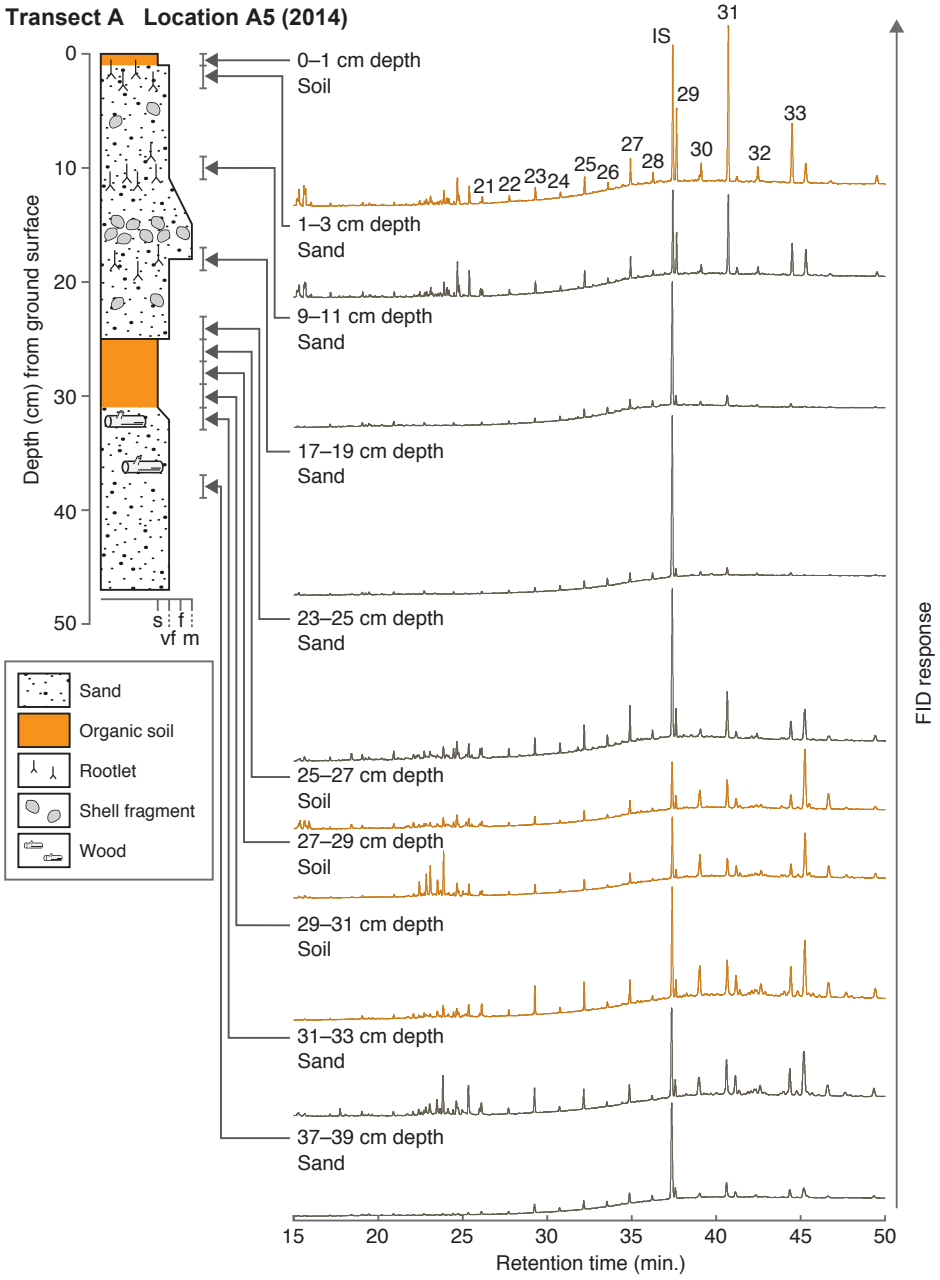

Fig. 4-14. Gas chromatographs of hydrocarbons at location A5 in 2014. Black and gray lines of chromatograph show the results of sand and soil, respectively. Numbers indicate carbon numbers of hydrocarbons, and IS is 5α-cholestane, used as an internal standard.

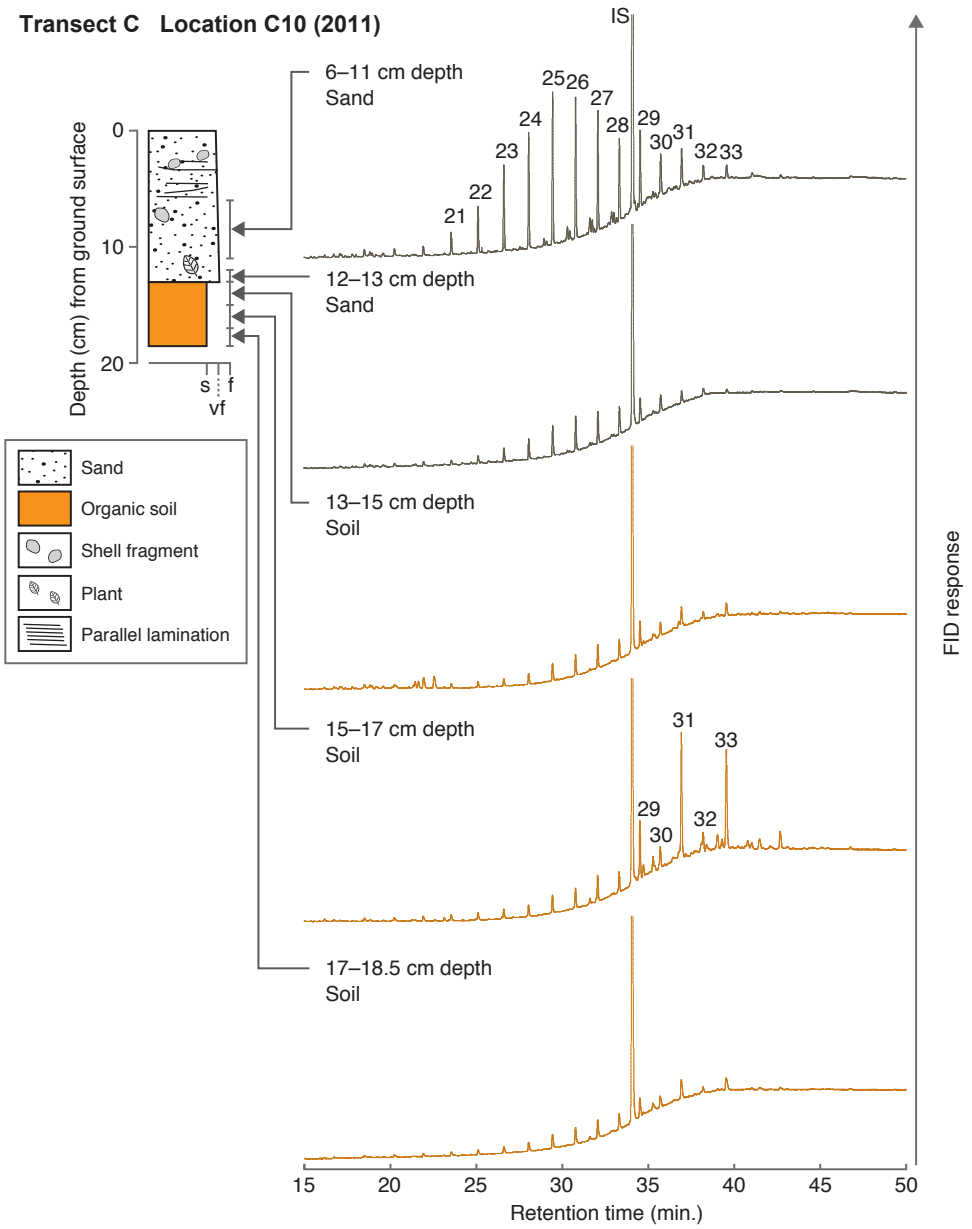

Fig. 4-15. Gas chromatographs of hydrocarbons at location C10 in 2011. Black and gray lines of chromatograph show the results of sand and soil, respectively. Numbers indicate carbon numbers of hydrocarbons, and IS is 5α-cholestane, used as an internal standard.

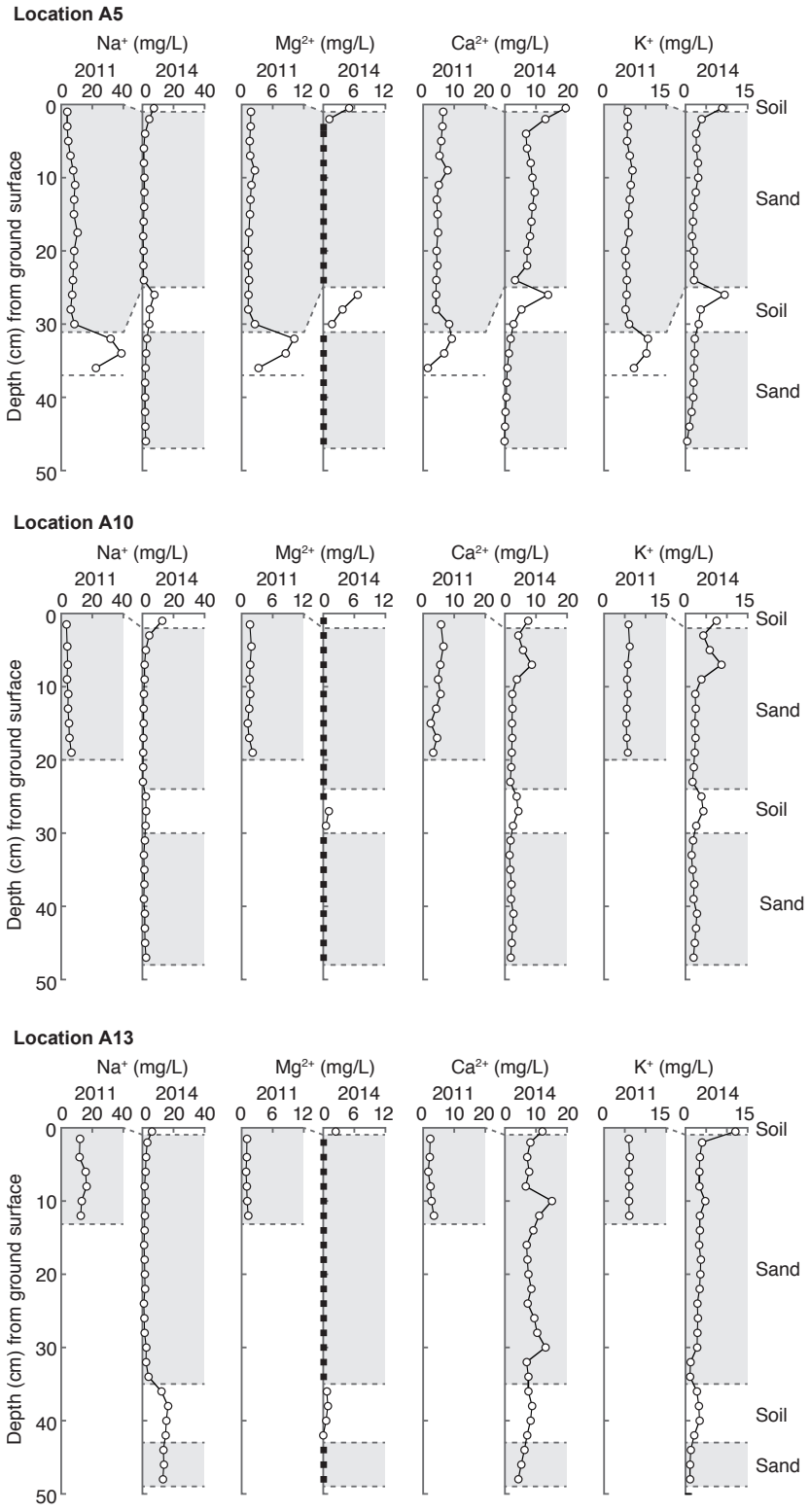

Fig. 4-16. Depth profiles of water-leachable cations (Na^+, Mg^{2+}, Ca^{2+}, and K^+) along transect A in 2011 and 2014. Black squares indicate values below the detection limit. The graphs of manganese and strontium were not posted because they were below the ICP-AES detection limit in every sample.

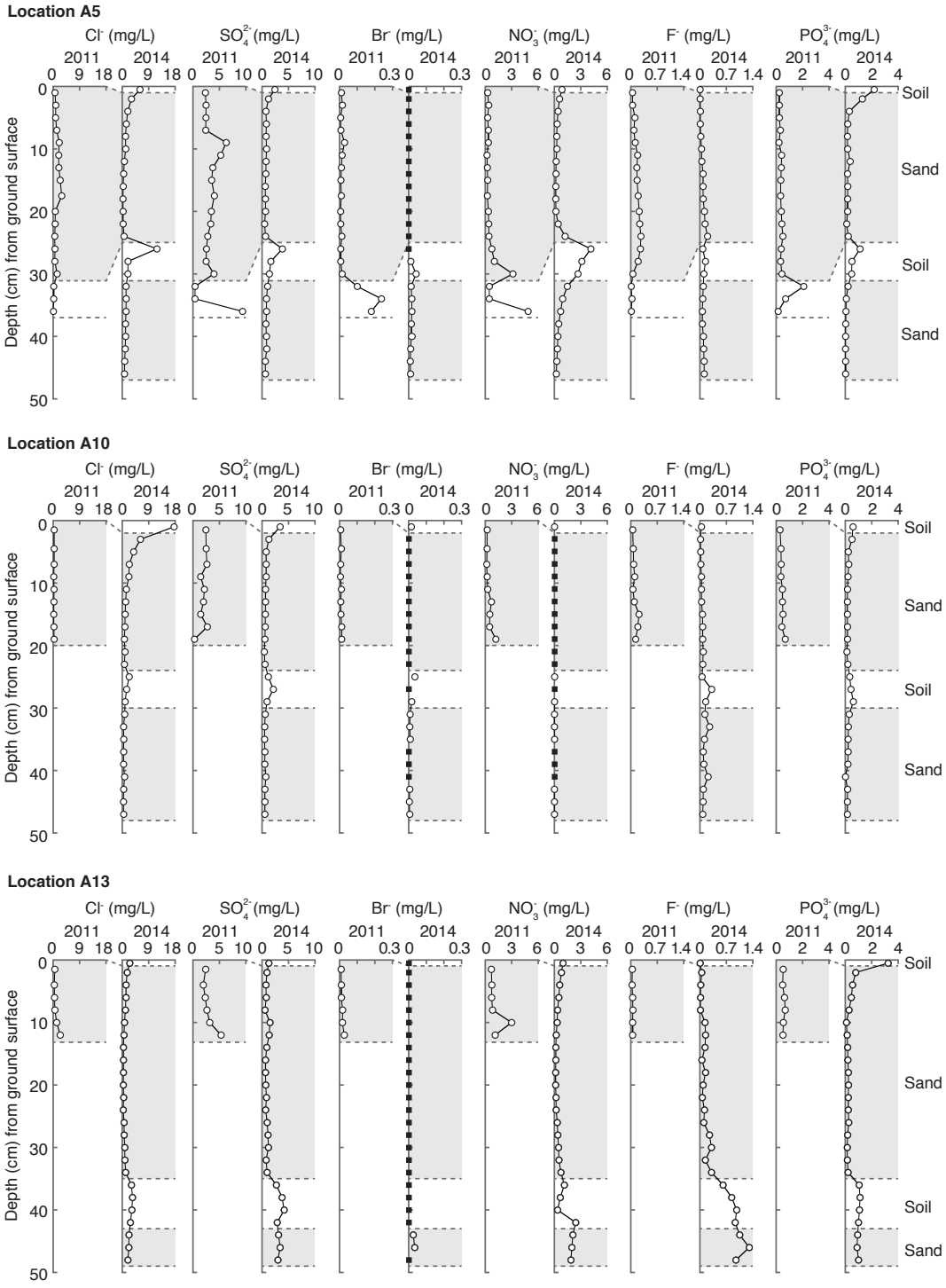

Fig. 4-17. Depth profiles of water-leachable anions (Cl^-, SO_4^{2-}, Br^-, NO^{3-}, F^- and PO_4^{3-}) along transect A in 2011 and 2014. Black squares indicate values below the detection limit.

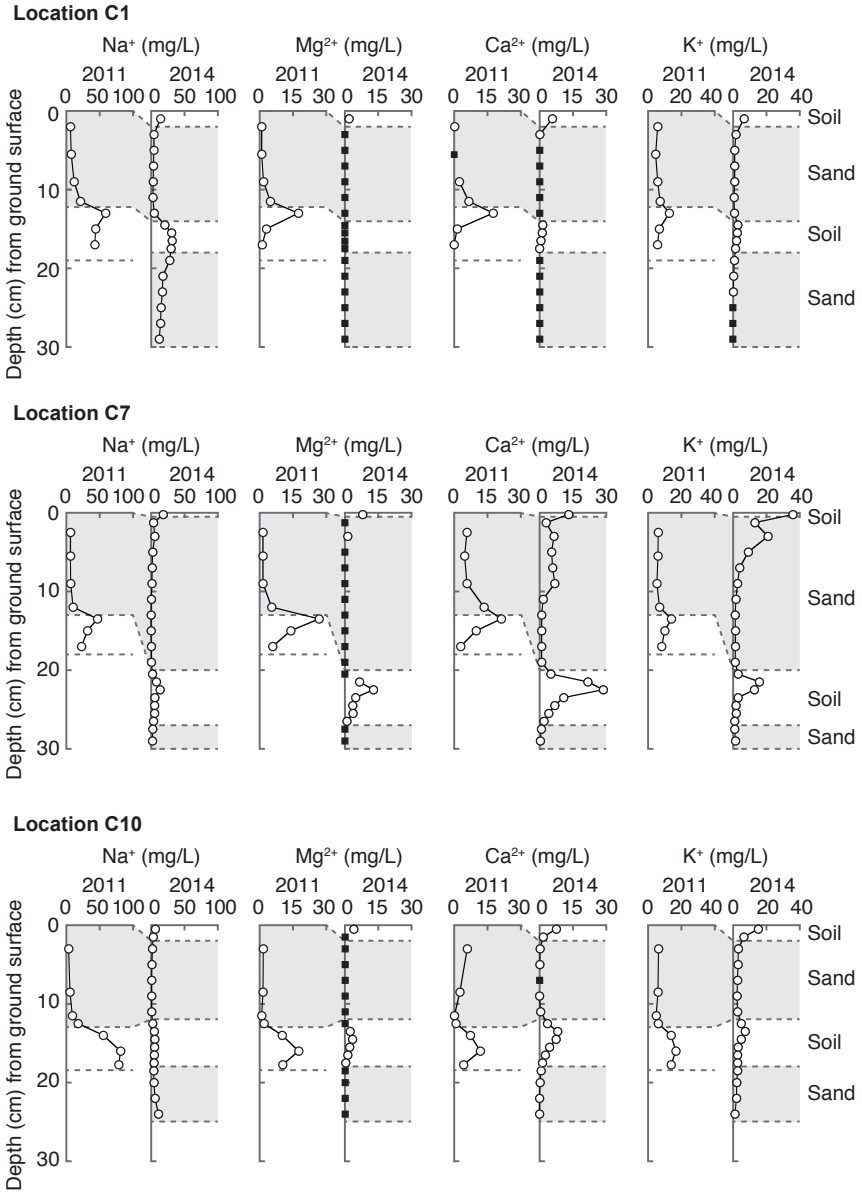

Fig. 4-18. Depth profiles of water-leachable cations (Na^+, Mg^{2+}, Ca^{2+}, and K^+) along transect C in 2011 and 2014. Black squares indicate values below the detection limit. The graphs of manganese and strontium were not posted because they were below the ICP-AES detection limit in every sample.

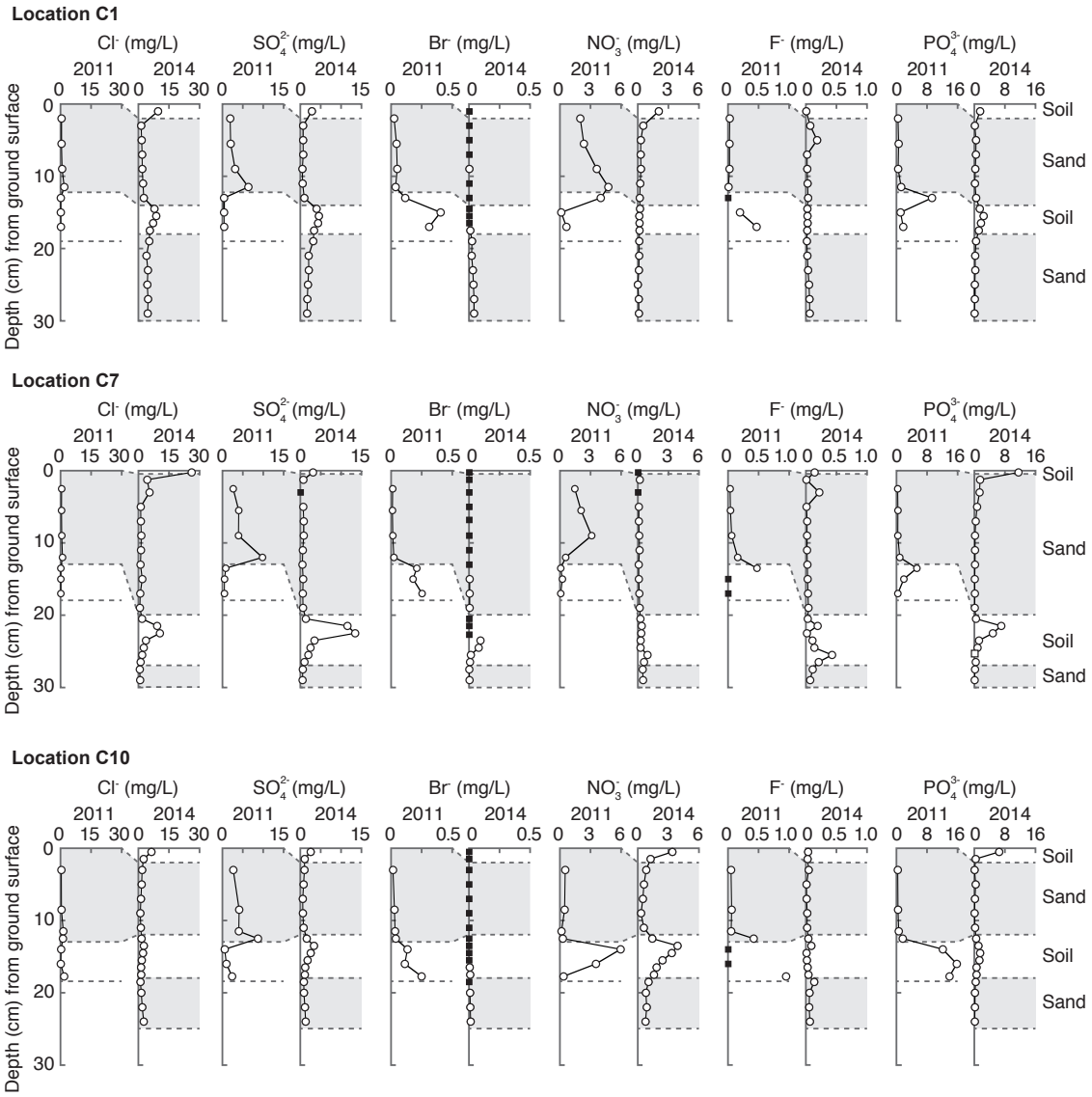

Fig. 4-19. Depth profiles of water-leachable anions (Cl^-, SO_4^{2-}, Br^-, NO^{3-}, F^- and PO_4^{3-}) along transect C in 2011 and 2014. Black squares indicate values below the detection limit.

4.4 Yamamoto

4.4.1 Sample information

All lake bottom sediments were collected at April 2014 using 3-m-long geoslicer on boat. Slices 1, 2, and 3 were taken at the same location (Fig. 2-5b). Because their stratigraphy was similar, Slice 3 was adopted as a representative of these three samples. Detail analyses, such as CT image, ^{14}C dating, tephra analysis, and diatom analysis, were only conducted for Slice 3 because the stratigraphy of the surface unit was similar among Slices 3, 4, and 5 and sediment below surface unit was organic-rich in Slice 3 compared with the other slices. All 'depth' used in the samples of *Suijin-numa* was expressed as depth from the lake floor.

4.4.2 Stratigraphy

Deposit beneath the lake floor was 20–60-cm-thick black mud in every sampling locations, and 7–15-cm-thick sand was deposited immediately below the black mud in Slice 3, 4, and 5 (Fig. 4-20). Sediments below the sand were, respectively, sandy deposits, peat, and gray silt seaward (Slices 5 and 6), central (Slice 3), and landward (Slice 4) of the lake (Fig. 4-20).

In Slice 3, 50-cm-thick black mud was deposited on top of the sediment samples. A 7-cm-thick very fine to medium sand layer (Sand 1) was observed immediately below the mud. It has a clear erosional base, as shown in the CT image (Fig. 4-20). Sand 1 contained angular gravels, rounded gravels, and granitic rocks (Fig. 4-21) at its lower part. Organic rich peat was observed below Sand 1. Two sand layers (Sands 2 and 3) were intercalated to the peat. Stratigraphy of the Slice 4 generally resembles that of the Slice 3, although it contains only one sand layer below Sand 1. Gray silt was dominant below Sand 1. Slice 5 was taken at the shallowest point (80 cm water depth). The black mud at the top was the thinnest (19-cm-thick) among the samples. A 6-cm-thick medium sand (=Sand 1) was observed immediately below the mud, but the contact between the black mud and sand was unclear. A fine to medium sand (39–54 cm depth) was intercalated by brown sandy mud. Coarse sand was present at the base of this sediment sample. Slice 6 was collected at the most seaward among the other sampling locations (Fig. 2-5b). Also, 45-cm-thick black mud was found at the top. The layer equivalent to Sand

1 was not observed from Slice 6. Thick medium sand found at the base of this sample (66–93 cm depth) contains abundant shell fragments.

4.4.3 Radiocarbon dating

From ^{14}C dating of organic sediment picked up from Slice 3, calendar age below Sand 3 was about 2900 cal yr BP, although it was about 2400 cal yr BP above the Sand 3 (Fig. 4-22 and Table 4-1). Calendar ages below and above Sand 2 were, respectively, about 2300 cal yr BP and 1100 cal yr BP. Extremely old age (ca. 11,000 cal yr BP) inferred from a sample just below Sand 2 is apparently reworked old organic materials because the age is too old to compare with below and above sediment. The age of peat between Sands 1 and 2 (57 and 67 cm depth) was about 700–1100 cal yr BP. Ages of the surface black mud ranged from modern to 200 cal yr BP (Fig. 4-22 and Table 4-1). Calendar ages obtained from leaves were, respectively, ca. 400 and 700 years younger than the age obtained from the same layer organic sediment at 65–66 and 81–82 cm depth.

4.4.4 Tephra

No remarkable tephra concentrated layer, a so-called visible tephra layer, was found in any sample obtained through this survey. Volcanic glass contents were measured in six layers (57–59, 59–61, 61–63, 63–65, 65–67, and 67–69 cm depth) from the sample of Slice 3. Moreover, the refractive-index of volcanic glass and orthopyroxene, and glass shard major element compositions were measured in three layers (57–59, 61–63, and 65–67 cm depth).

In Slice 3, although no visible tephra layer exists at peat between 57 and 67 cm depth (Fig. 4-20), characteristic features were found at 57–59, 61–63, and 65–67 cm depth based on the analysis of volcanic glass content (Fig. 4-23). Contents of heavy minerals were high (17.6%) at 57–59 cm depth. A peak of volcanic glass (4.4%), although not noticeable, was found at 61–63 cm depth. Heavy minerals were more concentrated, from 4.2% at 67–69 cm depth to 6.8% at 65–67 cm depth. Especially, orthopyroxene concentrations were higher, but the amphibole contents were decreased.

Refractive-indices of volcanic glass and orthopyroxene (Table 4-2), and glass shard major element compositions (Table 4-3) were measured in three layers (57–59, 61–63, and 65–67 cm depth). Results showed refractive-index and major element compositions for 57–59, 61–63, and 65–67 cm depth, probably indicating a mixture of volcanic glasses that originate from Hr-FA and Hr-FP (two sixth-century eruptions of Haruna volcano, central Japan: Soda, 1989). That inference is supported by the presence of amphibole. In addition to these tephra, volcanic glasses origin from A.D. 915 To-a might be mixed at these three layers, as inferred from the results of the color and shape of volcanic glass, and the refractive-index of orthopyroxene.

4.4.5 Diatom

Diatom analysis was conducted at five layers (0–3, 8–13, 18–23, 28–33, and 38–43 cm depth) from the surface black mud in Slice 3 (Fig. 4-24). Total 115 taxa was identified. *Staurosira construens* var. *binodis*, *Staurosirella pinnata*, and *Pseudostaurosira brevistriata* showed a high percentage in every layer. Although *Suijin-numa* was freshwater environment before the 2011 tsunami judging from the diatom data obtained by Sawai et al. (2008), brackish-marine and marine diatoms were mixed from top to bottom of the surface black mud (Fig. 4-24).

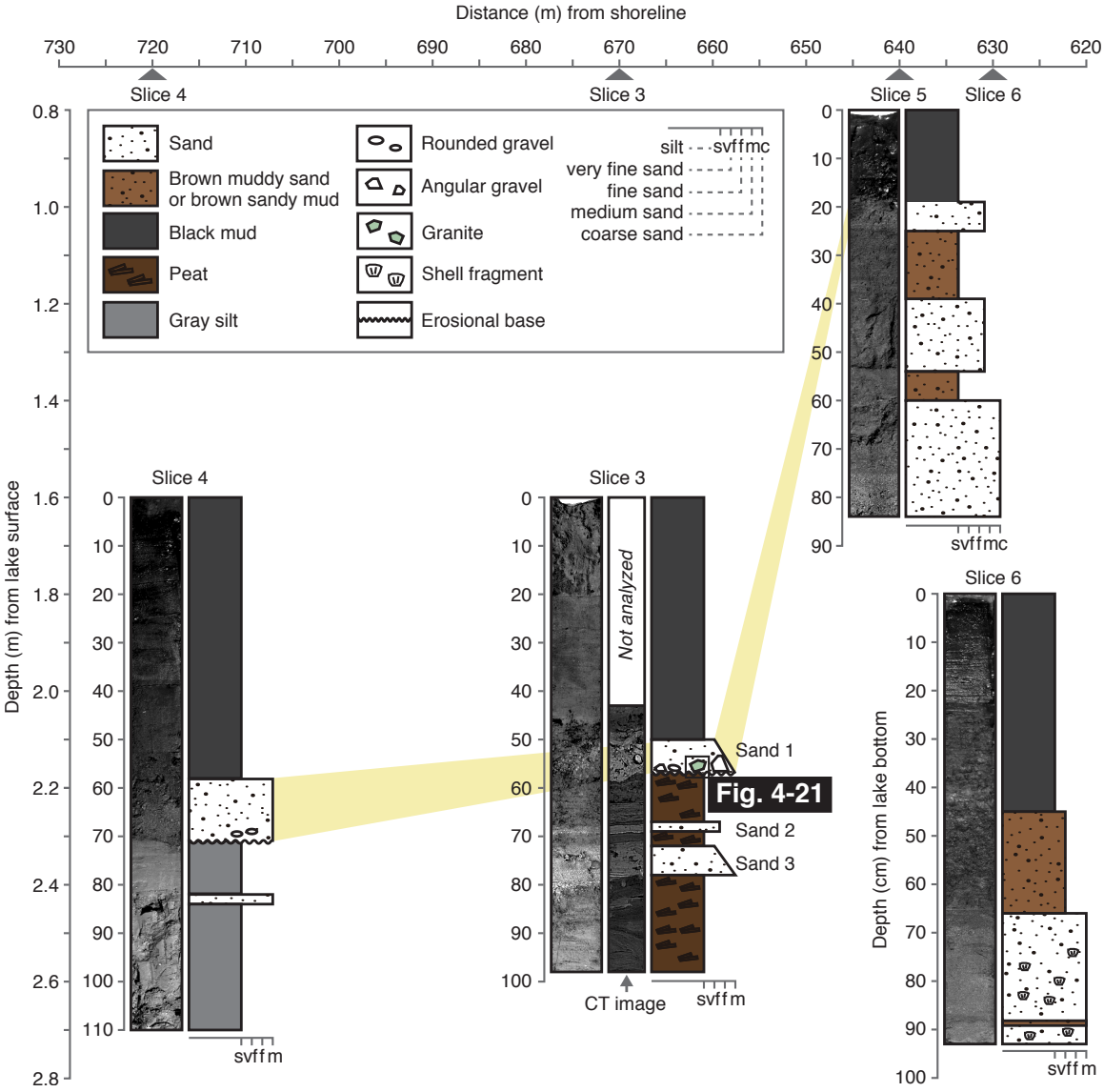

Fig. 4-20. Stratigraphy of sediment below the lake floor of *Suijin-numa*.

Fig. 4-21. Photograph of granitic pebble contained at bottom of Sand 1 from Slice 3.

Table 4-1. Radiocarbon data for organic sediments and leaves from sample Slice 3.

Sample ID	Depth (cm)	Material	^{14}C age (yr BP)	δ^{13}C (‰)	Calendar age (2σ)(cal yr BP)	Lab. code
Slice 3	8–13	Organic sediments	170±30	-27.2	130–230	Beta-412363
Slice 3	18–23	Organic sediments	90±30	-26.9	20–140	Beta-412364
Slice 3	28–33	Organic sediments	60±30	-27.0	Modern	Beta-412365
Slice 3	38–43	Organic sediments	130±30	-26.9	60–150	Beta-412366
Slice 3	57–58	Organic sediments	890±30	-26.6	730–830	Beta-387433
Slice 3	58–59	Organic sediments	920±30	-26.1	780–920	Beta-380294
Slice 3	59–60	Organic sediments	860±30	-26.4	700–800	Beta-387434
Slice 3	60–61	Organic sediments	1220±30	-26.5	1060–1190	Beta-387435
Slice 3	61–62	Organic sediments	910±30	-26.3	760–920	Beta-378684
Slice 3	62–63	Organic sediments	890±30	-27.0	730–830	Beta-387436
Slice 3	63–64	Organic sediments	940±30	-26.0	790–920	Beta-387437
Slice 3	64–65	Organic sediments	890±30	-26.5	730–830	Beta-387438
Slice 3	65–66	Organic sediments	1140±30	-25.3	970–1100	Beta-378685
Slice 3	65–66	Leaves	590±30	-29.2	580–650	Beta-413685
Slice 3	66–67	Organic sediments	930±30	-26.7	790–920	Beta-387439
Slice 3	69–70	Organic sediments	9950±30	-26.2	11250–11410	Beta-387440
Slice 3	70–71	Organic sediments	2270±30	-25.9	2300–2350	Beta-378686
Slice 3	71–72	Organic sediments	2330±30	-25.9	2310–2390	Beta-387441
Slice 3	78–79	Organic sediments	2900±30	-24.1	2950–3080	Beta-387442
Slice 3	79–80	Organic sediments	2980±30	-24.6	3060–3250	Beta-387443
Slice 3	80–81	Organic sediments	2850±30	-24.2	2880–3060	Beta-378687
Slice 3	81–82	Organic sediments	2930±30	-24.4	2980–3170	Beta-387444
Slice 3	81–82	Leaves	2270±30	-29.6	2300–2350	Beta-413686
Slice 3	82–83	Organic sediments	2940±30	-24.0	2990–3180	Beta-387445

The radiocarbon ages were converted to calendar ages by using the INTCAL13 database (Reimer et al., 2013) and the Calib 7.1 program (http://calib.qub.ac.uk/calib/). Radiocarbon and calendar ages are expressed as yr BP and cal yr BP, respectively.

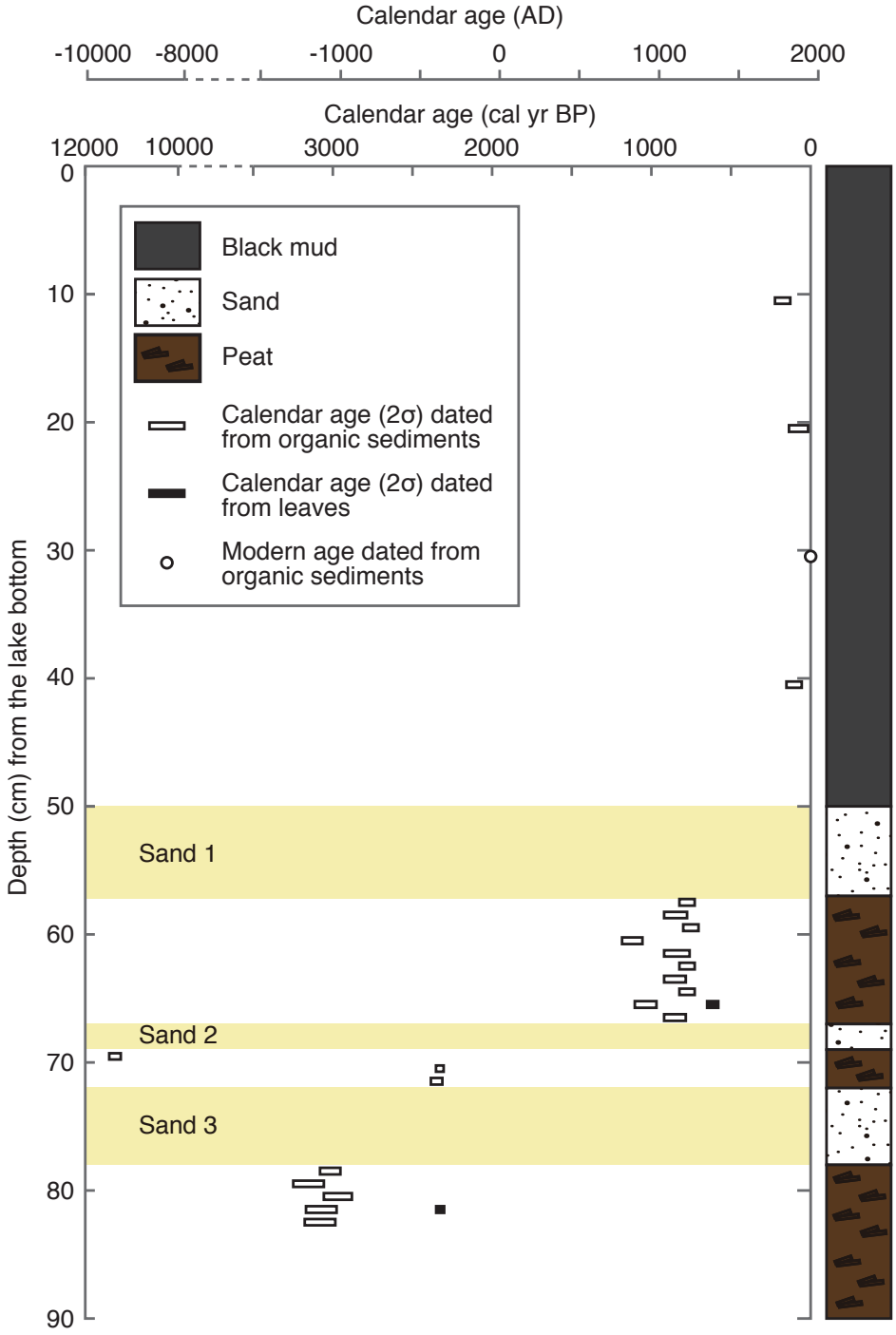

Fig. 4-22. Results of ^{14}C dating for Slice 3. ^{14}C data show 2 σ range and are presented in Table 4-1. ^{14}C age measured by organic sediment and leaves are indicated respectively in white and black bars. White circles represent modern values obtained from organic sediment.

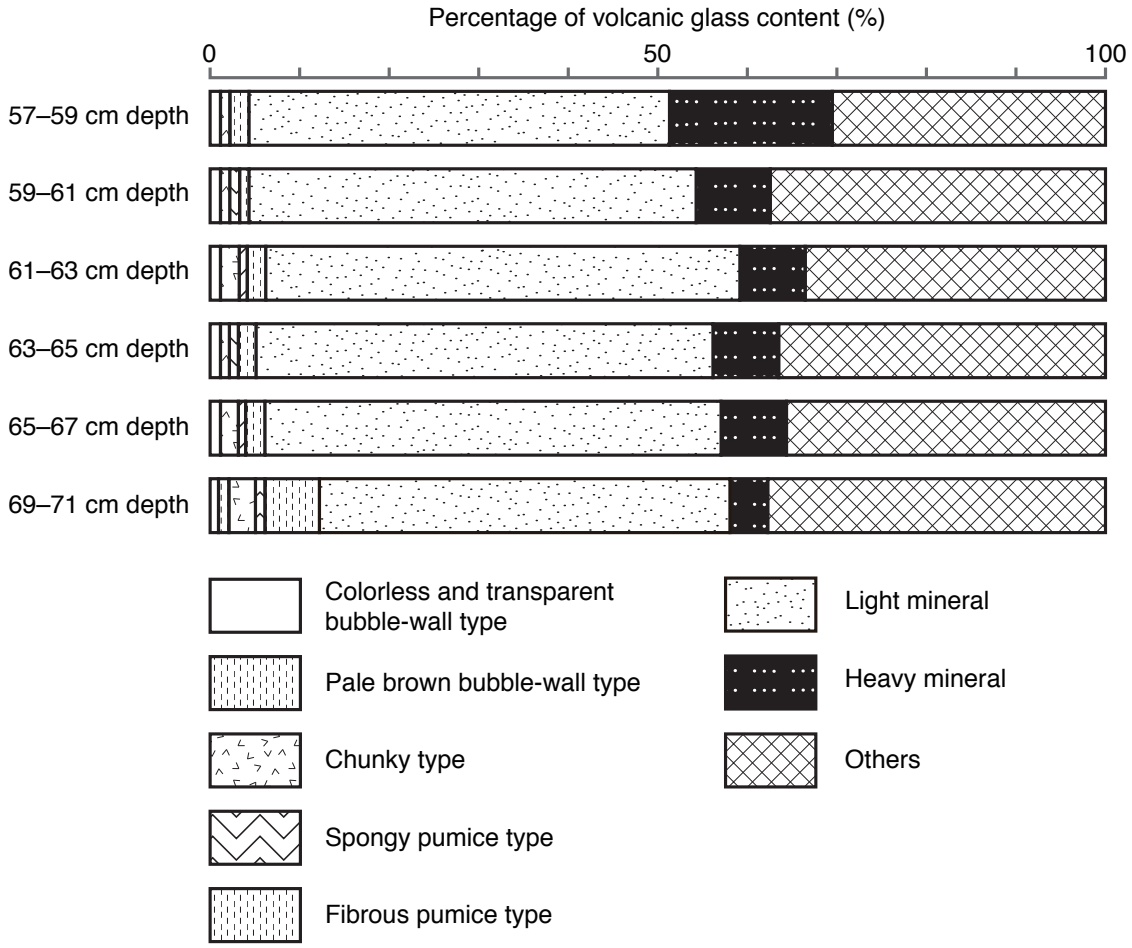

Fig. 4-23. Diagram of volcanic glass content for Slice 3. Percentages of different types volcanic glass, light, and heavy minerals were estimated from observations of 250 particles ranging from 1/4 to 1/8 mm.

Table 4-2. Refractive-indices of glass and orthopyroxene in Slice 3 and marker tephra around the Miyagi-Fukushima Pacific coast for last 30 ka.

Sample ID	Volcanic glass		Orthopyroxene		Reference
	Refractive index (n)	Counted particle	Refractive index (γ)	Counted particle	
57–59 cm depth	1.496–1.508	34	1.705–1.726	33	This study
61–63 cm depth	1.498–1.510	31	1.708–1.727	30	This study
65–57 cm depth	1.497–1.505	34	1.708–1.724	31	This study

Marker tephra	Volcanic glass	Orthopyroxene	Reference
	Refractive index (n)	Refractive index (γ)	
As–A: A.D.1783	1.507–1.512	1.707–1.712	1)
As–Kk: A.D.1128		1.706–1.710	2)
B–Tm: 10th century	1.511–1.522		1)
To–a: A.D.915	1.503–1.507	1.706–1.708	1)
Hr–FP: middle 6th century	1.501–1.504	1.707–1.711	1)
Hr–FA: early 6th century	1.498–1.505	1.707–1.711	1)
Nm–N: 5 ka	1.500–1.505	1.706–1.708	1)
To–Cu: 6 ka	1.508–1.512	1.703–1.709	1)
K–Ah: 7.3 ka	1.508–1.516		1)
Hj–O: 11–12 ka	1.499–1.504	1.712–1.715	1)
To–H: 15 ka	1.505–1.509	1.708–1.712	1)
As–K: 15–16.5 ka	1.501–1.503	1.708–1.712	1)
As–YP: 15–16.5 ka	1.501–1.505	1.707–1.712	1)
AT: 28–30 ka	1.499–1.501		1)
To–Of: ≧32ka	1.505–1.511	1.707–1.711	1)

1) Machida and Arai (2011), 2) Soda (1996).

Table 4-3. Glass shard major element compositions of Slice 3 and marker tephra for about 30 ka; *n.d.*, no data.

Sample ID		SiO_2	TiO_2	Al_2O_3	FeO	MnO	MgO	CaO	Na_2O	K_2O	P_2O_5	Counted particle
57–59 cm depth	type 1-1	78.49	0.07	12.52	1.08	0.06	0.04	0.64	2.24	4.83	0.04	4
	type 1-2	79.85	0.06	12.41	1.06	0.03	0.04	0.51	3.26	2.76	0.03	2
	type 1-3	79.09	0.11	12.41	1.25	0.06	0.07	0.84	2.86	3.33	0.04	4
61–63 cm depth	type 2-1	79.34	0.20	12.66	1.73	0.09	0.22	1.51	2.61	1.61	0.05	5
	type 2-2	79.62	0.09	12.39	1.02	0.07	0.05	0.63	2.99	3.1	0.03	4
	type 2-3	78.47	0.06	12.83	0.98	0.06	0.03	0.72	2.40	4.42	0.03	2
65–67 cm depth	type 3-1	78.54	0.19	12.38	1.54	0.03	0.2	1.59	2.97	2.55	0.01	3
	type 3-2	80.18	0.17	12.35	1.51	0.07	0.14	1.30	2.32	1.91	0.04	7
	type 3-3	79.58	0.06	12.52	1.23	0.08	0.03	0.41	2.88	3.2	0.02	1

Marker tephra	SiO_2	TiO	Al_2O_3	FeO	MnO	MgO	CaO	Na_2O	K_2O	P_2O_5	Reference
To-a	77.87	0.37	12.81	1.75	0.1	0.42	2.00	3.29	1.34		1)
Nm-N	78.10	0.24	12.10	1.14	0.09	0.19	1.34	3.35	3.45		2)
To-Cu	75.08	0.44	13.28	2.46	0.08	0.63	2.63	4.04	1.29		1)
K-Ah	75.24	0.53	12.85	2.42	0.08	0.47	2.02	3.32	3.00		1)
Hj-O	77.79	0.16	12.76	1.05	*n.d.*	0.44	1.09	3.61	3.10		2)
To-H (pfl) upper	78.30	0.29	12.67	1.52	0.06	0.29	1.73	3.84	1.30		2)
To-H (pfl) lower	76.38	0.40	13.43	1.90	0.11	0.44	2.22	3.88	1.24		2)
As-YP	78.15	0.27	11.99	1.33	0.04	0.26	1.30	3.72	2.89		1)
Nr-KU	77.98	0.22	12.28	1.22	*n.d.*	1.01	1.59	4.23	1.47		2)
AT	78.25	0.13	12.14	1.26	0.04	0.11	1.09	3.41	3.56	0.02	1)
To-Of (pfl)	77.82	0.36	12.45	1.88	0.08	0.33	1.87	3.97	1.25		2)

Volatile-free compositions normalized to 100% were listed in table.

1) Yagi (unpublished data), 2) Aoki and Arai (2000).

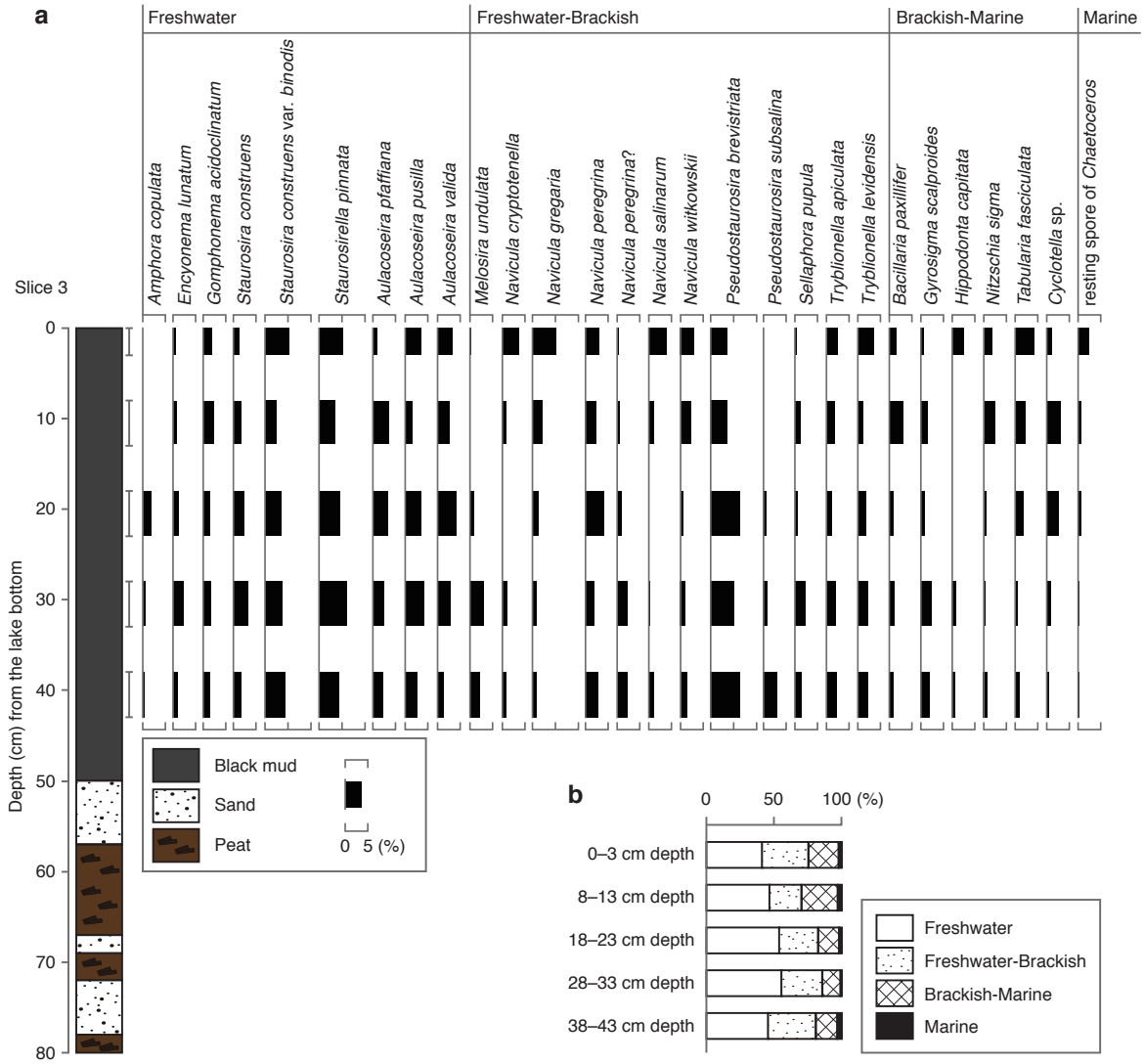

Fig. 4-24. Results of diatom analysis for Slice 3. (a) Vertical changes in diatom assemblages in Slice 3 (exceeding 2% relative to counted total diatom valves). (b) Relative abundance of diatom assemblages classified into four salinity groups (freshwater, freshwater-brackish, brackish-marine, and marine).

Chapter 5. Discussion

5.1 Stable carbon isotope ratio

In Hasunuma, $\delta^{13}C_{bulk}$ in the sand was about 15‰ higher than $\delta^{13}C_{org}$ in the sand layer, on the other hand, $\delta^{13}C_{bulk}$ and $\delta^{13}C_{org}$ were almost identical in the soil (Figs. 4-11 and 4-12). The LOI550 of samples collected in 2011 shows that the organic carbon content was very low in the sandy tsunami deposit (Figs. 4-11 and 4-12). In contrast, LOI950 was high in the sand at locations A5, C1, C7, and C10, which indicates the presence of carbonate: shell fragments that were also visible to the naked eye. Shell fragments were contained at sand layer but they were absent in the soil. Therefore, the difference between $\delta^{13}C_{bulk}$ and $\delta^{13}C_{org}$ in the sand layer strongly suggests the presence of shell fragments. $\delta^{13}C_{org}$ ranged from –22‰ to –31‰ in both sand and soil layers, indicating that most of the organic carbon originates from C3 terrestrial plants (Lamb et al. 2006).

The $\delta^{13}C_{org}$ values in SND-14 were, respectively, –26.3‰ and –27.9‰ to –27.0‰ in the sand and soil (Fig. 4-1). While, the $\delta^{13}C_{org}$ values in samples of Hasunuma were, respectively, –29.7‰ to –22.9‰ and –29.8‰ to –27.7‰ in the sand and soil (Figs. 4-11 and 4-12). Chagué-Goff et al. (2012a) also reported $\delta^{13}C$ from the sample of tsunamigenic sand, and soil both within and beyond tsunami inundation limit at the Sendai Plain. These $\delta^{13}C$ values were almost same with both sand and soil from SND-14 and soil from Hasunuma samples. However, a part of $\delta^{13}C$ at sand layer was ca. 3‰ heavier than the samples of the Sendai Plain: SND-14 and samples reported by Chagué-Goff et al. (2012a). It is possible that the difference represents contribution of marine organic matter. It was not analyzed $\delta^{13}C$ of original soil (unaffected by tsunami), seawater particle organic carbon, or marine sediment. However, $\delta^{13}C$ of marine organic carbon (dissolved organic carbon, particle organic carbon, and algae) is typically in the range of –25 to –16‰, whereas $\delta^{13}C$ of terrestrial C3 and C4 plants, respectively, are –32 to –21‰ and –17 to –10‰ (Lamb et al. 2006). The heaviest value of sand layer $\delta^{13}C_{org}$ (–22.9‰) recorded from sand deposit collected at Hasunuma might represent a mixture of terrestrial C3 plant and marine organic matter. Anyhow, the values (–22.9‰) were within the range of $\delta^{13}C$ of marine organic matter and terrestrial C3 plant (Lamb et al. 2006).

It is difficult to distinguish marine organic carbon using merely $\delta^{13}C$ because the ranges of $\delta^{13}C$ of terrestrial C3 plant and marine organic matter were partly overlapped. Moreover, marine organic matter transported by tsunami inundation might be mixed with terrestrial organic matter. In that case, obtained $\delta^{13}C$ value apparently shifts to the value of terrestrial organic carbon, and we cannot identify the source of organic matter. It is important to know endmember of background level of original soil unaffected by tsunami, seawater particle organic carbon, and sea-bottom sediment. On that base, we might be able to estimate how much amount of marine-source organic matter is supplied to coastal land.

5.2 Allogenic biomarkers

5.2.1 Source of biomarkers

Living organisms produce specific organic compound. The distribution of hydrocarbons had a maximum at C_{29} with other larger peaks at the odd-numbered *n*-alkanes (C_{23}, C_{25}, C_{27}, C_{31}, and C_{33}), whereas lesser peaks occurred at the even-numbered *n*-alkanes (C_{24}, C_{26}, C_{28}, C_{30}, and C_{32}) in most of the layers measured at Sendai, Odaka, and Hasunuma (Figs. 4-3, 4-4, 4-6, 4-13, 4-14, and 4-15). This distribution pattern primarily indicates a contribution by higher plants (Eglinton and Hamilton, 1963). On the other hand, short-chain (C_{17}, C_{18}, and C_{19}) *n*-alkanes, pristane, and phytane are originated from marine and/or aquatic organism. C_{17} and C_{19} *n*-alkanes are predominant in algae (Gelpi et al., 1970), and C_{18} *n*-alkane is derived from fish (Mackie et al., 1974). Pristane is predominately derived from zooplankton (Blumer et al., 1963), benthos, and fish (Mackie et al., 1974). Phytane is derived predominately from zooplankton (Blumer and Thomas, 1965) or sediment itself by biological activity (Ikan et al., 1975).

Long-chain C_{37}–C_{39} unsaturated methyl and ethyl ketones, namely alkenones, are derived from several species of haptophytes, including the widely distributed coccolithophorids *Emiliania huxleyi* and *Gephyrocapsa oceanica* (Volkman et al., 1980; Marlowe et al., 1984; Conte et al., 1994). Alkenones are also one of good indicator for marine sources.

Cholesterol, stigmasterol, and *β*-sitosterol were detected at every measured layer from all study sites. Animals tend to make cholesterol, whereas higher plants typically produce stigmasterol and *β*-sitosterol (Peters et al., 2007a). Dinosterol originated from marine dinoflagellates (e.g. Boon et al., 1979) and is considered to be a good indicator as a marine biomarker.

Unresolved complex mixture (UCM) is an evidence for contamination of biodegraded or low-maturity petroleum in sediment or water sample (Meyers and Takeuchi, 1981; Gough and Rowland, 1990). If UCM is contained in sample, it represents the broad and pronounced rise of the baseline on gas chromatograms (Peter et al., 2007b).

5.2.2 Biomarkers deposited by the 2011 tsunami

Characteristic hydrocarbons, such as short-chain *n*-alkanes, pristane, and phytane, were detected in the soil layer underlying the tsunami deposits in both the Sendai (SND-14) and Odaka (ODA-2) sediment samples (Figs. 4-3 and 4-6). Additionally, dinosterol originated from marine dinoflagellates was detected in the tsunamigenic mud layer (5–6 cm depth) at Odaka (Figs. 4-7 and 4-8). Because these aquatic hydrocarbons and marine-source dinosterol were absent in the deeper soil layer in each location and surface modern soil layer in Odaka, these biomarkers are likely to have been transported by abrupt event. Both sampling locations were sufficiently far from the shoreline (1.6 km inland in Sendai and 2.6 km inland in Odaka) and Tohoku region does not receive severe typhoon damage in recent years. Moreover, these biomarkers found from the layer associated with the 2011 tsunami deposit although they were not at sandy tsunami deposit itself. Therefore, these aquatic biomarkers (short-chain *n*-alkanes, pristine, phytane, and dinosterol) seem to have been transported from the ocean by the 2011 tsunami.

In addition to the presence of aquatic biomarkers, another notable feature was observed from sample of Odaka. There was a broad and marked rise of the baseline (Fig. 4-6) at the 20–21 cm depth that the layer was contained aquatic biomarker. It is probably as a result of contamination with UCM (see subsection 5.2.1). Because there is no evidence for UCM in either terrigenous or marine organic matter under natural condition, their presence in this layer indicates that they were contaminated by the

tsunami as well as the aquatic biomarkers. The UCM contamination might have originated from low-maturity oil deposited on the seafloor or oil spilled from broken vehicles and ships. Although there is no conclusive evidence of the source of UCM contamination, an important point is that UCM is never derived from recent organic matter. The presence indicates that it was provided by abrupt event—in this case, the tsunami.

From the results at Hasunuma, on the other hand, aquatic biomarkers were absent both the sandy tsunami deposit and in the soil in either 2011 and or 2014 (Figs. 4-13, 4-14, and 4-15). One possibility is that aquatic biomarkers were transported but they were not preserved at both sand and soil layers. They might be disappeared by external force, for example groundwater movement. Another possibility is that contributions of marine source organic matter were too low. Aquatic biomarkers might be transported by the tsunami inundation, however, it was too low to detect by GC. Although aquatic biomarkers were found at Sendai and Odaka, no aquatic biomarkers were found at Hasunuma. The difference whether transported biomarkers were detected or not may be attributable to specific environmental attributes of the study area, i.e., difference of original soil and organic content both sand and soil.

Transported (aquatic) biomarkers seem to adsorb to fine mineral particles and organic matter but not to large, sand-sized particles because they were detected from only soil layer or tsunamigenic mud. Allogenic biomarkers were transported together with sand by the tsunami. They might leach out of the sand layer due to sand possess much porosity, and then they concentrated in the soil below the sand layer. Or, aquatic biomarkers adsorbed and deposited to surface tsunamigenic mud like the results of Odaka. Organic content at overlying and underlying mud represented by LOI550 was similar among Sendai, Odaka, and Hasunuma. However, soil at Hasunuma contains sand-sized particle from beach by wind because sampling locations were close to beach (within ca. 350 m; Fig. 2-4). The soil scattering sand might enrich permeability of allochthonous organic carbon. Therefore, transported biomarkers, at Hasunuma, might pass through the soil layer by groundwater movement.

Marine-sourced biomarkers were not detected in the sand layer of the B-18 sample collected 3 months after the tsunami (Fig. 4-4). It cannot be speculated on whether characteristic hydrocarbons had penetrated the underlying soil because there were no soil samples available from the time shortly after

the tsunami. The data suggests that detectable amounts of marine-sourced biomarkers were not preserved in the sand layer at least 3 months after the tsunami.

In Odaka, allogenic biomarkers were not observed in the mud layer (15–18 cm depth) intercalated between the two sand layers (8–15 cm and 18–20 cm depth). One possibility is that the mud layer did not originate from the sea-bottom but from another source, such as paddy soil. Results of detailed analyses of grain size distributions and diatom (Szczucinski et al., 2012) at the Sendai Plain imply that the main sources of muddy tsunami deposits were local land soil although sampling location at Odaka is not the Sendai Plain and is located between narrow valley. If it can be adapt to the case of Odaka, mud drape intercalated between the sands is consisted of terrestrial organic matter. However, even freshwater mud transported by seawater could contain marine organisms. Another possibility is that marine-sourced organic materials were diluted by terrestrial organic materials. Therefore, marine-sourced biomarkers were apparently absent in detectable amounts. A large contribution of terrestrial organic matter may blind a presence of marine-sourced biomarkers. Actually, LOI in the mud drape was higher than the underlying soil (Fig. 4-5).

In the same reason, alkenones and marine-source sterols were absent or not detected in almost layers analyzed at three sites. It seems quite probable that terrestrial organic matter is largely contained in geological layer compared with marine one. Removal of plant materials, for example picking of large terrestrial plant or sieving, before biomarker analysis may effective to detect marine-source biomarkers more accurately.

Marine-source biomarkers seem to be generally transported on land by tsunami inundation. From the results of Sendai and Odaka, the conceptual process of deposition of marine-source biomarkers is considered as below (Fig. 5-1): (1) Marine organisms, such as zoo- and phytoplankton, fish, benthos, and algae, composed of organic molecular structural materials are contained at seawater. The partly degraded marine organism is deposited at the bottom of the sea. (2) When tsunami occur, both marine organisms in seawater and degraded organic matter deposited in the sea-bottom are transported to land with sediment origin from sea-bottom, sand dune, and local land soil. (3) Sediments (sand and mud) and marine organisms are deposited on land. (4) After several days to months, marine organisms decompose by biodegradation or carbonate skeletons dissolve in the acidified soil. However, their

organic molecular structures remain in the soil and it can be detected as biomarker. Marine-sourced biomarkers are concentrated in the mud layer overlying the sand or in the soil underlying sandy deposits, or in both.

The aquatic hydrocarbons were concentrated 2 cm below the sandy tsunami deposits in SND-14 (Fig. 4-3), whereas they were detected immediately beneath the sandy tsunami deposits in ODA-2 (Fig. 4-6). It is possible that seawater penetrated 2 cm downward into the soil layer via dense roots. Rice paddy soil contains plant materials, and the region was fallow in March when the tsunami occurred. However, there could be more than one possible interpretation in the case of paleotsunami deposits. If there is a slight gap between a sand layer and a layer containing marine-sourced biomarkers, we cannot necessarily differentiate whether they were formed by a single tsunami event or by multiple tsunami events. If there was a single tsunami event, the depositional process was likely as follows (Fig. 5-2a): Sand is deposited on the surface by tsunami inundation, and marine-source biomarkers are then concentrated in the underlying soil by seawater penetration via roots. It is similar to the case of the Sendai sample. If there were multiple tsunami events, the depositional process was likely as follows (Fig. 5-2b): (1) Marine-sourced biomarker deposition is caused by tsunami inundation without sand deposition. (2) Soil accumulates naturally over time. (3) Sand is deposited by another tsunami without deposition of marine-source biomarker. The latter case is not likely, however, because there was no evidence of marine-source biomarkers in the second tsunami event, even though sand was transported by seawater flow. From this viewpoint, even if there is a slight gap between a sand layer and the layer containing marine-source biomarkers, it seems quite probable that these depositions were formed by a single tsunami event. However, we must be noted that evidence of allogenic biomarker can a few cm away from event deposit.

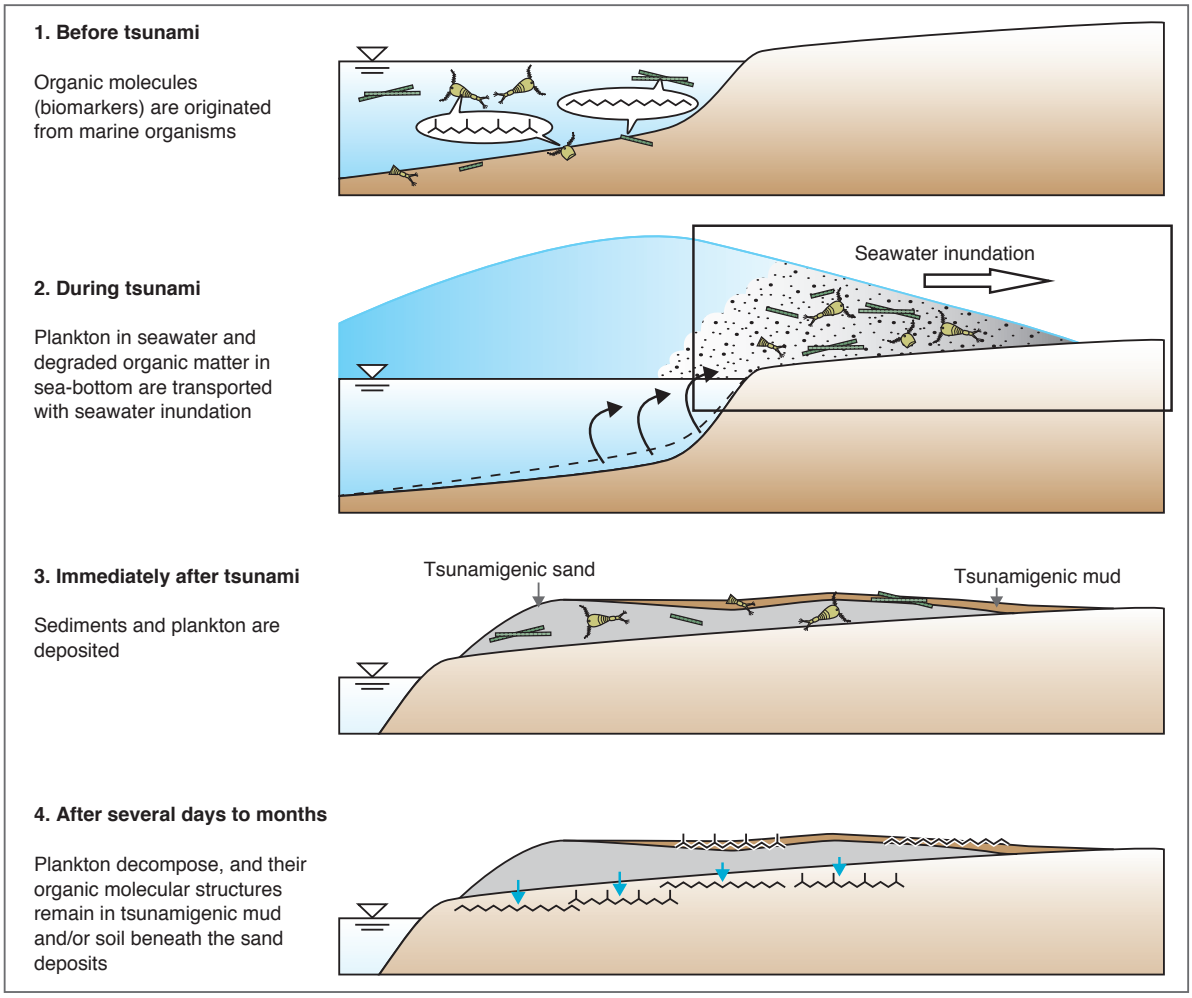

Fig. 5-1. Marine biomarker depositional process: (a) before tsunami, (b) during tsunami, (c) immediately after tsunami, and (d) after several days to months.

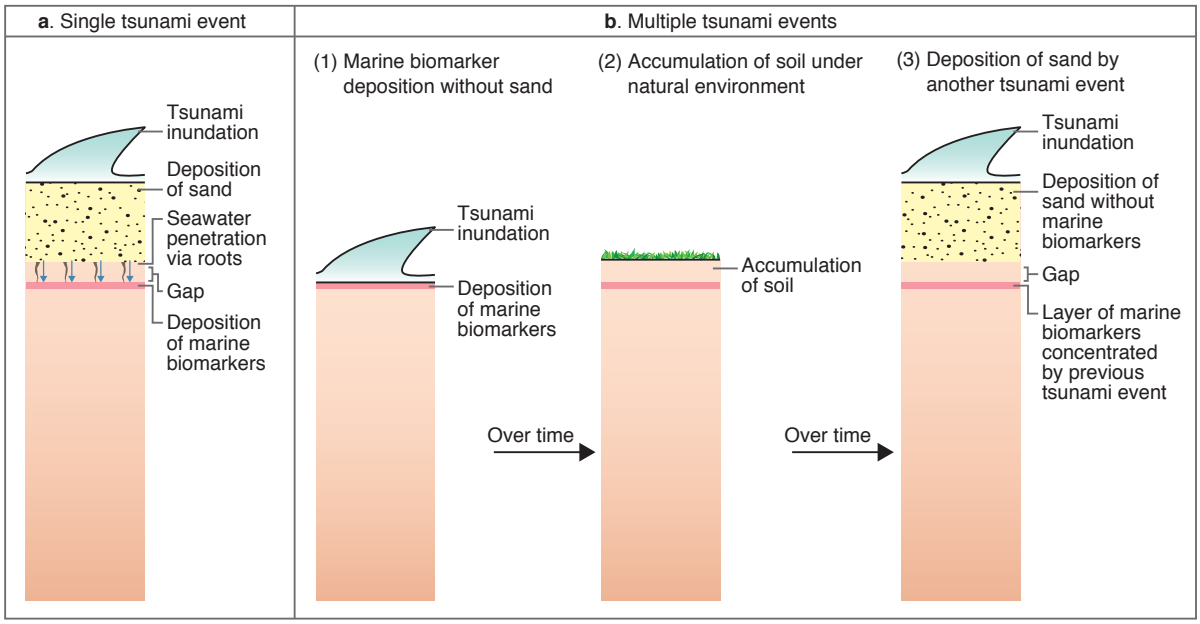

Fig. 5-2. Illustration showing how a slight gap can be formed between a sand layer and a layer with concentrated marine biomarkers: (a) single event and (b) multiple events.

5.3 Behavior of water-leachable ions

Concentrations of almost water-leachable ions in the 2011 samples of Hasunuma were low in the sandy tsunami deposit (Figs. 4-16–4-19). They were highest in the soil just below the sand layer and then they were gradually decreased with depth in the soil (Figs. 4-16–4-19). This distribution suggests that characteristics of saltwater represented by water-leachable ions easily preserved at soil not at sand. It is highly possible that saltwater flooded together with or after sand deposition penetrates the sand layer and reached the underlying soil. The pattern of gradually decrease with depth at soil probably represent downward penetration. Because the finer textured and organic rich soil can hold more water than the sand, many seawater components likely became concentrated in the soil below the surface sand layer.

Chagué-Goff et al. (2012b, 2014) also reported similar trend from the analysis of samples collected at the Sendai Plain. They found that the concentrations of water-leachable ions (Cl^-, Br^-, SO_4^{2-}, and Na^+) were low in the 20 cm thick sandy tsunami deposit. The concentrations marked highest values at soil just below the sand layer and then they were decreased with depth. However, at another site in Chagué-Goff et al. (2014), concentrations were higher in the thin sandy tsunami deposits (1 cm thickness) than in the soil below the sand. At Hasunuma, thickness of sandy tsunami deposits was more than 10 cm, and the concentrations of water-leachable ions were generally low in every sample. It suggests that water-leachable ions derived from seawater may penetrate at thick (≥10 cm) sand layer but remain at thin sand layer.

The concentrations of water-leachable cations decreased from 2011 to 2014 in both the tsunami sand layer and the underlying soil (Figs. 4-16 and 4-18). Concentrations of water-leachable anions, especially sulfate, bromide, and nitrate, also decreased between 2011 and 2014 (Figs. 4-17 and 4-19). Similar patterns that are decreasing of concentrations over time were reported for tsunami deposits and underlying soil on the Sendai Plain (Chagué-Goff et al. 2012b, 2014). Chagué-Goff et al. (2014) collected samples at paddy field from the Sendai Plain 2, 5, 9, and 11 months after the tsunami. In May 2011 (2 months after the tsunami), they observed high concentrations of chloride, bromide, sulfate, and sodium just below a 20-cm-thick sandy tsunami deposits. At least up to one year after tsunami

inundation, the concentrations generally decreased with time. The report and the results of Hasunuma suggest that decreasing of concentrations of water-leachable ions is not local event, and it can be occurred in anywhere.

Although seawater origin water-leachable ions concentrated by tsunami inundation seems to be generally decreased with time, the behavior is actually complicated. Concentrations of calcium ion at locations A5 and A13 were higher in 2014 than in 2011 samples (Fig. 4-16). In general, cation is easy to adsorb in organic-rich sediment. Moreover, divalent cation is more adsorb than monovalent one. In the case of Hasunuma study area, seawater compositions were usually derived to coastal forest by sea spray, and they were penetrated the ground constantly. Because sandy tsunami deposits collected in 2014 contain much fine roots (Fig. 4-9), divalent cation could be adsorbed at sand layer. Therefore, concentration of calcium ion might increase at sand layer from 2011 to 2014 nevertheless the other ions decreased.

While, Chagué-Goff et al. (2014) reported that chloride concentration was higher in February 2012 than in October 2011 at least at one site. The concentration had increased immediately above the almost hard pan that is puddled soil and reduce water loss for rice farming. The presence of the impermeable hard pan underneath the rice paddy soil impeded downward leaching and resulting downward increase in chloride concentration. In Hasunuma, samples were collected at coastal forest where there is no hard pan. Therefore, water-leachable ions might leach further downward and diluted by precipitation and groundwater movement. Thus, although water-leachable ions derived from tsunami inundation can be collected in high concentrations at soil below a thick sand layer, they are leached with time unless a low-permeability layer can halt the downward leaching, as previously reported by Chagué-Goff et al. (2014).

5.4 Erosion of paleo-tsunami deposit

5.4.1 Identification of the 2011 tsunami deposit

In *Suijin-numa*, the 2011 tsunami likely deposited the 7–15-cm-thick sand layer (Sand 1) observed in slices of the lake floor (Fig. 4-20) for the following reasons: (1) no sand deposit that is equivalent to

the Sand 1 was observed before the 2011 event represented by Sawai et al. (2008), (2) an erosional unconformity underlies Sand 1, and (3) Sand 1 contained granite rock fragments (Figs. 4-20 and 4-21). The basement geology around this area is alluvium and the Pliocene sandstone (Fig. 2-5a). Therefore, the presence of granite rock fragments is unnatural. It is noteworthy that the granite rock is typically used for tombstones or flagstones in recent Japanese culture. Therefore, granite rock fragments were expected to have derived from artifacts, which were probably transported from tsunami-devastated residential areas.

A 20–60-cm-thick black mud layer above Sand 1 probably settled out of suspension in the hours and days after the tsunami. In fact, post-tsunami satellite images showed that muddy seawater and debris stagnated for a few days around the pond because of the topographic lows. The tsunami, with abundant sand and gravel, inundated the lake. At that time, black mud deposited on lake bottom was stirred up and land soil was flowed in the lake. After gravel and sand were firstly deposited, the suspended black mud was re-settled through the water column and was deposited on the sand layer. The existence of brackish-marine and marine diatoms throughout the surface black mud in Slice 3 (Fig. 4-24) proves that seawater incursion stirred the lake water and mud. The combination of lower sandy and upper muddy tsunami deposits was typically reported on the Sendai Plain (Abe et al., 2012) including the small valley surrounding *Suijin-numa* (Abe et al., 2014). Therefore, the results indicate that stratigraphically similar tsunami deposits can also be formed both on land and in the lake.

Results of detailed analyses of grain size distributions, diatom assemblages (Szczuciński et al., 2012), mineralogy, and foraminifera (Putra et al., 2013) at the Sendai Plain imply that the main sources of sandy and muddy tsunami deposits are beach and dune sand, and local soil, respectively. As true also for the Sendai Plain, the source of sand at the narrow valley around *Suijin-numa* is probably the beach and dune, as shown by a comparison of grain size distributions in tsunami sand, beach sand, and dune sand (Abe et al., 2014). The muddy tsunami deposits formed at the narrow valley were probably transported from the paddy field and lake bottom because mud has mainly freshwater diatoms, in addition, the mud thickness increased rapidly around *Suijin-numa* (Abe et al., 2014). If one assumes that the source of sandy and muddy tsunami deposits at *Suijin-numa* is the same as that around the

narrow valley, then sand was transported from beach and dune. Mud was transported from the paddy field and re-settled from lake bottom.

5.4.2 Lake bottom erosion and reworking

Sediment data of Sawai et al. (2008) are useful as a reference of the pre-tsunami lake bottom deposits. Slice 3 was collected near the location of Core 1 by Sawai et al. (2008) (Fig. 2-5b). In Core 1, tsunamigenic sand deposits, which were formed by the 1611 Keicho tsunami and the 869 Jogan tsunami, plus the 915 To-a layer were intercalated in peat and mud deposits (Sawai et al., 2008). Peat is predominant in lower sediments, whereas mud is contained in upper sediments. The boundary is almost at the depth of 1611 Keicho tsunami deposit (Sawai et al., 2008). Before the 2011 tsunami, peat and mud deposited above the To-a layer were about 1.4-m-thick at the center of the lake (Sawai et al., 2008). The 1611 Keicho tsunami deposit was observed at the central to landward area, whereas the 915 To-a tephra layer was observed throughout the lake (Sawai et al., 2008).

After the tsunami, however, the combination of lower sandy and upper muddy deposit that is interpreted as the 2011 tsunami deposit (see subsection 5.4.1) was observed at upper part of lake bottom sediment. The surface mud layer that is interpreted as the 2011 muddy tsunami deposit was only 50-cm-thick in Slice 3. The 1611 Keicho tsunami sandy layer was not observed in post-tsunami sample not only in Slice 3 but also in other slices (Fig. 4-20). Furthermore, no tephra layer was observed in any post-tsunami sediment (Fig. 4-20). The results of tephra analyses (Fig. 4-23, Tables 4-2 and 4-3) demonstrated that mixtures of volcanic glasses of Hr-FA, Hr-FP, and To-a were contained especially at 57–59, 61–63, and 65–67 cm depth. They were apparently reworked because the depositional ages of these volcanic glasses are completely different (six-century in Hr-Fa and Hr-FP; AD915 in To-a). Based on the evidence that (1) the 1611 Keicho tsunami sandy deposit was absent and (2) no tephra layer was observed from post-tsunami deposit, it is proposed that lake bottom sediments were strongly eroded by the 2011 tsunami.

To estimate the erosional depth, an age-depth model might be useful. In fact, absence of the 1611 Keicho tsunami deposit and the 915 To-a tephra layer in post-tsunami sediment is consistent with the

large time gap separating the period when Sand 1 was deposited (2011) and the age of the peat underlying Sand 1 (ca. 600–1100 yr BP) (Fig. 4-22). However, several difficulties are associated with the age-depth model used to estimate the erosional depth. The age-depth model established in this study cannot be compared directly with the age-depth model of Sawai et al. (2008) because of the difference between dated materials: ^{14}C data of Slice 3 were mainly obtained from organic sediments. However, ^{14}C data of Sawai et al. (2008) were obtained from plant macrofossils. Age difference observed between organic sediment and leaves in Slice 3 were, respectively about 400 and 700 years at 65–66 and 81–82 cm depth. It is noteworthy that it is difficult to validate which material is better to ascertain the correct age of sediments. Results of Slice 3 showed that a tsunami can erode lake bottom sediments considerably and rework sediments on the top. Similar processes might have occurred in the past. If so, leaves might be reworked and bulk organic carbon might be a mixture of various reworked sediments.

Considering the large variability of ^{14}C dating results, it is inferred that absence of To-a layer in post-tsunami sediment is more reliable to estimate erosional depth. When one assumes that the tsunami eroded at least the stratigraphic level of the To-a layer, then the erosional depth of the lake bottom sediment reached approximately 1.4 m in the lake center. Extensive erosion might not be a local effect in the lake center; it might extend over the entire lake floor (Fig. 5-3). In fact, the To-a layer was found at all samples in pre-tsunami sediment (Sawai et al., 2008), although it was absent in post-tsunami sediment. The lake bottom seems to have been eroded entirely by the 2011 tsunami, at least deeper than the depth of the To-a layer. The eroded thickness can be estimated at least from 80 cm to 150 cm when it is compared the closest pre- and post-tsunami sediments.

Strong lake floor scour at the seaward end of the lake reported in a small lake along the western coast of Norway was probably caused by the Storegga tsunami, which occurred between 7000 and 7200 years BP (Bondevik et al., 1997), although no such report is tested in the case of modern examples. Occurrence of such selective scouring in the lake can be confirmed from *Suijin-numa*. High tsunami flow velocity at the seaward end of the lake scoured the lake bottom, but left no sandy deposit observed from Slice-6 (Fig. 4-20). Results of a flume experiment reproduced in the coastal lake environment suggest that the seaward edge of the lake is scoured strongly by a hydraulic jump because

of the sudden increase of the water depth in the lake (Yamaguchi and Sekiguchi, 2015). They also suggested that deposition was slight near the seaward edge of the lake (Yamaguchi and Sekiguchi, 2015). Large erosion and the absence of sand deposits observed in Slice 6 (Fig. 4-20) are consistent with their experiment, so it is explainable by the similar scouring process near the seaward edge of the lake. This finding is expected to be important for future investigations of paleo-tsunami deposits at any lake. The preservation potential of the tsunami deposit might be high near the center to the landward edge of the lake rather than the seaward edge.

5.4.3 Implication for paleo-tsunami study

Coastal lakes and lagoons are considered to be promising places to reconstruct paleo-tsunami history. However, results in *Suijin-numa* imply that even the paleo-tsunami history in coastal lake and lagoon settings is more complex than previously thought because possible large-scale erosion and reworking of the lake floor by a large tsunami cannot be overlooked. The extensive erosion of lake bottom sediments might or might not occur depending on several factors such as cohesion of lake bottom sediments and bed shear stress induced by tsunami flow. In fact, soft mud in *Suijin-numa* was eroded significantly in meter-order whereas a hard peat layer, i.e. the lower To-a layer, would not have been eroded to such a degree. Lake bottom erosion is also expected to be related to the power of tsunami flow at the lake, which is controlled by several factors such as the initial wave size, water-depth of the lake, distance from the shoreline, and elevation. For example, *Suijin-numa* is 2.6 m in maximum water depth, which might be shallow when compared to the flow depth of the tsunami at the lake (approximately 10 m). Moreover, *Suijin-numa* is located near the shoreline (about 600 m inland). For that reason, the tsunami flow velocity might not have been weakened when the tsunami inundated the lake. Therefore, the extent of marked erosion of the paleotsunami record depends on the local setting and tsunami size: it should be evaluated in each survey area and for each tsunami event. Further hydraulic experiments must be conducted to elucidate the relations among these factors and the extent of lake bottom erosion.

Thick reworked sediment confuses estimation of the depositional age of the tsunami deposit. The age below Sand 1 is older than at least AD915 because the To-a layer was eroded. Black mud above Sand 1 contains organic matter with various ages. The age in reworked mud was recorded as the modern age to ca. 200 cal yr BP in Slice 3 (Fig. 4-22 and Table 4-1). It is not a medium age for past 1100 years but shifted slightly to a younger age, i.e., modern to ca. 200 cal yr BP. This result is explainable that young organic carbon exists more than old organic carbon because of the decomposition of old carbon. Therefore, if one overlooks the fact that the mud above Sand 1 was deposited by the tsunami and if one estimates the depositional age of Sand 1 using organic sediments immediately below and above Sand 1 without knowing that the upper mud was deposited in 2011, then the obtained depositional age of Sand 1 might be inferred as a few hundred years older than the actual age (Fig. 5-4).

Identification of muddy tsunami deposits is extremely important to ascertain an appropriate age of paleo-tsunami deposits. Muddy tsunami deposits were not usually identified in earlier studies for lake sediments because they closely resemble the mud that was deposited originally in the lake before the tsunami. However, an evidence of seawater incursion in reworked black mud was found based on diatom analysis (Fig. 4-24). Moreover, recent works have suggested that muddy tsunami deposits might be identified using geochemical analysis (e.g., Goto et al., 2011; Chagué-Goff, 2015). Such analyses are strongly sought for the careful identification of muddy tsunami deposits above the sandy tsunami deposit. It might engender a better understanding of an appropriate age.

Revealing paleotsunami history at the coasts near the subduction zone such as the Pacific coast of Tohoku including the Sanriku coast (e.g., Sawai et al., 2012, 2015a; Goto et al., 2015; Ishimura and Miyauchi, 2015) has yielded important contributions of tsunami geology to future tsunami risk evaluation. However, tsunami history might not always be complete, even in a low-energy environment, because tsunami deposits are not necessarily formed; moreover, they can be disturbed by bioturbation (Szczuciński, 2011). The results of *Suijin-numa* further imply that, in some cases, it is insufficient to date only above and below an event deposit to clarify whether extreme erosion occurred. Soil deposited on the previous tsunami deposit might still be thin and soft if a large tsunami recurrence

interval is short (e.g., a few hundred years). Therefore, it is likely that such soil and even previous tsunami deposits have been eroded.

To overcome these issues and to reconstruct paleotsunami history accurately, it is important to confirm the continuity of sediment among tsunami deposits. Numerous dating experiments might be effective to clarify the existence of erosion. Sawai et al. (2009) reported the recurrence interval of tsunamis based on numerous dating experiments of plant macrofossils in eastern Hokkaido, northern Japan, along the southern Kuril trench. Continuous ^{14}C data confirmed that the depositional ages of peat were consistent with the stratigraphic order and that no severe age gap was observed. Even though extensive erosion and reworking occurred because of the tsunami, as in the case of *Suijin-numa*, they are distinguishable by ^{14}C data from the entire sediment. Such confirmation of the completeness of the geologic record is crucially important for accurate understanding of the tsunami history.

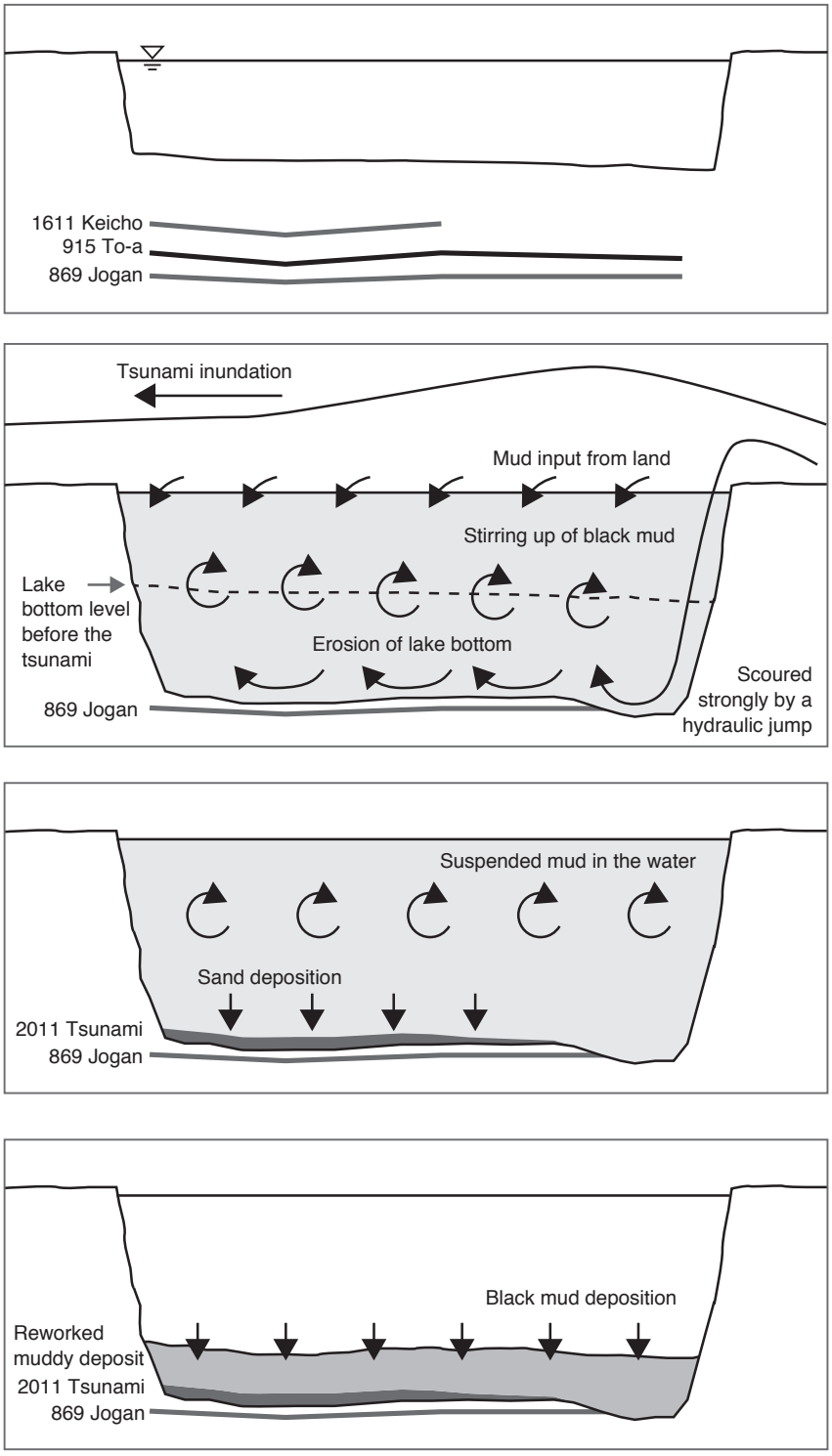

Fig. 5-3. Illustration showing the lake bottom erosion and reworking caused by tsunami inundation.

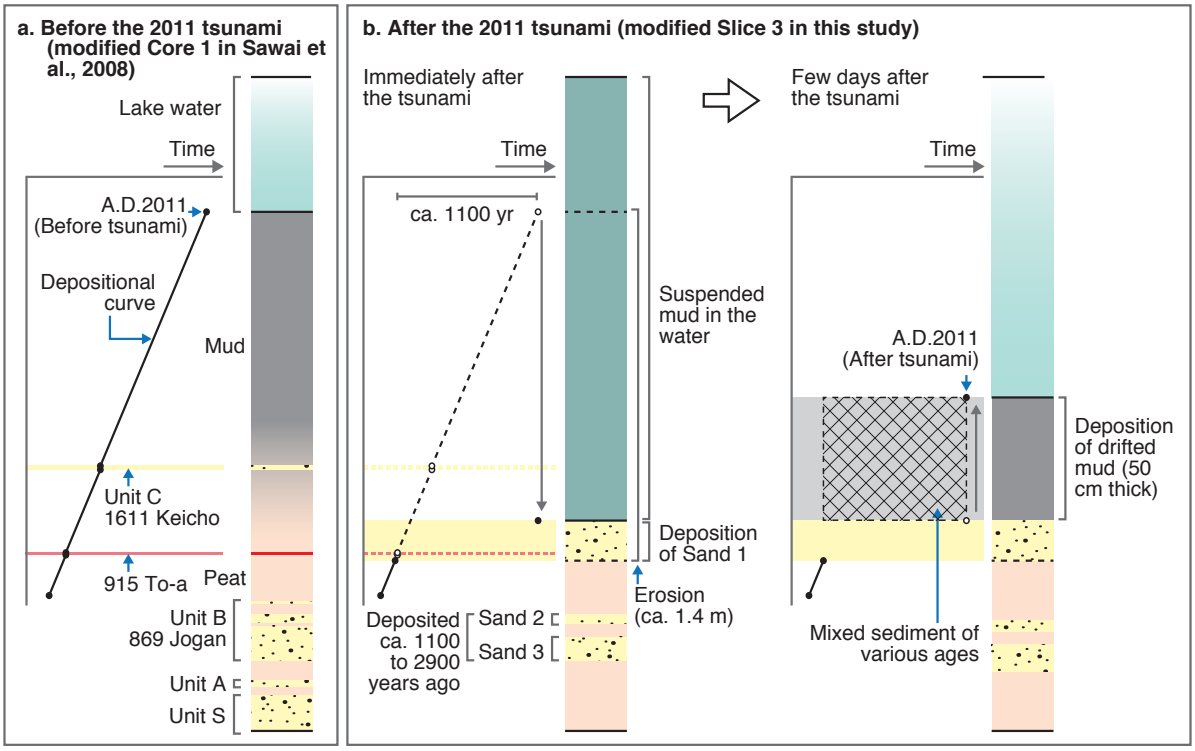

Fig. 5-4. Conceptual model of depositional and erosional process. (a) Columnar section before the 2011 tsunami (modified after Core 1 in Sawai et al., 2008). Linear graph shows a depositional curve. The accumulation rate is assumed as constant. (b) Columnar section after the 2011 tsunami (modified after Slice 3 in this study). Immediately after the tsunami (left panel in b), approx. 1.4 m thick mud is eroded, which is consistent with ca. 1100 years. A large time gap occurred below and above Sand 1. A few days after the 2011 tsunami (right panel in b), suspended mud was deposited on Sand 1. The mud contains organic materials of various ages. The age of the mud deposit became a few hundred years older than the actual age. Correct age of the post 2011 sediment can only be estimated if one measures the sediments that will be deposited above the black mud in the future.

5.5 Implication of geochemical analysis for paleo-tsunami research

Preservation potential of geochemical characteristics associated with tsunami inundation is important for applying these features to tsunami research, for example identifying paleo-tsunami deposit or estimating inundation limit of paleo-tsunami. Evidence of marine-sourced biomarkers was detected at Sendai and Odaka although they were absent at Hasunuma either 2011 or 2014. Tsunami-derived water-leachable ions were concentrated at soil just below thick sandy tsunami deposit, and then they were decreased with time.

One of important factor for preservation of geochemical evidence is meteoric water. Rainfall and seepage probably account for the decreasing or disappearance of geochemical characteristics. For example, salinization caused by the 2004 Indian Ocean tsunami (as indicated by electrical conductivity, pH, and Na^+, K^+, Ca^{2+}, Mg^{2+}, and Cl^- contents) had almost disappeared just one rainy season after the tsunami (Szczuciński et al., 2007; Chandrasekharan et al., 2008; Kume et al., 2009; Raja et al., 2009; Nakaya et al., 2010). Nakaya et al. (2010) reported that soil salinity could be almost completely eliminated by 1000 mm or more of rainfall. In the case of the Sendai Plain, high concentration of water-leachable ions was detected from sample collected at May 2011 but they were generally decreased at February 2012 (Chagué-Goff et al., 2014). Total rainfall at Sendai was, respectively, about 320 mm and 1220 mm between March 2011 to May 2011 and February 2012 (Japan Meteorological Agency). These reports suggest that the concentration of water-leachable ions could decrease over time, most likely because it can easily be diluted by water flow such as precipitation and groundwater movement.

In the case of Hasunuma, samples were collected in June and August 2011 and in October 2014 (Table 2-1). Precipitation between the 2011 tsunami and the 2011 sampling date (about 620 and 760 mm from March to June and August 2011, respectively; Japan Meteorological Agency) was too low to eliminate soil salinity at Hasunuma. Therefore, it is not surprising that water-leachable ions were still measureable in the 2011 samples. Between March 2011 and October 2014, however, they may have been eliminated by the high amount of precipitation since the tsunami (about 5630 mm; Japan Meteorological Agency).

More than 2340 mm of precipitation was recorded between March 2011 and February 2013 in Sendai, and more than 3400 mm was recorded between March 2011 and September 2013 in Haramachi (the closest meteorological weather station to Odaka, about 10 km away; Japan Meteorological Agency). Even though both sites had a high level of precipitation, the marine-sourced biomarkers were still observed, especially it was detected at Sendai 2 years after the tsunami and at Odaka 2.5 years after the tsunami. It suggests that biomarkers have resistance characteristic against to water movement although secular change of allogenic biomarkers was not confirmed. It is important to emphasize that the marine-sourced biomarkers were preserved for at least 2 years. Moreover, biomarkers are utilized in paleoenvironmental and paleoclimate research (Eglinton and Eglinton, 2008), it is expected to be preserved in geological layer for long time. It suggests that biomarkers have a potential as tsunami deposit identifying proxy.

Moreover, biomarkers may be useful to estimate tsunami inundation area correctly. Goto et al. (2011) found that high concentration of water-leachable chloride was observed at muddy tsunami deposit beyond sandy tsunami deposit. Inundation area of paleotsuanmi is estimated from distribution of sand deposit because it can be identified from geological layer compared with muddy tsunami deposit. However, sand deposit does not always distribute up to the inundation limit. According to the case of the 2011 tsunami, ≥0.5 cm thick sand layer reached 57–76% of the inundation distance where the tsunami inundated more than 2.5 km inland (Abe et al. 2012). It is not unique to the case of the 2011 tsunami. Chagué-Goff et al. (2015) also reported that high concentration of water-leachable chloride and sulfur were observed beyond the extent of the sandy tsunami deposit associated with the 2010 Maule earthquake and subsequent tsunami caused at Chile. If we could find an evidence of tsunami inundation using water-leachable ions as results of Goto et al. (2011) and Chagué-Goff et al. (2015), we can estimate tsunami inundation areas more precisely. Therefore, it is important to estimate tsunami inundation area using geochemical analysis. In this study, it was revealed that water-leachable ions are generally disappeared with time. While, biomarkers seem to be preserved for a long time. If biomarkers can be detected from tsunami inundation area where is no sedimentation, it can be estimate precise inundation area (Fig. 5-5). This estimation leads to better understanding of reconstruction of magnitude and epicenter of past earthquake.

Geochemical characteristics might be preserved at coastal lake as reported by Minoura and Nakaya (1991) and Minoura et al. (1994). However, coastal lake is sometimes incurred severe erosion and reworking by tsunami incursion like the result of *Suijin-numa*. Especially, reworked mud is incredibly difficult to distinguish by eye observation from geological layer. In that case, it might be able to identify by using geochemical analysis, such as biomarkers. However, we should take more precise biomarker analysis because some biomarkers, such as short-chain *n*-alkanes, are made by freshwater organism. To identify an evidence of seawater incursion, it is required using marine-sourced biomarker, such as dinosterol, brassicasterol mainly derived by diatom (e.g., Rubinstein and Goad, 1974), and alkenones. However, measurable amount of marine-source biomarkers possibly cannot be deposited by tsunami inundation, in fact, they were almost not detected from terrestrial samples excavated in this study. In order to detect such marine-source biomarkers, it is required to improve analytical technique. For example, visible terrestrial plant materials are removed by picking up or sieving and then sample amount is increased. Large amount of terrestrial organic materials seem to blind a low contribution of marine-source organic materials, therefore removal of visible terrestrial plants is probably effective to detect marine-source biomarkers. In that case, consideration of biomarker analysis for lake bottom sediment is valuable because it may be able to identify reworked mud deposit as well as sandy tsunami deposit.

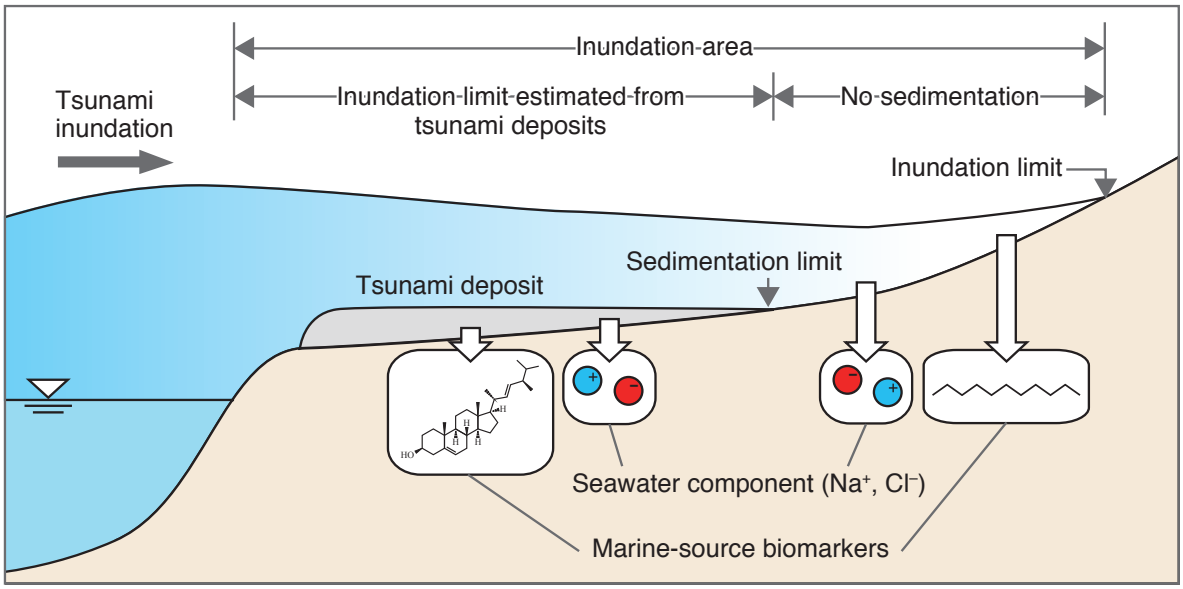

Fig. 5-5. Illustration showing the deposition of sediment and chemical components by tsunami inundation. Sandy deposit does not always reach to tsunami inundation limit. Chemical component can be detected from inundation area even though beyond sedimentation limit.

Chapter 6. General conclusions

In this thesis, I applied biomarker and water-leachable ion analyses for the samples of 2011 Tohoku-oki tsunami deposit and underlying and overlying soil collected at Senadi, Odaka, and Hasunuma. Moreover, significant lake-bottom erosion caused by the tsunami inundation was discussed based on the comparison of pre- and post-tsunami lake bottom deposits at Yamamoto. Based on these analyses, I found the following points:

1) Marine-origin biomarkers were transported and deposited in the soil below the sandy tsunami deposit or in the tsunamigenic mud by the 2011 tsunami.
2) Transported biomarkers can adsorb to fine particles and organic-rich sediment not to sand-sized particles, and it can be preserved at least 2-years.
3) Water-leachable ions originated from seawater compositions can be concentrated at coastal soil layer just below thick sand layer by tsunami inundation. However, the concentrations can be diluted by rainfall or groundwater movement, and the evidence of seawater incursion can be disappeared for several months to a year.
4) Severe lake bottom erosion (0.8–1.5 m) including geological record, such as paleotsunami deposit and volcanic ash layer, was caused by the 2011 tsunami at coastal lake.
5) Coastal lake is considered to be suitable area for tsunami research, however, these area also be caught a severe damage and can be lost valuable geological records.
6) Thick (20–60 cm) mud was reworked at lake floor by the tsunami. The mud contained old organic materials, suggesting that identifying reworked mud is required to reconstruct tsunami history precisely.

Geochemical characteristics seem to be preserved in organic silty mud rather than sand. Both water-leachable ions and biomarkers were transported on land by tsunami, and especially, biomarkers have a possibility that it can be preserved for long time. The findings show the potential of using biomarkers as proxies for identifying marine-originated deposits on coastal land. Moreover, it can be

utilized to estimate inundation area correctly. It leads to high-accuracy reconstruction of tsunami occurrence interval, inundation area, and magnitude of paleo-earthquake. In order to apply geochemical proxy for paleotsunami research, further case studies are required; for example gathering a modern analogue of geochemical features, finding geochemical characteristics from paleotsunami deposit that is identified as tsunami-origin based on sedimentological or paleontological features. Although it is required for more case studies for applying geochemical analysis to paleotsunami deposit, I proposed in this thesis that the possibility of geochemical analysis in the field of tsunami deposit research.

Acknowledgements

I am greatly indebted to Associate professor Shigehiro Fujino (University of Tsukuba), Associate professor Kazuhisa Goto (Tohoku University), and Dr. Yuki Sawai (National institute of Advanced Industrial Science and Technology) for providing valuable and constructive comments. I thank Professor Minoru Ikehara (Kochi University) and Dr. Junko Hara (National institute of Advanced Industrial Science and Technology) for their help with geochemical analyses and for providing valuable comments. I thank Professor Ken-ichiro Hisada and Associate professor Yoshihiko Kamata for their valuable comments and suggestions. I thank Dr. Takashi Chiba for diatom analysis. The TC, TN, $\delta^{13}C$, and biomarker analyses and CT image scanning were performed under the cooperative research program of the Center for Advanced Marine Core Research, Kochi University (Accept Nos. 13A028, 13B043, 14A006, 14A019, and 14B017). Water-leachable ions were analyzed at the National Institute of Advanced Industrial Science and Technology. This research was supported by the Program to Disseminate Tenure Tracking System, MEXT, Japan, and JSPS research funds (no. 26242033 and 15K05334). Finally, I am deeply grateful to my family for all of their supports.

References

Abe, H., Sugeno, Y., Chigama, A., 1990. Estimation of the height of the Sanriku Jogan 11 Earthquake-tsunami (A.D. 869) in the Sendai Plain. *Journal of the Seismological Society of Japan (Zishin)* **43**, 513–525 (in Japanese with Engligh abstract).

Abe, T., Goto, K., Sugawara, D., 2012. Relationship between the maximum extent of tsunami sand and the inundation limit of the 2011 Tohoku-oki tsunami on the Sendai Plain, Japan. *Sedimentary Geology* **282**, 142–150.

Abe, T., Goto, K., Sugawara, D., 2014. Spatial distribution of the 2011 Tohoku-oki tsunami deposits in a narrow valley at the southern end of Sendai Plain. *19th International Sedimentological Congress*, Geneva, Abstract, p. 10.

Abelson, P.H., 1954. Organic constituents of fossils. *Carnegie Institution of Washington Year Book* **53**, 97–101.

Alpar, B., Ünlü, S., Altınok, Y., Özer, N., Aksu, A., 2012. New approaches in assessment of tsunami deposits in Dalaman (SW Turkey). *Natural Hazards* **60**, 27–41.

Aoki, K., Arai, F., 2000. Late Quaternary tephrostratigraphy of marine core KH94-3, LM-8 off Sanriku, Japan. *The Quaternary Research* **39**, 107–120 (in Japanese with English abstract).

Atwater, B.F., 1987. Evidence for great Holocene earthquakes along the outer coast of Washington State. *Science* **236**, 942–944.

Blumer, M., Thomas, D.W., 1965. Phytadienes in zooplankton. *Science* **147**, 1148–1149.

Blumer, M., Mullin, M.M., Thomas, D.W., 1963. Pristane in zooplankton. *Science* **140**, 974.

Bondevik, S., Svendsen, J.I., Mangerud, J., 1997. Tsunami sedimentary facies deposited by the Storegga tsunami in shallow marine basins and coastal lakes, western Norway. *Sedimentology* **44**, 1115–1131.

Boon, J.J., Rijpstra, W.I.C., Lange, F.D., Leeuw, J.W.D., Yoshioka, M., Shimizu, Y., 1979. Black Sea sterol–a molecular fossil for dinoflagellate blooms. *Nature* **277**, 125–127.

Brassell, S.C., 1993. Applications of biomarkers for delineating marine paleoclimatic fluctuations during the Pleistocene. In: Engel, M.H., Macko, S.A., (eds.) *Organic geochemistry*, Plenum Press, New York, 699–738.

Calib 7.1. CALIB Radiocarbon Calibration [online]. Available from: http://calib.qub.ac.uk/calib/calib.html.

Chagué-Goff, C., Andrew, A., Szczuciński, W., Goff, J., Nishimura, Y., 2012a. Geochemical signatures up to the maximum inundation of the 2011 Tohoku-oki tsunami — Implications for the 869AD Jogan and other palaeotsunamis. *Sedimentary Geology* **282**, 65–77.

Chagué-Goff, C., Dawson, S., Goff, J.R., Zachariasen, J., Berryman, K.R., Garnett, D.L., Waldron, H.M., Mildenhall, D.C., 2002. A tsunami (ca. 6300 years BP) and other Holocene environmental changes, northern Hawke's Bay, New Zealand. *Sedimentary Geology* **150**, 89–102.

Chagué-Goff, C., Goff, J., Nichol, S.L., Dudley, W., Zawadzki, A., Bennett, J.W., Mooney, S.D., Fierro, D., Heijnis, H., Dominey-Howes, D., Courtney, C., 2012c. Multi-proxy evidence for trans-Pacific tsunamis in the Hawai'ian Islands. *Marine Geology* **299–302**, 77–89.

Chagué-Goff, C., Goff, J., Wong, H.K.Y., Cisternas, M., 2015. Insights from geochemistry and diatoms to characterise a tsunami's deposit and maximum inundation limit. *Marine Geology* **359**, 22–34.

Chagué-Goff, C., Niedzielski, P., Wong, H.K.Y., Szczuciński, W., Sugawara, D., Goff, J., 2012b. Environmental impact assessment of the 2011 Tohoku-oki tsunami on the Sendai Plain. *Sedimentary Geology* **282**, 175–187.

Chagué-Goff, C., Schneider, J.-L., Goff, J.R., Dominey-Howes, D., Strotz, L., 2011. Expanding the proxy toolkit to help identify past events — Lessons from the 2004 Indian Ocean Tsunami and the 2009 South Pacific Tsunami. *Earth-Science Reviews* **107**, 107–122.

Chagué-Goff, C., Wong, H.K.Y., Sugawara, D., Goff, J., Nishimura, Y., Beer, J., Szczuciński, W., Goto, K., 2014. Impact of tsunami inundation on soil salinisation: up to one year after the 2011 Tohoku-oki tsunami. In: Kontar, Y.A., Santiago-Fandiño, V., Takahashi, T., (eds.) *Tsunami Events and Lessons Learned: Ecological and Societal Significance*. Springer, Dordrecht, 193–214.

Chandrasekharan, H., Sarangi, A., Nagarajan, M., Singh, V.P., Rao, D.U., Stalin, P., Natarajan, K., Chandrasekaran, B., Anbazhagan, S., 2008. Variability of soil-water quality due to Tsunami-2004 in the coastal belt of Nagapattinam district, Tamilnadu. *Journal of Environmental Management* **89**, 63–72.

Conte, M.H., Volkman, J.K., Eglinton, G., 1994. Lipid biomarkers of the Haptophyta. In: Green, J.C., Leadbeater, B.S.C., (eds.) *The Haptophyte Algae*, Clarendon Press, Oxford, 351–377.

Dawson, A.G., Hindson, R., Andrade, C., Freitas, C., Parish, R., Bateman, M., 1995. Tsunami sedimentation associated with the Lisbon earthquake of 1 November AD 1755: Boca do Rio, Algarve, Portugal. *The Holocene* **5**, 209–215.

Dawson, A.G., Long, D., Smith, D.E., 1988. The Storegga slides: evidence from eastern Scotland for a possible tsunami. *Marine Geology* **82**, 271–276.

Dean, W.J., 1974. Determination of carbonate and organic matter in calcareous sediments and sedimentary rocks by loss on ignition: comparison with other methods. *Journal of Sedimentary Petrology* **44**, 242–248.

Eglinton, G., Hamilton, R.J., 1963. The distributions of alkanes. In: Swan, T., (ed.) *Chemical Plant Taxonomy*, Academic Press, San Diego, California, 187–217.

Eglinton, T.I., Eglinton, G., 2008. Molecular proxies for paleoclimatology. *Earth and Planetary Science Letters* **275**, 1–16.

Fujikawa, T., Okazawa, H., Nakamura, T., Takeuchi, Y., Komamura, M., 2011. Physical and chemical properties of tsunami deposits in the northeast area of Fukushima Prefecture after the Tohoku-Kanto Earthquake. *Internatinal Journal of GEOMATE* **1**, 44–49.

Gelpi, E., Schneider, H., Mann, J., Oró, J., 1970. Hydrocarbons of geochemical significance in microscopic algae. *Phytochemistry* **9**, 603–612.

Geospatial Information Authority of Japan. Geospatial Information Authority of Japan [online]. Available from: http://www.gsi.go.jp/kikaku/kikaku40014.html.

Goff, J., Chagué-Goff, C., Nichol, S., Jaffe, B., Dominey-Howes, D., 2012. Progress in palaeotsunami research. *Sedimentary Geology* **243–244**, 70–88.

Goff, J., Nichol, S., Chagué-Goff, C., Horrocks, M., McFadgen, B., Cisternas, M., 2010. Predecessor to New Zealand's largest historic trans-South Pacific tsunami of 1868AD. *Marine Geology* **275**, 155–165.

Goff, J.R., Wells, A., Chagué-Goff, C., Nichol, S.L., Robert J, N., Devoy, 2004. The elusive AD 1826 tsunami, South Westland, New Zealand. *New Zealand Geographer* **60**, 28–39.

Goto, K., Chagué-Goff, C., Fujino, S., Goff, J., Jaffe, B., Nishimura, Y., Richmond, B., Sugawara, D., Szczuciński, W., Tappin, D.R., Witter, R.C., Yulianto, E., 2011. New insights of tsunami hazard from the 2011 Tohoku-oki event. *Marine Geology* **290**, 46–50.

Goto, K., Hashimoto, K., Sugawara, D., Yanagisawa, H., Abe, T., 2014. Spatial thickness variability of the 2011 Tohoku-oki tsunami deposits along the coastline of Sendai Bay. *Marine Geology* **358**, 38–48.

Goto, K., Sugawara, D., Abe, T., Haraguchi, T., Fujino, S., 2012a. Liquefaction as an important source of the A.D. 2011 Tohoku-oki tsunami deposits at Sendai Plain, Japan. *Geology* **40**, 887–890.

Goto, K., Sugawara, D., Ikema, S., Miyagi, T., 2012b. Sedimentary processes associated with sand and boulder deposits formed by the 2011 Tohoku-oki tsunami at Sabusawa Island, Japan. *Sedimentary Geology* **282**, 188–198.

Goto, T., Satake, K., Sugai, T., Ishibe, T., Harada, T., Murotani, S., 2015. Historical tsunami and storm deposits during the last five centuries on the Sanriku coast, Japan. *Marine Geology* **367**, 105–117.

Gough, M.A., Rowland, S.J., 1990. Characterization of unresolved complex mixtures of hydrocarbons in petroleum. *Nature* **344**, 648–650.

Hemphill-Haley, E., 1996. Diatoms as an aid in identifying late-Holocene tsunami deposits. *The Holocene* **6**, 439–448.

Ikan, R., Baedecker, M.J., Kaplan, I.R., 1975. Thermal alteration experiments on organic matter in recent marine sediment–II. Isoprenoids. *Geochimica et Cosmochimica Acta* **39**, 187–194.

Ishimura, D., Miyauchi, T., 2015. Historical and paleo-tsunami deposits during the last 4000 years and their correlations with historical tsunami events in Koyadori on the Sanriku Coast, northeastern Japan. *Progress in Earth and Planetary Science* **2**, 16.

Jackson, K.L., Eberli, G.P., Amelung, F., McFadden, M.A., Moore, A.L., Rankey, E.C., Jayasena, H.A.H., 2014. Holocene Indian Ocean tsunami history in Sri Lanka. *Geology* **42**, 859–862.

Jagodziński, R., Sternal, B., Szczuciński, W., Chagué-Goff, C., Sugawara, D., 2012. Heavy minerals in the 2011 Tohoku-oki tsunami deposits—insights into sediment sources and hydrodynamics. *Sedimentary Geology* **282**, 57–64.

Jankaew, K., Atwater, B.F., Sawai, Y., Choowong, M., Charoentitirat, T., Martin, M.E., Prendergast, A., 2008. Medieval forewarning of the 2004 Indian Ocean tsunami in Thailand. *Nature* **455**, 1228–1231.

Japan Meteorological Agency. Japan Meteorological Agency [online]. Available from: http://www.jma.go.jp/jma/index.html.

Kelsey, H.M., Nelson, A.R., Hemphill-Haley, E., Witter, R.C., 2005. Tsunami history of an Oregon coastal lake reveals a 4600 yr record of great earthquakes on the Cascadia subduction zone. *Geological Society of America Bulletin* **117**, 1009–1032.

Komai, T., Kawabe, Y., Hara, J., Sakamoto, Y., Zhang, M., 2012 Geochemical survey of tsunami sediments and transport of toxix elements from offshore environment –Urgent investigation for earthquake March 11, 2011–. *Proceedings of the Twenty-second (2012) International Offshore and Polar Engineering Conference*, 49–53.

Kume, T., Umetsu, C., Palanisami, K., 2009. Impact of the December 2004 tsunami on soil, groundwater and vegetation in the Nagapattinam District, India. *Journal of Environmental Management* **90**, 3147–3154.

Lamb, A.L., Wilson, G.P., Leng, M.J., 2006. A review of coastal palaeoclimate and relative sea-level reconstructions using $\delta^{13}C$ and C/N ratios in organic material. *Earth-Science Reviews* **75**, 29–57.

Machida, H., Arai, F., 2011. *Atlas of Tephra in and around Japan (revised edition)*. University of Tokyo Press, Tokyo, 336 p (in Japanese).

Mackie, P.R., Whittle, K.J., Hardy, R., 1974. Hydrocarbons in the Marine Environment I. *n*-Alkanes in the Firth of Clyde. *Estuarine and Coastal Marine Science* **2**, 359–374.

Marlowe, I.T., Green, J.C., Neal, A.C., Brassell, S.C., Eglinton, G., Course, P.A., 1984. Long chain (n-C_{37}–C_{39}) alkenones in the Prymnesiophyceae. Distribution of alkenones and other lipids and their taxonomic significance. *British Phycological Journal* **19**, 203–216.

Matsumoto, D., Sawai, Y., Tanigawa, K., Fujiwara, O., Namegaya, Y., Shishikura, M., Kagohara, K., Kimura, H., submitted. Tsunami deposit associated with the 2011 Tohoku-oki tsunami in Hasunuma site of the Kujukuri coastal plain, Japan. *Island Arc*.

Meyers, P.A., Takeuchi, N., 1981. Environmental changes in Saginaw Bay, Lake Huron recorded by geolipid contetns of sediments deposited since 1800. *Environmental Geology* **3**, 257–266.

Minoura, K., Gusiakov, V.G., Kurbatov, A., Takeuti, S., Svendsen, J.I., Bondevik, S., Oda, T., 1996. Tsunami sedimentation associated with the 1923 Kamchatka earthquake. *Sedimentary Geology* **106**, 145–154.

Minoura, K., Imamura, F., Sugawara, D., Kono, Y., Imamura, T., 2001. The 869 Jogan tsunami deposit and recurrence interval of large-scale tsunami on the Pacific coast of northeast Japan. *Journal of Natural Disaster Science* **23**, 83–88.

Minoura, K., Nakaya, S., 1991. Traces of tsunami preserved in inter-tidal lacustrine and marsh deposits: some examples from Northeast Japan. *The Journal of Geology* **99**, 265–287.

Minoura, K., Nakaya, S., Sato, H., 1987. Traces of tsunamis recorded in lake deposits —An example from Jusan, Shiura-mura, Aomori—. *Journal of the Seismological Society of Japan (Zishin)* **40**, 183–196 (in Japanese with Engligh abstract).

Minoura, K., Nakaya, S., Uchida, M., 1994. Tsunami deposits in a lacustrine sequence of the Sanriku coast, northeast Japan. *Sedimentary Geology* **89**, 25–31.

Nakata, T., Shimazaki, K., 1997. Geo-slicer, a newly invented soil sampler, for high-resolution active fault studies. *Journal of Geography (Chigaku zassi)* **106**, 59–69 (in Japanese with English abstract).

Nakaya, T., Tanji, H., Kiri, H., Hamada, H., 2010. Developing a Salt-Removal Plan to Remedy Tsunami-caused Salinity Damage to Farmlands: Case Study for an Area in Southern Thailand. *Japan Agricultural Research Quarterly: JARQ* **44**, 159–165.

Nanayama, F., Furukawa, R., Shigeno, K., Makino, A., Soeda, Y., Igarashi, Y., 2007. Nine unusually large tsunami deposits from the past 4000 years at Kiritappu marsh along the southern Kuril Trench. *Sedimentary Geology* **200**, 275–294.

Nanayama, F., Satake, K., Furukawa, R., Shimokawa, K., Atwater, B.F., Shigeno, K., Yamaki, S., 2003. unusually large earthquakes inferred from tsunami deposits along the Kuril trench. *Nature* **424**, 660–663.

Nichol, S.L., Chagué-Goff, C., Goff, J.R., Horrocks, M., McFadgen, B.G., Strotz, L.C., 2010. Geomorphology and accommodation space as limiting factors on tsunami deposition: Chatham Island, southwest Pacific Ocean. *Sedimentary Geology* **229**, 41–52.

Ohkouchi, N., Kawamura, K., Taira, A., 1997. Molecular paleoclimatology: reconstrcution of climate variabilities in the late Quaternary. *Organic Geochemistry* **27**, 173–183.

Okazaki, H., Ohki, J., 2012. Tsunami deposits and coastal change in Kujukuri coast at the 2011 Tohoku earthquakes. *Journal of the Natural History Museum and Institute, Chiba* **12**, 1–15 (Japanese with English abstract).

Ozawa, S., Nishimura, T., Suito, H., Kobayashi, T., Tobita, M., Imakiire, T., 2011. Coseismic and postseismic slip of the 2011 magnitude-9 Tohoku-Oki earthquake. *Nature* **475**, 373–376.

Peters, K.E., Walters, C.C., Moldowan, J.M., 2007a. Biochemistry of biomarkers. In: Peters, K.E., Walters, C.C., Moldowan, J.M., (eds.) *The Biomarker Guide volume 1: Biomarkers and isotopes in the Environment and Human History petroleum exploration and Earth history.* Cambridge University Press, Cambridge, 45–71.

Peters, K.E., Walters, C.C., Moldowan, J.M., 2007b. Biomarkers in the environment. In: Peters, K.E., Walters, C.C., Moldowan, J.M., (eds.) *The Biomarker Guide volume 1: Biomarkers and isotopes in the Environment and Human History petroleum exploration and Earth history.* Cambridge University Press, Cambridge, 274–321.

Peters, K.E., Walters, C.C., Moldowan, J.M., 2007c. Source- and age-related biomarker parameters. In: Peters, K.E., Walters, C.C., Moldowan, J.M., (eds.) *The Biomarker Guide volume 2: Biomarkers and isotopes in petroleum exploration and Earth history.* Cambridge University Press, Cambridge, 483–607.

Pilarczyk, J.E., Horton, B.P., Witter, R.C., Vane, C.H., Chagué-Goff, C., Goff, J., 2012. Sedimentary and foraminiferal evidence of the 2011 Tōhoku-oki tsunami on the Sendai coastal plain, Japan. *Sedimentary Geology* **282**, 78–89.

Putra, P.S., Nishimura, Y., Nakamura, Y., Yulianto, E., 2013. Sources and transportation modes of the 2011 Tohoku-Oki tsunami deposits on the central east Japan coast. *Sedimentary Geology* **294**, 282–293.

Raja, R., Chaudhuri, S.G., Ravisankar, N., Swarnam, T.P., Jayakumar, V., Srivastava, R.C., 2009. Salinity status of tsunami-affected soul and water resources of South Andaman, India. *Current Science* **96**, 152–156.

Reimer, P.J., Bard, E., Bayliss, A., Beck, J.W., Blackwell, P.G., Ramsey, C.B., Buck, C.E., Cheng, H., Edwards, R.L., Friedrich, M., Grootes, P.M., Guilderson, T.P., Haflidason, H., Hajdas, I., Hatté, C., Heaton, T.J., Hoffmann, D.L., Hogg, A.G., Hughen, K.A., Kaiser, K.F., Kromer, B., Manning, S.W., Niu, M., Reimer, R.W., Richards, D.A., Scott, E.M., Southon, J.R., Staff, R.A., Turney, C.S.M., Plicht, J.v.d., 2013. IntCal13 and Marine13 radiocarbon age calibration curves 0–50,000 years cal BP. *Radiocarbon* **55**, 1869–1887.

Richmond, B., Szczuciński, W., Chagué-Goff, C., Goto, K., Sugawara, D., Witter, R., Tappin, D.R., Jaffe, B., Fujino, S., Nishimura, Y., Goff, J., 2012. Erosion, deposition and landscape change on the Sendai coastal plain, Japan, resulting from the March 11, 2011 Tohoku-oki tsunami. *Sedimentary Geology* **282**, 27–39.

Rubinstein, I., Goad, L.J., 1974. Occurrence of (24S)-24-methylcholesta-5, 22E-dien-3β-ol in the diatom Phaepdactylum tricornutum. *Phytochemistry* **13**, 485–487.

Santisteban, J.I., Mediavilla, R., López-Pamo, E., Dabrio, C.J., Zapata, M.B.R., a, M.J.G., Castaño, S., Martínez-Alfaro, P.E., 2004. Loss on ignition: a qualitative or quantitative method for organic matter and carbonate mineral content in sediments? *Journal of Paleolimnology* **32**, 287–299.

Sawai, Y., 2012. Study on paleotsunami deposits in geologic stratum. *Journal of the Geological Society of Japan* **118**, 535–558 (Japanese with English abstract).

Sawai, Y., 2014. Diatom fossil analysis as an aid for paleoseismology. *Diatom* **30**, 57–74 (Japanese with English abstract).

Sawai, Y., Fujii, Y., Fujiwara, O., Kamataki, T., Komatsubara, J., Okamura, Y., Satake, K., Shishikura, M., 2008. Marine incursions of the past 1500 years and evidence of tsunamis at Suijin-numa, a coastal lake facing the Japan Trench. *The Holocene* **18**, 517–528.

Sawai, Y., Kamataki, T., Shishikura, M., Nasu, H., Okamura, Y., Satake, K., Thomson, K.H., Matsumoto, D., Fujii, Y., Komatsubara, J., Aung, T.T., 2009. Aperiodic recurrence of geologically recorded tsunamis during the past 5500 years in eastern Hokkaido, Japan. *Journal of Geophysical Research* **114**, B01319.

Sawai, Y., Namegaya, Y., Okamura, Y., Satake, K., Shishikura, M., 2012. Challenges of anticipating the 2011 Tohoku earthquake and tsunami using coastal geology. *Geophysical Research Letters* **39**, L21309.

Sawai, Y., Namegaya, Y., Tamura, T., Nakashima, R., Tanigawa, K., 2015a. Shorter intervals between great earthquakes near Sendai: Scour ponds and a sand layer attributable to A.D. 1454 overwash. *Geophysical Research Letters* **42**, 4795–4800.

Sawai, Y., Tanigawa, K., Tamura, T., Namegaya, Y., 2015b. Medieval coastal inundation revealed by a sand layer on the Ita lowland adjacent to the Suruga Trough, central Japan. *Natural Hazards* **80**, 505–519.

Shinozaki, T., Fujino, S., Ikehara, M., Sawai, Y., Tamura, T., Goto, K., Sugawara, D., Abe, T., 2015a. Marine biomarkers deposited on coastal land by the 2011 Tohoku-oki tsunami. *Natural Hazards* **77**, 445–460.

Shinozaki, T., Goto, K., Fujino, S., Sugawara, D., Chiba, T., 2015b. Erosion of a paleo-tsunami records by the 2011 Tohoku-oki tsunami along the southern Sendai Plain. *Marine Geology* **369**, 127–136.

Shinozaki, T., Sawai, Y., Hara, J., Ikehara, M., Matsumoto, D., Tanigawa, K., submitted. Biomarkers and water-leachable ions in tsunami deposits associated with the 2011 Tohoku-oki tsunami at Hasunuma, Kujukuri coastal plain, Japan. *Island Arc*.

Soda, T., 1989. Two 6th century eruptions of Haruna volcano, central Japan. *The Quaternary International* **27**, 297–312 (in Japanese with English abstract).

Soda, T., 1996. Characteristics of marker-tephra layers above On-Pml ocurring in Kanto and the southern part of Tohoku, Japan. *Summaries of Researches using AMS at Nagoya University* **7**, 256–267 (in Japanese).

Srinivasalu, S., Thangadurai, N., Jonathan, M.P., Armstrong-Altrin, J.S., Ayyamperumal, T., Ram-Mohan, V., 2008. Evaluation of trace-metal enrichments from the 26 December 2004 tsunami sediments along the Southeast coast of India. *Environmental Geology* **53**, 1711–1721.

Szczuciński, W., 2011. The post-depositional changes of the onshore 2004 tsunami deposits on the Andaman Sea coast of Thailand. *Natural Hazards* **60**, 115–133.

Szczuciński, W., Kokociński, M., Rzeszewski, M., Chagué-Goff, C., Cachão, M., Goto, K., Sugawara, D., 2012. Sediment sources and sedimentation processes of 2011 Tohoku-oki tsunami deposits on the Sendai Plain, Japan — Insights from diatoms, nannoliths and grain size distribution. *Sedimentary Geology* **282**, 40–56.

Szczuciński, W., Niedzielski, P., Kozak, L., Frankowski, M., Zioła, A., Lorenc, S., 2007. Effects of rainy season on mobilization of contaminants from tsunami deposits left in a coastal zone of Thailand by the 26 December 2004 tsunami. *Environmental Geology* **53**, 253–264.

Szczuciński, W., Niedzielski, P., Rachlewicz, G., Sobczyński, T., Zioła, A., Kowalski, A., Lorenc, S., Siepak, J., 2005. Contamination of tsunami sediments in a coastal zone inundated by the 26 December 2004 tsunami in Thailand. *Environmental Geology* **49**, 321–331.

Takada, K., Nakata, T., Miyagi, T., Haraguchi, T., Nishitani, Y., 2002. Handy geoslicer – new soil sampler for Quaternary geologist. *Chishitsu News* **579**, 12–18 (in Japanese with English abstract).

Tamura, T., Murakami, F., Watanabe, K., 2010. Holocene beach deposits for assessing coastal uplift of the northeastern Boso Peninsula, Pacific coast of Japan. *Quaternary Research* **74**, 227–234.

Tanaka, G., Naruse, H., Yamashita, S., Arai, K., 2012. Ostracodes reveal the sea-bed origin of tsunami deposits. *Geophysical Research Letters* **39**, L05406.

Tanaka, H., Adityawan, M.B., Mano, A., 2014. Morphological changes at the Nanakita River mouth after the Great East Japan Tsunami of 2011. *Coastal Engineering* **86**, 14–26.

Tappin, D.R., Evans, H.M., Jordan, C.J., Richmond, B., Sugawara, D., Goto, K., 2012. Coastal changes in the Sendai area from the impact of the 2011 Tōhoku-oki tsunami: Interpretations of time series

satellite images, helicopter-borne video footage and field observations. *Sedimentary Geology* **282**, 151–174.

The 2011 Tohoku Earthquake Tsunami Joint Survey Group, 2011. Nationwide Field Survey of the 2011 Off the Pacific Coast of Tohoku Earthquake Tsunami. *Journal of Japan Society of Civil Engineers, Series B* **67**, 63–66.

Ünlü, S., Alpar, B., Altınok, Y., Özer, N., 2012. Rapid coastal changes and tsunami impacts at the Patara Harbour (Turkey). *Proceedings of the International Conference, Land-Sea Interaction in the Coastal Zone LANDSI-2012*, 411–418.

Volkman, J.K., Eglinton, G., Corner, E.D.S., Forsberg, T.E.V., 1980. Long chain alkense and alkenones in the marine coccolithophorid Emiliania huxleyi. *Phytochemistry* **19**, 2619–2622.

Yamaguchi, N., Sekiguchi, T., 2015. Effects of tsunami magnitude and terrestrial topography on sedimentary processes and distribution of tsunami deposits in flume experiments. *Sedimentary Geology* **328**, 115–121.

Yamamoto, M., Polyak, L., 2009. Changes in terrestrial organic matter input to the Mendeleev Ridge, western Arctic Ocean, during the Late Quaternary. *Global and Planetary Change* **68**, 30–37.

Yoshii, T., Imamura, M., Matsuyama, M., Koshimura, S., Matsuoka, M., Mas, E., Jimenez, C., 2013. Salinity in Soils and Tsunami Deposits in Areas Affected by the 2010 Chile and 2011 Japan Tsunamis. *Pure and Applied Geophysics* **170**, 1047–1066.